Fabrication of Composite Membranes for O_2/N_2 Separation

By

Syed Shujaat Karim

School of Chemical and Materials Engineering

National University of Science and Technology

Islamabad, Pakistan

2020

Fabrication of Composite Membranes for O_2/N_2 Separation

Name: Syed Shujaat Karim

Registration Number: 00000276153

This thesis is submitted as a partial fulfillment of the requirements for the degree of

MS Chemical Engineering

Supervisor Name: Dr. Sarah Farrukh

School of Chemical and Materials Engineering (SCME)

National University of Science and Technology (NUST)

H-12 Islamabad, Pakistan

December, 2020

Dedication

I dedicate this work to my beloved parents, siblings, friends, respectable teachers and especially thanks my supervisor, whose continuous and tireless support makes this work possible.

Acknowledgements

All praise belongs to **Almighty Allah**, the most Benevolent, the most Merciful, Who has granted me the strength, courage and willpower to complete my research work, and to overcome all the hindrance that come in my way. I consider myself highly fortunate to be able to complete this work in the time allocated to me.

My utmost gratitude to my supervisor, **Dr. Sarah Farrukh** for her invaluable guidance and support throughout my post graduate research work. I am thankful to her for always believing in my abilities, and always being there for my assistance. I would also sincerely thank **Dr. Arshad Hussain** for his invaluable research direction during this work.

I would also like to thank my Guidance and Examination Committee (GEC) members, **Dr. Tayyaba Noor** and **Dr. Muhammad Ahsan**, for their advice in easing the difficulties and removing the problems in my research project. I am also thankful to them for their moral support as well as material assistance.

I would also like to thank the Lab staff for their assistance in conducting the necessary characterization testing. I am thankful, especially to Mr. Zarrar Salah ud din from MEMAR Lab, Mr. Zafar from SEM Lab, Mr. Nouman from Chemical analysis Lab, Mr. Khurram from XRD Lab and Mr. Khawar from Mechanical Testing Lab SCME NUST.

Finally, I am immensely gratified to my family and friends, who have been the source of endless support and encouragement for me, especially when I was in troubled regarding my project. They have given me much needed moral support and help, to complete my research work.

Abstract

Air separation for the enrichment of oxygen (O_2) and nitrogen (N_2) gas has gained substantial importance in both industrial and medical applications. Therefore, it is imperative to separate O_2 and N_2 gases from air mixture. For this purpose, it is proposed to use composite membrane, which is regarded as one of the most innovative technology in 21st century due to its remarkable characteristics. This research aiming for developing high performance perm-selective composite membrane for O_2/N_2 gas separation for the commercial applications such as blood oxygenator (Artificial Lungs). In-order to achieve this purpose, initially through theoretical model and experimental phase diagram the selection of polymer, compatibility between the layers and morphology of support membrane were predicted. In second step, PVA support membranes were fabricated using non-solvent induced phase separation (NIPS) process, which have the spongy morphology, accordingly as predicted. Which were then optimized using variation in two main parameters, polymeric concentration and coagulation residence time. In third step, a thin mixed matrix membrane (MMMs) based selective layer was coated on the skin layer of PVA asymmetric membranes, having thickness of 7.06 μm forming a multi-layer composite (MLC) membrane. This MMMs layer was composed of CA/PEG blend with incorporated ZIF-8 particles. Through different characterization, the influence of membrane thickness and PEG addition with respect to gas permeance and mechanical properties were analyzed. In which SEM, XRD, FT-IR and UTM were used to study the morphology, chemical structure, presence of different functional groups and membrane mechanical properties respectively. In gas permeation test, it revealed that by reducing thickness of membrane up-to 7.06 μm and addition of PEG, resulted in maximum O_2 gas permeance up-to 0.75 GPU at 2 bar. Which concludes that, by reducing membrane thickness and addition of plasticizer, increases the gas permeance.

Keywords: Composite Membranes; Oxygen enrichment; Air Separation; O_2/N_2 Separation; Optimization Analysis; Multi-layer composite membrane (MLCM); Blood Oxygenator Membrane.

Table of Contents

List of Figures

List of Tables

Nomenclature

DLC	Dual layer composite	mPDA	mphenylenediamine
GS	Gas separation	HoP	Hot pressing method
PSA	Pressure swing adsorption process	MMMs	Mixed matrix membranes
CVD	Chemical vapor deposition	CD	Cryogenic Distillation
PI	Polyimide	PVC	Polyvinylchloride
PVP	Polyvinylpyrrolidene	FT-IR	Fourier Transform Infrared
SEM	Scanning electron microscopy	PAN	Polyacrylonitrile
PVDF	Polyvinyldiene fluoride	PES	Polyethersulfone
CNT	Carbon nano-tube	PC	Polymer Concentration
ZIF	Zeolitic imidazolate frame work	CNT	Carbon nano-tube
XSBR	Styrene-butadiene carboxylated latexes	CRT	Coagulation residence Time
CMS	Carbon molecular sieves	PDMS	Polydimethylsiloxane
LS	Loeb-Sourirajan	PEG	Poly ethylene glycol
CC	Cynanuric chloride	CA	Cellulose acetate
TMC	Trimesoylchloride	NIPS	Non-solvent induced Phase separation
PIP	Piperazine	M.W	Molecular Weight
mPD	m-phenylenediamine	K.D	Kinetic Diameter
TFC	Thin-film composite	DETA	Di-ethlyenetriemine
MBGS	Membrane based gas separation	PI	Polyimide

Chapter 1 - Introduction

1.1 Air Separation Background

Over the past few decades, air separation, for the purpose of enrichment of oxygen (O_2) and nitrogen (N_2) has gained quite a substantial value in the commercial process industries. As air is the main source of both oxygen (O_2) and nitrogen (N_2) as mentioned in Table 1.1, it consists of 20.95 % of O_2 and 78.09 % of N_2. Whereas, remaining 0.96 % comprises of other gaseous mixture. The purpose for its enrichment is that the O_2 gas has many application in chemical industries and medical sectors. In chemical industries, O_2 gas is utilized in oxidation process in different chemical processes such as gasification and natural gas purification, coal fired combustion engine and industrial furnace [1-3]. Aside from these application, it has been used waste water treatment process [4]. In medical application, enrichment of O_2 gas has also got extensive importance. As it is well known that O_2 gas has been used in various medical treatment and therapy such as, oxygen therapy for the treatment of toxicity in blood (e.g. carbon monoxide toxicity reduction) [5], other than this it is used in the treatment of novel corona virus (COVID-19) [6], open heart surgeries and lungs transplantation [3, 7, 8]. The nitrogen (N_2) gas can also be used in variety of applications such as in food industries, pharmaceutical and chemical industries like packaging, medicine and fertilizer production process [9]. Therefore a wide range of conventional methods have been used for the applications of gas separation, which are pressure swing adsorption (PSA), absorption and cryogenic distillation process unit. Through PSA process 20-100 tons/day of O_2 gas can be produced having purity of 92 %. Whereas, through cryogenic method 100 tons/day with 99% of purity of oxygen can be produced [10].

1.2 Comparison between membrane technology and conventional technology

These conventional technologies have numbers of drawbacks such as these process are highly energy intensive process, required large area (large footprint) and difficult to scale-up due to its high cost of unit. Whereas, since 1970, Membrane based separation for air (O_2/N_2) separation had attracted attention in both academia research and industrial sector

[11, 12]. The membrane technology has numerous advantages over the conventional technologies for gas separation in industrial sector, which are mentioned below [9, 13]:

(1) It required no complex instrumentation to install the process.

(2) Gas separation (GS) is carried out continuously.

(3) Energy consumption is lower as compared to conventional technologies.

(4) Membrane technology can easily be combined with other separation technologies to form a hybrid technology for GS application.

(5) It can be easily scale-up.

(6) Required no mass transfer agent or additive for the separation process.

(7) Membrane technology has greater flexibility in adjusting variable and designing system.

(8) It's a clean technology with operational ease, also considered as one of the green technology system.

Table 1.1 - Unpolluted dry air composition by volume with K.D and M.W

Gases	Percentage or volume (ppm)	Kinetic Diameter (Å)	Molecular Weight	REF #
Nitrogen	78.084 %	3.64	28	[14, 15]
Oxygen	20.946 %	3.46	32	[14, 15]
Argon	0.934 %	3.40	40	[14, 16]
Carbon dioxide	360 ppm (variable)	3.30	44	[14, 15]
Neon	18.18 ppm	2.75	20	[14, 16]
Helium	5.24 ppm	2.60	4	[14, 17]
Methane	1.6 ppm	3.80	16	[14, 15]
Krypton	1.14 ppm	3.60	84	[14, 16]
Hydrogen	0.5 ppm	2.89	2	[14, 15]
Nitrous Oxide	0.3 ppm	3.30	44	[14, 17]
Xenon	0.087 ppm	3.96	131	[14, 16]

1.3 Membrane Technology

Membrane is a perm-selective barrier between two phases, which has the capability to separate the feed stream into retentate and product streams through a certain driving force gradient. The driving force can be concentration, pressure, temperature and electrical potential gradients between the species of the feed gas stream. The membrane GS process is depicted in Figure 1.1. Which represents that, the binary gaseous mixture stream is separated through membrane into two stream, (a) product stream consist of component A, enriched O_2 stream gas and (b) remaining retentate stream with component B, enriched with N_2 gas.

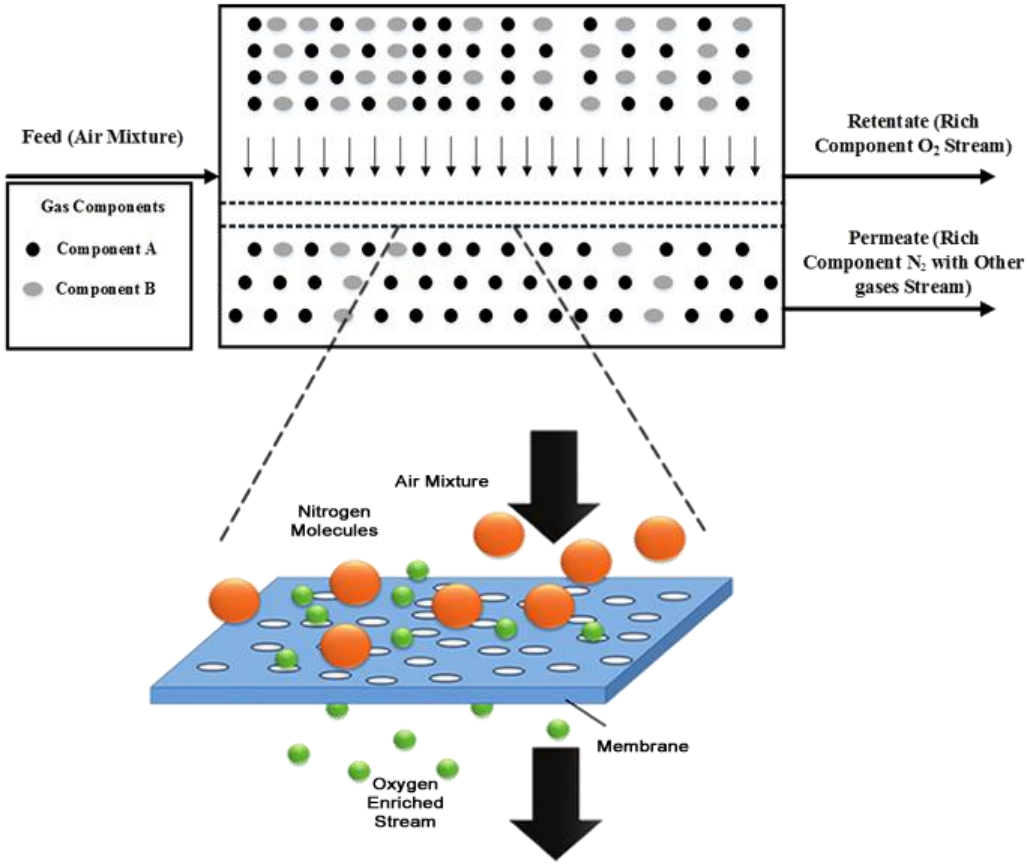

Figure 1.1. MBGS system diagram for air (O_2/N_2) separation

The following is the schematic diagram of membrane classification on the basis of nature, structure, transport mechanism and geometrical configuration.

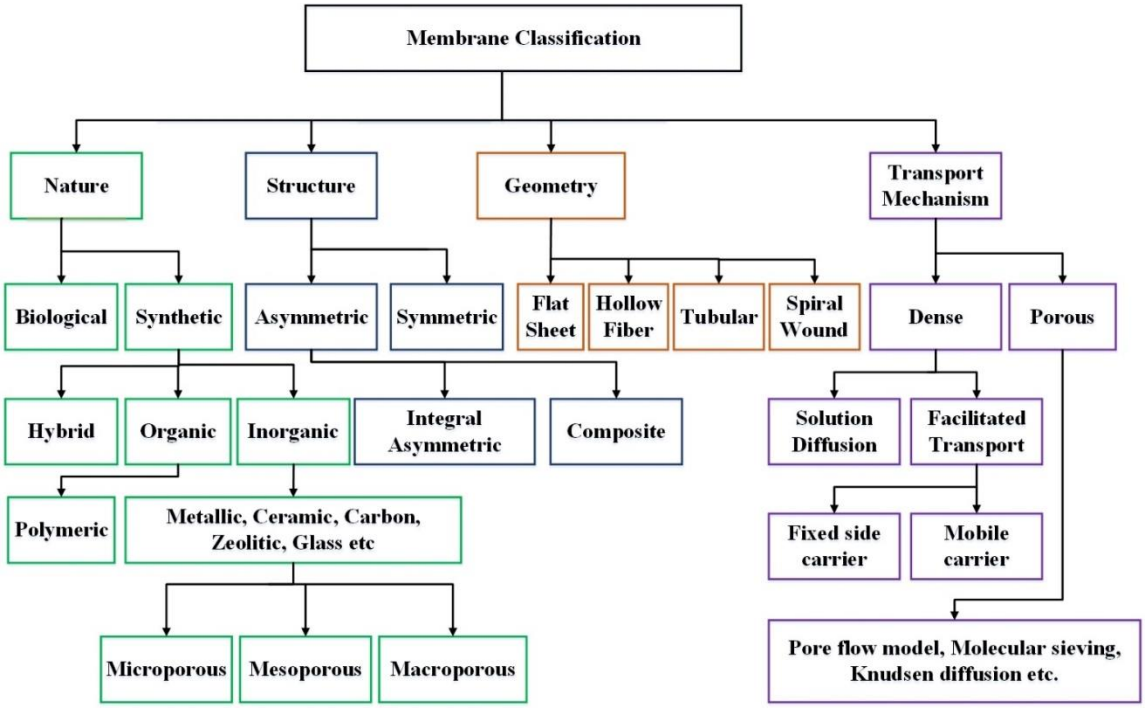

Figure 1.2. Membrane classification schematic diagram

1.4 Composite Membranes

Composite membrane have the structure similar to asymmetric membrane, which consist of one or more layer on top of porous support composed of different materials. The top thin dense layer act as selective layer, helps in separating gas mixture components. Whereas the bottom porous layer act as mechanical support provides negligible resistance towards the gas transport. These membrane are preferred and used in various commercial GS application. Due to this structural arrangement, these membrane are highly selective towards components of gas mixture with high permeate flux at bearable high pressure range. As compared to asymmetric membrane, composite membrane, shows numerous advantages, such as (a) independent selection of materials for each layer (e.g. selective layer and porous support layer) are possible. (b) Both selective and porous layer can be independently prepared and then combined together. (c) As only thin selective layer, is require on top of porous support in composite membrane, due to this reason expensive materials for the selective layer can be use in less quantity [18]. Composite membrane consist of two or more layers, dual-layer composite (DLC) membrane consist of two

layers as illustrated in Figure 1.3 (a), However to enhance its lifespan, protective layer are also applied on top of selective layer as illustrated in Figure 1.3 (b).

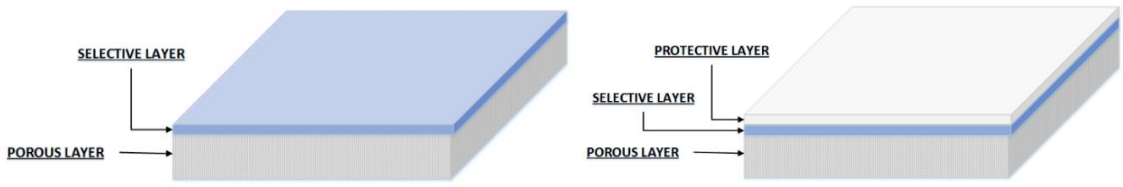

(a) (b)

Figure 1.3. Composite membrane types (a) DLC membrane, (b) DLC membrane with protective layer

1.4.1 Dense Membrane (Selective Layer)

Dense selective membranes follows solution diffusion model, which relies on Fick's law of diffusion. The driving force of gas molecules transport is due to concentration gradient through the membrane. In composite membrane, dense selective layer can be composed of one or more than one polymer with addition of nano-particles. Which includes MOFs, COFs, ZIFs, Zeolites, magnetic particles and MWCNTs etc. Gas permeability of membrane depends on two main factors, which are diffusion and sorption coefficient. Whereas, diffusion of gas molecules through a dense layer also depends on the thickness of membrane. Gas permeation rate can be increased by reducing the thickness of membrane. But the major problem is that, by the reducing its thickness, the membrane become fragile. This issue can be overcome, by using a porous mechanical support in composite membrane. Through which, the membrane shows, durability and high perm-selective nature in MBGS process [9, 19, 20].

1.4.2 Porous Membrane (Support Layer)

In a composite membrane, porous support layer provides mechanical support to the selective thin dense layer, which shows negligible resistance towards the gas transport and follows pore flow model as represented in Figure 1.4. These membranes are generally fabricated from the phase inversion method proposed by Loeb-Sourirajan (LS), which involves immersion precipitation of polymeric solution in a coagulation bath. This technique is also called as non-solvent induced phase separation - NIPS method for the preparation of anisotropic porous membrane. However, some porous support membrane

may have a thin dense top layer, that doesn't consist of any pores. In this scenario, the support layer materials also contributes to the gas selectivity nature of the membrane separation process. Which depends on the properties of the materials and thickness of asymmetric membrane skin layer.

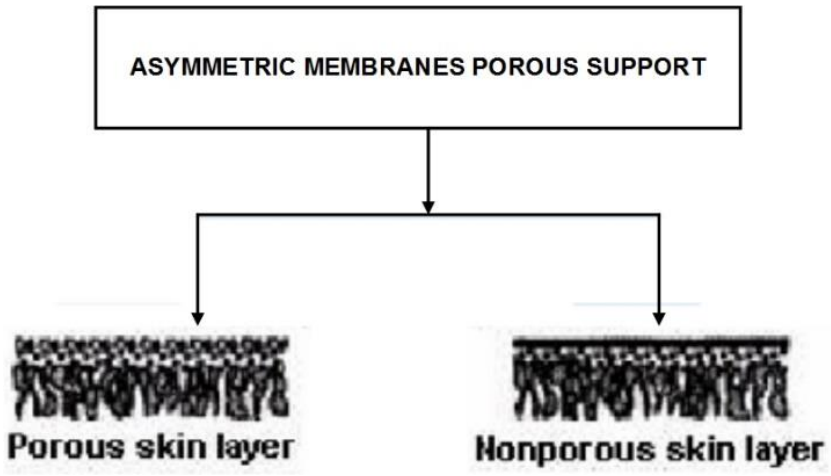

Figure 1.4. Types of Asymmetric structure polymeric porous support membranes

Although, there are other method for the fabrication of support layer. These method includes, Porogen addition, Track-etch and expanded film method. But through these methods, isotropic (symmetric) porous membrane are fabricated [9, 19, 20].

1.4.3 Protective Layer (Additional Layer)

In composite membrane, additional layer made of different polymer (e.g. Pebax polymer) are usually applied on top of selective dense layer. Which protects the soft surface selective layer of the membrane from being damaged during the handling of membrane and module fabrication process, e.g. fabrication of membrane module having high packing density and plug the defective area of surface [9, 20-22].

1.5 Composite membrane criteria for GS applications

The selection of material for the composite membrane for GS process relies on its physical and chemical properties of materials, since these material are used to fabricate into composite membrane for the GS applications. In order to separate gas mixture, composite membrane should possess number of properties, which are mentioned below [23].

- The selective layer should have high selectivity towards the required component of gas mixture.
- The composite membrane should have good adhesion and compatibility between layers.
- High permeability/flux towards the selected component of the gas mixture stream.
- It should be thermally and chemically stable.
- Having long shelf life.
- Fouling resistance.
- Higher mechanical strength.
- Plasticization resistance.
- It should be cost effective (economically good).
- Should be able to cheaply produced and manufactured into various modules of membrane.

1.6 Gas transport mechanism of composite membrane

A membrane separates a gaseous mixture components on the basis of difference in their permeability through the membrane materials. In-order to achieve higher performance MBGS, a greater difference between the permeability of both component i and j needs to be required. For that purpose, gas molecules physical and chemical properties as well as its interaction with membrane material needs to be considered. There are different mechanism of gas transport that can be employed in composite membrane. As by incorporating, nano-particles such as MOFs, COFs, ZIFs, MWCNTs, magnetic particles, silica etc. in polymer matrix, these membrane can exhibits the following mentioned mechanism.

1.6.1 Solution Diffusion

Dense selective membrane has no pores or channels for the transport of gas, it follow solution diffusion mechanism. There are three main steps occurred in this transport mechanism. (a) It absorbs a specific gas component of the mixture at higher pressure. (b) In second step, due to the concentration gradient, absorbed gas diffuses through the membrane. (c) At last step, the gas desorbs at the permeate side, under lower pressure. In

this mechanism, the gas components of the mixture separates on the basis of difference in their permeability through membrane [9, 20, 24].

1.6.2 Molecular Sieving Effects

In this mechanism, the separation of gas components takes place due to difference in their kinetic diameter (K.D) as mentioned in Table 1.1. By incorporating different nano-particles in dense polymeric membrane, the selective layer can also exhibits molecular sieving effects with the combination of solution diffusion mechanism. As different nano-particles, such as (MOFs, COFs, MWCNTs, etc.) have different sizes of pore aperture, which acts as molecular sieve towards the gas components of mixture [9, 20, 25-27].

1.6.3 Facilitated Transport

This mechanism of gas transport also works with the combination of solution diffusion in composite membrane. In this mechanism, the gas components of the mixture is separated, by forming a complexes through temporary bonding with carrier. These complexes, then diffuses across the membrane, due to the concentration gradient. Afterwards, complexes undergoes through reversible reaction, which releases gas component at the permeate side under lower pressure [9, 28-30].

1.6.4 Factors affecting MBGS in dense selective layer

Membrane act as a selective barrier towards the species present in gaseous mixture. Which represents the separation of air (O_2/N_2) through a composite membrane. The gas separation performance relies on the Fick's law. The product stream is enriched with desired gas component such as O_2 gas, whereas retentate stream is enriched with remaining (undesired gas) components of the mixture such as N_2 gas. There are two main factors, that represents the performance of membrane (i) permeability of desired gas component (P_{ij}), (ii) Selectivity (α_{ij}) of gas components passes through membrane as represented in below mentioned mathematical equations.

$$P_i = \frac{Q\Delta L}{A\Delta P} \qquad \text{Eq (1.1)}$$

$$P = S \times D \qquad \text{Eq (1.2)}$$

$$\alpha_{i/j} = \frac{P(i)}{P(j)} \qquad \text{Eq (1.3)}$$

Where Q = Flowrate of permeate gas. A = Area of membrane, ΔL = membrane thickness. ΔP = pressure difference, P_i = permeability of desired component. P_j = permeability of undesired component and its unit is Barrer = 10^{-10} (cm^3. (STP).cm/cm^2.s.cmHg). Whereas, in thermodynamics term permeability is the product of solubility (S) and diffusivity (D) of the gas permeate through membrane. The selectivity (α) term defines, the affinity of membrane towards the gas components of mixture. In mathematical term, it is a ratio between the permeability of binary gas components. However, in some cases permeance is used to express the ability of a gas to permeate through a membrane having a specific thickness. It's unit is GPU = 10^{-6} (cm^3 (STP)/cm^2.s.cmHg) [9, 20].

1.7 Composite Membrane Fabrication Methodologies

Composite membranes generally fabricated by deposition of a thin top dense layer on a porous sub-layer, composed of different materials. During past years, many methods have been developed for fabricating defect free composite membrane such as solution casting, dip coating, spin coating, interfacial polymerization, and chemical vapor deposition (CVD).

1.7.1 Solution casting

Solution casting is one of the most commonly used method for the fabrication of composite membrane in lab scale. In this technique, an automatic or manual membrane caster consist of doctor blade, is generally used to apply coating on the surface of porous support membrane. The thickness of coated layer is control by adjusting distance between the doctor blade and porous substrate. The selective layer thickness can be controlled below 10 μm, but practically fabricating thickness below 1μm is quite challenging task [9, 20].

1.7.2 Dip coating

Dip coating method is simplest method for the fabrication of composite membrane. In which, selective layer is deposited by dipping the porous support layer in the polymer solution for some time and then lifting at a controlled speed. The main parameter to control the thickness of coating are as mentioned below:

- Polymeric solution concentration.
- Dipping time.
- The speed for the withdrawal of porous support.
- Evaporation rate and environmental impact.

On the basis of these parameter several predictive mathematical models have been developed to predict the coated layer thickness such as Landau and Levich model equation as mentioned below

$$h = c * \frac{(\eta U)^{2/3}}{\gamma^{1/6}(\rho g)^{1/2}} \qquad \text{Eq (1.4)}$$

In which h is the coating thickness, c is a constant (0.944 for Newtonain liquids), η denoted as the liquid viscosity, U is the speed of withdrawal, whereas γ is the surface tension of liquid against air and ρ is the liquid density. However, through this method, the coated layer thickness can be fabricated below 5 μm [19, 31].

1.7.3 Interfacial Polymerization

Interfacial polymerization, is another method for the fabrication of composite membrane, proposed by John Cadotte, which is further developed by North Star Research. In this method a porous support layer is dipped in a reactive coating solution in-order to deposit it, in the pores of porous layer. This coated support layer was then immersed in a reactant bath for some time, forming highly crosslinked selective layer on the surface of porous substrate. At the end, heat treatment is often applied in-order to complete the fabrication process. Through this method, the dense layer thickness, can be achievable up-to a range of 0.1 μm or less. This type of membrane showed high selectivity and high permeability due to its thinner selective layer and highly crosslinked material on the surface of porous substrate. However, the selectivity of membrane depends on the nature of material used in the fabrication of composite membrane. Aside from the GS application, this technique has also used for the fabrication of reverse osmosis (RO) membranes, which showed higher permeation flux and salt rejection as compared to commercially prepared RO membranes [9]. The major problem in the composite membrane prepared through this method is less crosslinked hydrogel formation in the pores of support membrane. When

dried, it becomes rigid and adds resistance towards the gas transport but in case of RO, this layer stayed hydrated during the process, which offers less resistance towards the water flux. This problem of less crosslinked hydrogel formation can be prevented by adding a gutter layer on the porous support before immersion of porous support in the reactive material solution [9, 32].

1.7.4 Spin-coating

Spin-coating is a film coating method, which is widely used for the fabrication of composite membrane. The device used for this process is called spin-coater. In this method a thin uniform coated layer is produced by spreading polymeric solution onto a rotating porous substrate through centrifugal forces. Whereas the solvent evaporation during this process is highly depended on the nature, properties and speed of spinning. As evaporation process is accelerated by air flow induced mechanism through high rotation speed. Due to this reason, the film solidified within a minute during the spin coating process. In industries, spin-coating method is usually used for the manufacturing of advanced electronic devices. The coating layer thickness can be controlled by changing the rotation speed and concentration of polymeric solution [33].

1.7.5 Chemical Vapor Deposition

Chemical vapor deposition (CVD) is a film deposition technique, in which through chemical treatment, vapors of materials are deposited on the surface of substrate [34]. The film deposition can be controlled through changing the parameters of chemical reaction. Which includes materials of substrates, temperature, total pressure applied, flow rate and composition of gas mixture used for reaction etc. [35]. CVD can also be used for material deposition process that are insoluble in nature. Another advantages of this method is that, it can be used for surface modification of substrate, such as narrowing the pore size by deposition of material on the surface of porous substrate [36-38].

1.7.6 Post-treatment

After fabrication of composite membrane, post treatment are required in most cases, which could leads to the high GS performance. Generally, many researcher used various techniques for the post treatment such as high temperature oven drying for few hours after freshly fabricated composite membrane, which remove residual solvent present in membranes [39-42].

1.8 Motivation

Air is the main source of both oxygen (O_2) and nitrogen (N_2) gas. Both these gases are used in different industrial and medical applications. Therefore it's imperative to separate O_2 and N_2 gas from air mixture. For that purpose, a cost effective separation process is required. Since composite membrane technology is considered as one of the most innovative technology in 21st century due to its remarkable characteristics and has fewer requirements in terms of cost, energy and maintenance. Which gives us motivation to explore this area further, in-order to make it more feasible at industrial scale for O_2/N_2 separation.

1.9 Aim of Research

The aim of this work is to, initially fabricate and optimized PVA based porous support through NIPS method. Afterwards, synthesized a mixed matrix based composite membrane, having active layer composed of Cellulose acetate (CA) and Polyethylene Glycol (PEG) blend incorporated with ZIF-8 as filler. Then characterized it using various analytical techniques, such as SEM, Gas permeation, FT-IR, XRD and mechanical testing in-order to investigate the morphology of composite membrane, O_2/N_2 gas separation performance, chemical structure, crystallinity and their mechanical properties accordingly.

1.10 Outlines of the Thesis

1st Chapter comprises, the introduction of air separation (O_2/N_2), convectional technology for air separation and its comparison with membrane technology, introduction to membrane technology, membrane classification, composite membrane and its components. The different gas transport mechanism of composite membrane and factors that affects the gas transport behaviour, state-of-the-art fabrication methodologies of composite membrane, motivation and objective of this research work are also included.

2nd Chapter comprises, the literature review of different dense, asymmetric and composite membrane material for O_2/N_2 separation. Additive in active layer such as incorporated nano-particle, active layer thickness, support layer thickness, fabrication methods of composite membrane, characterization, module/configuration, operating conditions and their GS properties are also included.

3rd Chapter summarizes theoretical solubility analysis of different solvents with the selected polymer, in-order to predict and ensure the compatibility between multiple layers of composite membrane.

4th Chapter summarizes materials selection, experimental techniques used to synthesize the composite membranes, and details of characterization techniques in-order to evaluate its properties.

5th Chapter comprises, results and discussion of data obtained from different characterization techniques utilized to evaluate quantitatively and qualitatively all fabricated membranes.

Lastly, we conclude the entire work followed by list of recommendations for future research work.

Chapter 2 – Literature Review

2.1 Membrane Technology for O_2/N_2 separation

Throughout the years, different membranes were produced for air separation (O_2/N_2) separation. As air is the main source of both oxygen (O_2) and nitrogen (N_2) gas as mentioned in Table 1.1, it consists of 20.95 % of O_2, 78.09 % N_2 and remaining 0.96 % comprises of other gaseous mixture [14]. For its separation, membrane technology is considered as one of the innovative green technology. These membranes includes pure polymer based membranes, polymer blend membranes, mixed matrix membranes (MMMs), composite membranes and facilitated transport membranes.

2.2 Polymeric membranes

Since 1970, polymeric membrane have been used for air (O_2/N_2) separation. These membranes have several economic benefits such as, ease of material availability, light weight, low cost, state-of-the-art membrane fabrication process and high selective nature. The performance of membrane depends on the nature of polymeric material used. On the basis of glass transition temperature (T_g), the polymeric materials are classified into two main types, glassy polymer and rubbery polymer.

2.2.1 Glassy Polymers

Glassy polymers have glass transition temperature (T_g), higher than the room temperature. These polymers showed high gas selectivity and low permeability as compared to rubbery polymers due to its tough and rigid structure. As gas permeation in polymers depends on the mobility of chain and free volume. These polymer possessed structure, that have steric hindrance around the main chain, which prohibits the rotation of segments around the main chain of the polymer [9, 20, 43]. However, glassy polymer have high gas permeability, possessed rigid and twisted backbone of macromolecules, which provides micro voids for the gas permeation such as in perfluropolymer, PIMS (polymers of intrinsic micro porosity) and some polyimides [44, 45].

Some of the glassy polymers that are used for the commercial scale fabrication of membranes are Cellulose acetate (CA), Polysulfone (PSF), Polyamide (PA), Polyetherimide (PEI) and Poly (propylene oxide) (PPO) as mentioned in Table 2.1.

Table 2.1 - GS Characteristics of glassy polymers for O_2/N_2 separation

Polymers	P(O_2) (Barrer)	$\alpha_{O2/N2}$	REF#
Cellulose Acetate (CA)	0.79	5.9	[46]
Cellulose Nitrate (CN)	1.95	16.8	[46]
Ethylene Cellulose (EC)	14.7	3.32	[46]
Polyvinyl Alcohol (PVA)	0.03	3.33	[47]
Poly propylene oxide (PPO)	16.8	4.4	[48]
Poly sulfone (PSF)	1.5	5.8	[49]
Poly amide (PA)	3.1	6.7	[50]
Polyetherimide (PEI)	0.4	8.2	[24]
Polycarbonate (PC)	1.5	5.8	[24]
Polymers of intrinsic micro porosity (PIM-1)	370	4	[45]
Polymers of intrinsic micro porosity (PIM-7)	190	4.5	[45]

2.2.2 Rubbery Polymers

Rubbery polymers have glass transition temperature (T_g), lower than room temperature (RT). In structure of these polymers, the segments of the polymer chain, can freely rotates around the main chain axis. Which makes them elastic and soft. Due to these characteristics, rubbery polymers like Polydimethylsiloxane (PDMS) and Poly (1-(tri-methylsilyl)-1 propyene) (PTMSP), showed higher permeability of gas as represented in Table 2.2. However, they have lower O_2/N_2 selectivity as compared to glassy polymer.

This might be due to the free volume present in the polymeric chain (-$(CH_3)_2$ SiO-) and flexibility of siloxane group (-SiO-).

Table 2.2 - GS Characteristics of rubbery polymers for O_2/N_2 separation

Polymers	P(O_2) (Barrer)	$\alpha_{O2/N2}$	REF#
PDMS	800	2.00	[51]
PTMSP	8800	1.375	[52]

2.3 Polymer Blends

Polymer blends is a combination of two or more polymers. In-order to combine their properties in the resultant membrane, the blending of polymers is done by mixing one polymer into other polymer in certain proportions. There are three types of blending of polymers (1) miscible polymer blends, in which the polymer blends are in homogeneous form, having single glass transition temperature (T_g), (2) Compatible polymer blends are miscible blends in a certain composition range and temperature and (3) immiscible polymer blends are in heterogeneous form, having two glass transition temperature (T_g) [53-55]. The polymeric blends, which have been studied for O_2/N_2 separation by many researchers are mentioned in Table 2.3.

Table 2.3 – GS characteristics of polymer blends membrane for the O_2/N_2 separation

Polymers	P(O_2) (Barrer)	$\alpha_{O2/N2}$	REF#
PVP/EC (50/50)	3.10	5.90	[56]
PLA Blend (10/0)	0.36	6.22	[57]
PLA Blend (8/2)	0.31	6.67	[57]
PU/PVAc (80/20)	2.71	4.92	[58]
SBR/NR (50/50)	602	5.80	[59]

Li et al. [56] investigated blends of PVP (poly (4-vinylprimidine) with EC (ethylene cellulose) at variable PVP content of (0 – 100 wt. %). The membrane were prepared using solution casting method. Afterwards, the membranes were tested at pilot scale in-order to study the permeability of different gases including O_2/N_2 gas through PVP/EC blends. They found that, by increasing the content of PVP from (0 - 100 wt. %), the selectivity for O_2/N_2 gas separation increased. Whereas, the permeability of O_2 reduced. In the range of 50 – 60 wt. % of PVP, sudden increased in selectivity was observed, however the permeability of O_2 gas decreased. This sudden increment resulted due to the increase in volume on mixing of the different polymers solution.

Komatsuka et al. [57] investigated PLA (poly (lactic acid)) based blended polymeric membranes. The PLA blend (10/0) membrane showed O_2/N_2 selectivity of 6.22 and O_2 gas permeability of 3.34 Barrer. Whereas, the selectivity of PLA blend (8/2) showed, higher O_2/N_2 selectivity of 6.67 and permeability of O_2 is much lower as compared to (10/0) PLA blend, which was 0.33 Barrer. This increment of O_2/N_2 gas selectivity and decrement of O_2 gas permeability was due to the enhancement of crystallinity. Ghalei et al. [58] studied PU - poly (urethane) with PVAc - poly (vinyl acetate) polymeric blends for GS applications including O_2/N_2 separation. They found that, by increasing the contents of PVAc up-to 20 wt. %, the selectivity of O_2/N_2 increased, whereas the permeability of O_2 gas decreased. S.C. George et al. [59] studied blend of styrene-butadiene rubber (SBR) with natural rubber (NR) and investigated its O_2/N_2 gas separation properties, They observed that, SBR/NR (50/50) has optimum O_2/N_2 selectivity of 5.80 with O_2 gas permeability of 602 Barrer. This high permeation rate of O_2 gas is due to the rubbery polymer having rotating segment, which allowed high permeation rate of gas.

2.4 Asymmetric membranes

Asymmetric membrane consist of two layers skin layer on top of porous support. However, both layers of these membranes are composed of same polymeric materials. These membranes are commercially prepared through phase inversion method. There are four (4) different approaches for phase inversion method. Which includes (a) Non-solvent induced phase separation (NIPS) method. (b) Vapor induced phase separation (VIPS)

method. (c) Solvent induced phase separation (SIPS) method. (d) Temperature induced phase separation (TIPS) method. Asymmetric membranes are used in different commercial scale GS processes, due to its highly compact and durable structural design [60]. The polymeric asymmetric membranes for O_2/N_2 separation are mentioned in Table 2.4.

Table 2.4 – GS characteristics of polymeric Asymmetric membranes for the O_2/N_2 separation

Polymers	**Skin Layer Thickness**	**P(O_2)**	**$\alpha_{O2/N2}$**	**REF#**
Cellulose Acetate (CA)	-	4.41 (GPU)	2.62	[61]
Polyimide (PI)	2.6 μm	3.2×10^{-7} (cm^3 (STP) /cm^2.s.cm.Hg)	11.5	[62]
Polysulfone (PSF)	0.12 μm	8 – 18 (GPU)	4.7 – 5.9	[63]
PLA	-	0.34 (GPU)	1.03	[64]

F. Mohamed et al. [61] studied CA asymmetric membrane for O_2/N_2 gas separation by varying coagulation bath solvents. Through this study, they observed that by using combination of methanol and n-hexane, the O_2 permeance increased up-to 4.41 (GPU), with highest O_2/N_2 selectivity of 2.62. Whereas, H. Kawakami et al. [62] studied PI based asymmetric membrane for O_2/N_2 separation performance. Which showed that, the fabricated asymmetric membranes have the highest O_2/N_2 selectivity of 11.5 with O_2 gas permeance of 3.2×10^{-7} (cm^3 (STP)/cm^2.s.cm.Hg). Pesek et al. [63] studied polysulfone (PSF) based asymmetric membranes for the O_2/N_2 GS application. The fabricated membrane showed O_2/N_2 selectivity in the range of 4.7 – 5.9 with O_2 gas permeance of 8 – 18 (GPU).

Another researcher F. Mohammed [64], investigated PLA flat sheet asymmetric membranes of variable concentration (15 – 25 wt.%) for O_2/N_2 separation. The main

advantage of using these membranes in GS application is due to its bio-degradable nature. The fabricated membranes were tested on pilot scale for gas permeation properties at a pressure range of (5 – 11 bar). Through this, study they observed that, PLA asymmetric membrane at 15 wt. % showed the highest selectivity of 1.03 and O_2 gas permeance of 0.34 (GPU).

2.5 Mixed Matrix membranes

Mixed matrix membranes (MMMs) are composed of an inorganic or a hybrid material (inorganic – organic) in the form of nano or micro particles incorporated within polymeric matrix. In which usually polymer phase is the continuous phase, while additives are in the form of discrete phase. By combining the properties of both inorganic particles and polymeric materials, these membrane possessed high selectivity, permeability and mechanical properties. Due to these properties, MMMs membrane have the capability to cross Robeson upper bound curve [9, 65-68].

For the effective development of MMMs, some of the factors needs to be considered, which are mentioned as: (1) Selection of polymeric materials and fillers is the most important aspect. As filler interaction with polymer depends on shape, size and filler concentration that effects the MMMs GS performance [69, 70]. (2) Compatibility between the polymeric matrix and the filler should be ensured. As poor compatibility between polymeric matrix and the fillers leads to the poor GS performance. In-order to ensure its compatibility, different compatibilizers have been used. Which enhances the interaction between the polymer and filler [71, 72]. Other methods to resolve this problem are priming [73] and annealing method [74]. (3) Concentration of fillers in polymeric matrix should be optimum in-order to prevent agglomeration. As high loading of filler caused agglomeration. Which leads to the development of voids and gaps, causes reduction of GS performance. This problem can also be resolve by proper stirring, sonication of mixture of polymeric solution and filler. Another method is by using charged surfactants in the solution, can also reduce this issue [75]. Some of the MMMs membranes for O_2/N_2 separation are mentioned in Table 2.5.

Table 2.5 – GS characteristics of mixed matrix membrane (MMMs) for the O_2/N_2 separation

Polymers	Filler		Operating Conditions	$P(O_2)$ (Barrer)	$\alpha_{O2/N2}$	REF#
	Types	Loading (%)				
Cellulose Acetate (CA)	ZIF-8	2	P = 2.5 – 4 bar T = 25 °C	3.15	4.11	[76]
		3.5		3.19	5.33	
		5		3.36	9.58	
		8		4.64	2.89	
		11		4.10	1.62	
PSF	MIL-101	8	T = 25 °C	2.53	5.42	[77]
		16		4.11	6.02	
		24		5.25	5.42	
Matrimid	MOF-5	10	T = 35 °C P = 3 atm	2.30	8.40	[78]
		20		2.90	7.20	
		30		4.12	7.90	
PSF	CMS	10	-	3.53	5.13	[79]
		20		7.96	5.97	
		30		6.71	3.69	
		35		17.03	2.84	

S. Azam et al. [76], studied cellulose acetate (CA) mixed matrix membranes (MMMs) incorporated with ZIF-8 at variable filler loading of 2 – 11 wt. %. Which showed that, by adding ZIF-8 in cellulose acetate – CA polymer increased its selectivity up-to 4 times higher than the pristine CA polymer. Jeazet et al. [77], investigated the influence of MIL-101-Cr (water-stable) as a filler for O_2/N_2 gas separation. Different MMMs were fabricated at a filler loading between 8 – 24 %. They reported that, the permeability of O_2 gas was enhanced up-to 6 Barrer and also the highest O_2/N_2 selectivity of 6 was documented.

Perez et al. [78] also studied MMMs for O_2/N_2 separation. In this Matrimid membrane MOF-5 nano-crystals were incorporated with different filler loading between 10 – 30 wt. %. Through this investigation, they founds that, by increasing MOF-5 filler loading from 10 – 30 wt. %, the permeability of O_2 increased, while the selectivity of O_2/N_2 remains constant as compared to pure matrimid membrane.

Ismail et al. [79], fabricated polysulfone (PSF) MMMs, incorporated with carbon molecular sieves (CMS) at different loading of 10 – 35 wt. %. Which signifies that, by increasing filler loading, the selectivity also increased. Whereas, at 20 wt.% filler loading showed the most highest O_2/N_2 selectivity of 5.97 with O_2 permeability of 7.96 Barrer.

2.6 Composite Membranes

Composite membrane are composed of multiple layers, having top dense selective layer beneath the porous support layer. However, unlike asymmetric membrane both layers are composed of different materials. The GS were carried out through the selective layer, whereas porous membrane, only provides mechanical support to the thin top dense layer, having lower or negligible resistance towards the permeated gas components [80]. Some of the composite membranes for O_2/N_2 separation are mentioned in Table 2.6.

Recently Nikpour N. et al. [81], fabricated flat-sheet DLC membrane, in which active layer was based on mixed matrix membranes (MMMs), composed of Pebax-1657 incorporated with $BaFe_{12}O_{19}$ nano-particles. It was coated on a PES porous support layer by using solution casting method. The GS performance of these membranes showed, O_2/N_2 selectivity of 3.34 – 4.01 and O_2 gas permeance in range of 0.08233 – 0.06377

(GPU) at a magnetic field (H = 0.5 T) and temperature of 25 °C. K.C. Chong et al [82] developed a DLC hollow fiber membrane for oxygen enrichment through dip-coating method. Which consist of active layer of Poly (ether block amide) having thickness of 50 $\pm$ 4 μm. Whereas, the support layer is composed of PSF polymeric material. The membrane showed O_2/N_2 gas selectivity of 3.71 and O_2 gas permeance of 39.81 (GPU) at a pressure of 5 bar. However further studies on PEBAX polymer as coating material needed to be considered for the improvement of air (O_2/N_2) separation performance.

M. Salehi Maleh et al. [83], produced three different flat-sheet DLC membranes, using solution casting method. These membranes consist of a MMMs based active layers and porous support. In which, three nano-fillers, such as NaX, ZIF-8 and SiO_2 particles were incorporated in each Pebax 1657 polymer matrix (active layer) on top of PES support membrane. These DLC membranes showed, O_2/N_2 gas selectivity of 6.06, 3.85 and 3.52 respectively. Whereas, O_2 gas permeance of 2.87, 4.01, 3.17 (GPU) were observed respectively, at a temperature of 25 °C and pressure of 4 bar. Mohammad R.M et al. [84], fabricated a hollow fiber multi-layer composite (MLC) membrane, by applying PDMS coating having thickness of (11.85 – 11.17 μm) on recycled/used RO membranes, that were composed of PSF/Polyester layer by layer assembly. Dip-coating method was used to fabricate the coated hollow fiber. The MLC membranes, showed maximum O_2/N_2 gas selectivity of 5.92, having O_2 gas permeance of 0.7104 (GPU).

S.A. Habibiannejad et al. [85], investigated functionalized multi-wall carbon nanotubes (MWCNTs) for GS separation. In which blend of Pebax-1657 and MWCNTs (fillers) based selective layers were coated on the PES porous support membranes by using solution casting method. The MWCNTs prior to embedding in the polymer matrix, were functionalized with carboxylic, amine groups and Triton X-100 as a strong surfactant. The thickness of active layer and porous support membranes were 20 $\pm$ 5 μm and 50 $\pm$ 5 μm respectively. The maximum O_2/N_2 gas selectivity in the range of 2.5 – 6.5 was achieved by CNTX-100 and CNT – NH_3 DLC membranes. Which showed O_2 permeability in the range of 4.2 – 5 (Barrer) and 2.7 – 3.5 (Barrer) at a pressure range of 3 – 7 bar accordingly.

H. Nagar et al. [28], investigated air (O_2/N_2) separation through facilitated transport membrane. In which O_2 gas permeated through Pebax polymeric membrane incorporated

with cobalt (CoPc) complexes. In this investigation, thin film composite (TFC) membrane were fabricated by thin coating layer of Pebax-1657 incorporated with a cobalt (II) pthalocyannine (CoPc) compound on a ultra-porous support membrane, composed of PES. Effects of feed pressure and concentration of CoPc compound were also evaluated, which showed enhanced selectivity from 2.9 to 8.5 by increasing the concentration of CoPc loading from 0 – 1 wt. % at a constant pressure of 2 bar. Whereas at maximum selectivity, the O_2 gas permeance of 1.12 $\pm$ 0.108 (GPU) was observed.

Table 2.6 – GS characteristics of Composite membranes for the O_2/N_2 separation

Active Layer/ Thickness	**Support Layer/Thickness**	**Fabrication Method**	**Module**	**Operating Condition**	**P(O_2)**	**α (O_2/N_2)**	**REF #**
Pebax 1657 – $BaFe_{12}O_{19}$ 4 μm	PES (-)	Solution-casting	Flat sheet	H = 0.5 T at 25 °C P = 2 – 10 bar	0.08233 – 0.06377 (GPU)	3.34 – 4.01	[81]
Poly (ether block amide) 50 $\pm$ 4 μm	PSF (-)	Dip-coating Method	Hollow Fiber	P = 5 bar	39.81 (GPU)	3.71	[82]
Pebax 1657/NaX (-)	PES (-)	Solution casting	Flat sheet	T = 25 °C, P = 4 bar	2.87 (GPU)	6.06	[83]
Pebax 1657/ZIF 8 (-)	PES (-)	Solution casting	Flat sheet	T = 25 °C, P = 4 bar	4.01 (GPU)	3.85	
Pebax 1657/SiO_2 (-)	PES (-)	Solution casting	Flat sheet	T = 25 °C, P = 4 bar	3.17 (GPU)	3.52	
PDMS (11.85 – 11.17 μm)	PSF (-) + Polyester Layer (-)	Dip-coating	Hollow Fiber	P = 1 – 5 bar	0.7104 (GPU)	5.92	[84]
Pebax 1657 (20 $\pm$ 5 μm)	PES (50 $\pm$ 5 μm)	Solution Casting	Flat Sheet	P = 3 – 7 bar	3 (Barrer)	3.00	[85]

Pebax 1657 CNT – $COOH_4$ (20 ± 5 µm)	PES (50 ± 5 µm)	Solution Casting	Flat Sheet	P = 3 – 7 bar	2.8 – 3.5 (Barrer)	2.5 – 3.00	[85]
Pebax 1657 CNT – NH_2 (20 ± 5 µm)	PES (50 ± 5 µm)	Solution Casting	Flat Sheet	P = 3 – 7 bar	2.7 – 3.5 (Barrer)	3.00 – 6.5	[85]
Pebax 1657 CNTX 100 (20 ± 5 µm)	PES (50 ± 5 µm)	Solution Casting	Flat Sheet	P = 3 – 7 bar	4.2 - 5 (Barrer)	2.5 – 6.3	[85]
Pebax 1657 CNT-$COOH_6$ (20 ± 5 µm)	PES (50 ± 5 µm)	Solution Casting	Flat Sheet	P = 3 – 7 bar	1.5 (Barrer)	3 – 5	[85]
Pebax 1657 Cobalt (II) phthalocyanime (CoPc) – 0 % (-)	PES (-)	Solution Casting	Flat Sheet	P = 2 bar	0.06 ± 0.005 (GPU)	2.9	[28]
Pebax 1657 Cobalt (II) phthalocyanime (CoPc) – 0.01 % (-)	PES (-)	Solution Casting	Flat Sheet	P = 2 bar	0.16 ± 0.015 (GPU)	4.1	
Pebax 1657 Cobalt (II) phthalocyanime (CoPc) – 0.1 % (-)	PES (-)	Solution Casting	Flat Sheet	P = 2 bar	0.38 ± 0.028 (GPU)	6.3	
Pebax 1657 Cobalt (II) phthalocyanime (CoPc) – 0.5 % (-)	PES (-)	Solution Casting	Flat Sheet	P = 2 bar	0.73 ± 0.049 (GPU)	8.1	

Pebax 1657 Cobalt (II) phthalocyanime (CoPc) – 1 % (-)	PES (-)	Solution Casting	Flat Sheet	P = 2 bar	1.12 ± 0.108 (GPU)	8.5	
PDMS (0.2 μm)	PPy (-)	Interfacial Polymerization	Flat sheet	T = 35 °C	40.20 (Barrer)	17.20	[86]
T (p-OCH_3) PPCoCl (1 μm)	Pebax-2533 (100 μm)	Dip-coating method	Flat sheet	P = 0.35 - 8 bar T = 18 °C	6.3 – 12.2 (Barrer)	2.2 – 7.6	[87]

Son W-I et al. [86], also produced DLC membrane, which was composed of polypyrrole (PPy)/Polydimethylsiloxane (PDMS) and having active layer thickness of 0.2 μm. This investigation described polymerization behaviour, as due to slow polymerization the diameter of pores reduced from 4.89 Å to 3.67 Å, having closed value similar to kinetic diameter of nitrogen (N_2) gas. Which was the reason, the fabricated membrane showed a very high O_2/N_2 selectivity of 17.20. Whereas, O_2 gas permeability of 40.20 (Barrer) was obtained at a constant temperature of T = 25 °C. Similarly, J. Han et al. [87], studied highly selective O_2/N_2 separation membrane based on facilitated transport mechanism by using a porphyrin based O_2 carrier (T (p-OCH_3) PPCoCl). In this investigation, dip-coating method was used, in-order to coat 1 μm thickness of active layer on Pebax-2533 (100 μm) based flat sheet porous support membrane. The resulted membrane showed O_2/N_2 gas selectivity in the range of 2.2 – 7.6 with O_2 gas permeability of 6.3 – 12.3 (Barrer), at a pressure range of 0.35 – 8 bar and a constant temperature of T = 18 °C.

2.7 O_2/N_2 Gas Separation Robson Curves

Membrane gas separation process, depends on two main factors permeability and selectivity. Which relies on the membrane morphology, membrane thickness, gas pressure gradient and area of membrane. However, there is a tradeoff between the selectivity and permeability of membrane. This relationship was first plotted and described in 1991 by Robeson as represented in Figure 2.1. Also known as Robeson Plot. At the time of graph plotting, more than 300 literature data were found and plotted against permeability and selectivity, which developed Robeson upper bound served as a benchmark [88].

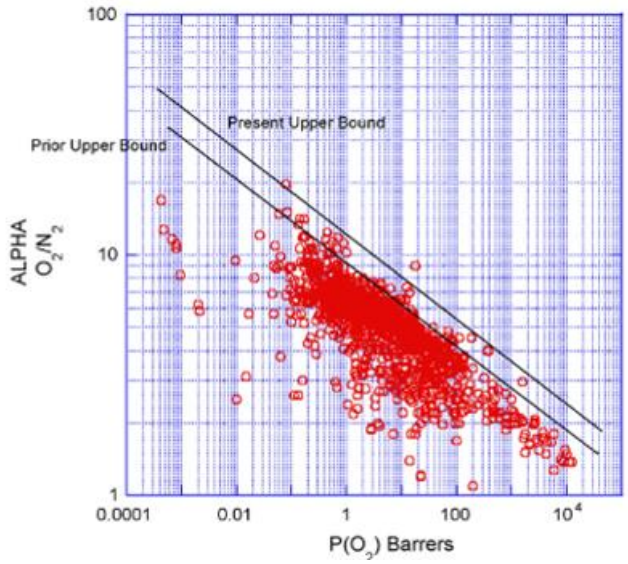

Figure 2.1. Robeson's Upper bound Curve (O_2/N_2)

For the past few years, due to intensive research on the GS process utilizing various types of membranes, the upper bound of Robeson plot has been revised in 2008. Which have been shifted upwards from the earlier bound of 1991, as shown in Figure 2.1. These modification in membrane were done through physical modification by adding fillers, chemical and surface modification by crosslinking it with functional groups. Membrane developed through addition of fillers are called as mixed matrix membranes (MMMs). Whereas, composites membrane are the combination of both thin selective layer (MMMs) and a porous support membrane. These membranes were known for their good perm-selective nature, mechanical strength, thermal and chemical resistive [88].

2.8 Literature Review Conclusion

2.8.1 Dense Layer Polymer Selection

According to literature survey, cellulose acetate (CA) polymer is selected as dense selective layer due to its glassy nature, high availability, environmental friendly, good performance and lower cost for the GS applications. In this polymer hydroxyl group are present in abundance. Which can be easily be activated by different process e.g. ligand coupling [48]. In this study, CA polymer has been used as main polymeric phase in MMMs based thin selective layer as shown in Figure 2.2.

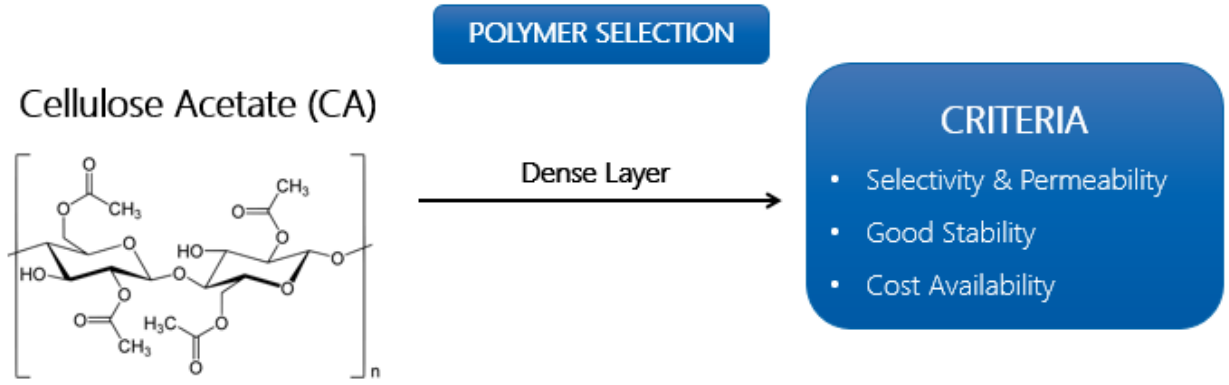

Figure 2.2. Dense Layer polymer selection: Cellulose acetate (CA) and Polymer selection criteria

2.8.2 Porous Support Polymer Selection

Poly vinyl alcohol (PVA) is considered as one of the inexpensive and environmental friendly green polymer, having variety of features such as it is well known for its high tensile strength, non-toxic, biodegradable, and bio-compatible nature as represented in Figure 2.3. Due to these qualities PVA is considered as a suitable polymer for the fabrication of porous support polymer [60].

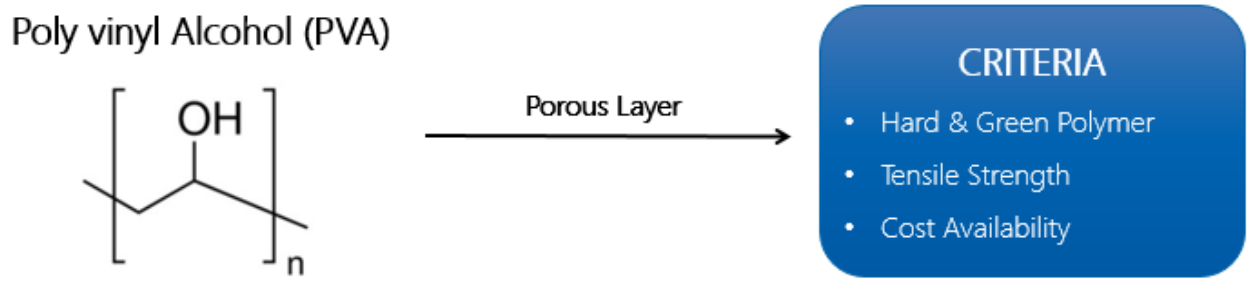

Figure 2.3. Porous Layer polymer selection: PVA polymer and Polymer selection criteria

2.8.3 Filler Selection

Metal organic framework (MOFs) are type of nano particles that can be used in dense layer to enhance the gas separation selectivity of membrane including for O_2/N_2 separation. Among different MOFs, Zeolite imidazolate framework (ZIFs) has excellent chemical and thermal stability, which can bear evaluated temperature up-to 400 ^oC and also have sieving property, tunable porosity and chemical functionality.

For O_2/N_2 separation ZIF-8, which has sodalite (SOD) topology shows most promising structure having pore aperture of 3.4 ^oA as shown in Figure 2.4. ZIF-8 consist of five membered imidazolate, which worked as a bridge between Zn (II) in the center and imparts angle of 145^o throughout the frameworks by coordinating N- atoms 1, 3-position of ring. The angle (145^o) made by metal-imidazolate-metal in ZIFs is similar to the bond angle made by Si-O-Si in many zeolites [76], as depicted in Figure 2.4.

The ZIFs also have the bonding capabilities with cellulose acetate (CA) and polyethylene glycol (PEG). However, PEG polymer was also added to enhance the flexibilities and mechanical strength of the membrane. Which acts as plasticizer in MMMs and also increases the permeability of gas due to the enhanced chain flexibility [89].

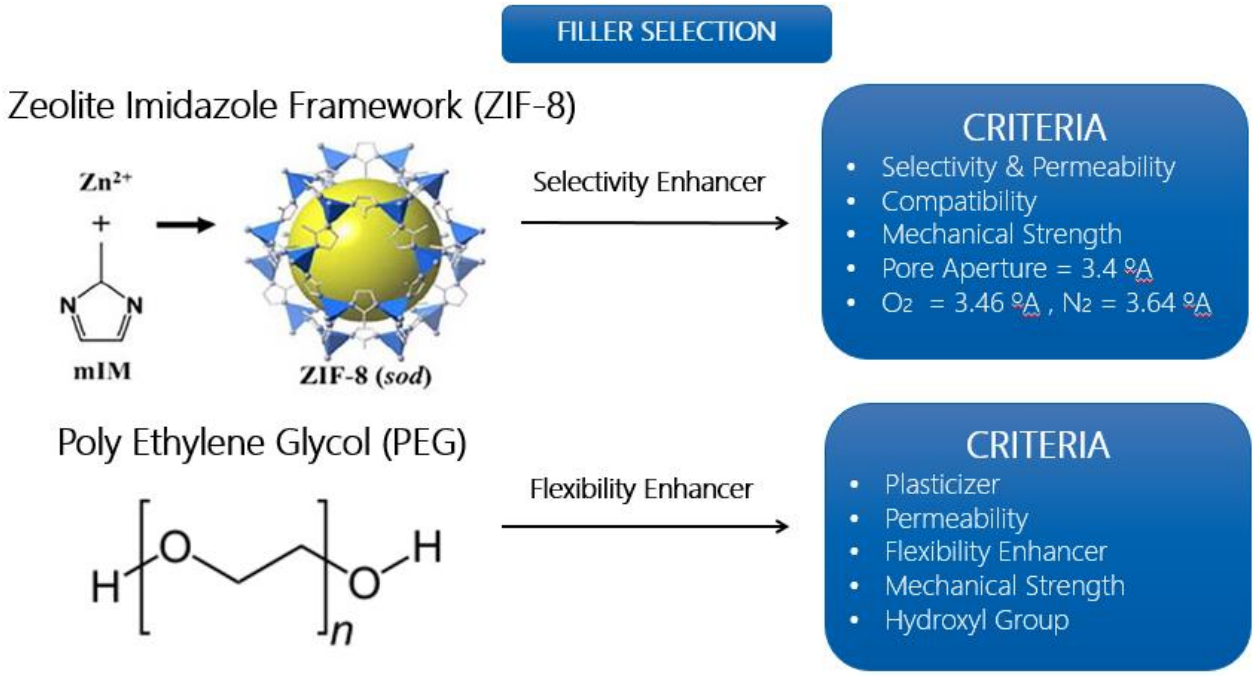

Figure 2.4. Filler selection: ZIF-8 and Poly ethylene glycol (PEG) selection criteria

Chapter 3 – Theoretical Solubility Model

3.1 Theoretical Solubility Analysis

The polymer solubility with various solvents can be predicted and estimated through Hansen solubility parameter (HSP) model. This model works on the basis of total cohesive energy, which further divided into three main parameters. Such as, dispersion force (δ_D) – atomic , polar bonding (δ_P) – molecular and hydrogen bonding (δ_H) – electron exchange as mentioned in equation 3.1 - 3.3. These cohesive energy is identical to liquid vaporizating energy also called as cohesive bond breaking energy [60, 90].

$$E = E_D + E_H + E_p \qquad \text{Eq (3.1)}$$

$$\frac{E}{V} = \frac{E_D}{V} + \frac{E_H}{V} + \frac{E_p}{V} \qquad \text{Eq (3.2)}$$

$$\delta_T = \delta D_D + \delta D_H + \delta D_P \qquad \text{Eq (3.3)}$$

In-order to determined the solubility distance (Ra) between the polymer and solvents, the following equation 3.4 was used

$$Ra = \sqrt{4\left(\delta D_s - \delta D_p\right)^2 + \left(\delta P_s - \delta P_p\right)^2 + \left(\delta H_s - \delta H_p\right)^2} \qquad \text{Eq (3.4)}$$

Where, the subscript of solvent and polymer is defined as S and P. In-order to determined the solubility likelihood between the polymer and solvents, the concept of Relative energy distance (RED) was introduced by C.M Hansen. Which can be calculated through following mentioned equation 3.5 [60, 90].

$$\text{RED} = \text{Ra}/\text{Ro} \qquad \text{Eq (3.5)}$$

Where Ra and Ro is the HSP distance and polymer solubility radius respectively. In HSP model, the solvent is considered to have good solubiliy with polymer if RED < 1. Whereas

if RED = 1, then solvent can caused swelling to the polymer. However, if RED > 1 the polymer is insoluble in solvent [60, 90].

Table 3.1 - Solubility Analysis between Polymer (PVA) and Solvents (THF & Water)

Parameter	PVA	THF	DIW	REF #
δ_D ($MP^{1/2}$)	15.00	16.80	18.10	[60, 90]
δ_P ($MP^{1/2}$)	17.20	5.70	17.10	[60, 90]
δ_H ($MP^{1/2}$)	17.80	8.00	16.90	[60, 90]
Ro	10.20	-	-	[60, 90]
Ra	-	15.53	7.62	[60]
RED	-	1.52	0.86	[60]

Table 3.2 - Solubility Analysis between Polymer (PEG) and Solvents (THF & Water)

Parameter	PEG	THF	DIW	REF #
δ_D ($MP^{1/2}$)	22.2	16.80	18.10	[90]
δ_P ($MP^{1/2}$)	11.2	5.70	17.10	[90]
δ_H ($MP^{1/2}$)	13.2	8.00	16.90	[90]
Ro	17	-	-	[90]
Ra	-	13.18	10.75	-
RED	-	0.775	0.632	-

Table 3.3 - Solubility Analysis between Polymer (CA) and Solvent (THF & Water)

Parameter	CA	THF	DIW	REF #
δ_D ($MP^{1/2}$)	14.90	16.80	18.10	[90]
δ_P ($MP^{1/2}$)	7.10	5.70	17.10	[90]
δ_H ($MP^{1/2}$)	11.1	8.00	16.90	[90]
Ro	12.4	-	-	[90]
Ra	-	5.10	13.21	-
RED	-	0.411	1.065	-

PVA* = Polyvinyl Alcohol, CA* = Cellulose Acetate, PEG* = Polyethylene Glycol,

THF* = Tetra-hydrofuran, DIW* = DI – Water (Total Solubility)*

3.2 Solubility Analysis Conclusion

The analysis data mentioned in Table 3.1 – 3.3 represented that, The RED between Tetrahydrofuran (THF) solvent with Cellulose acetate (CA) and Polyethylene glycol (PEG) polymer are 0.411 and 0.775 respectively. As these values are less than 1, so THF is considered as good solvent for the both polymer (CA & PEG). However, the RED value between THF and PVA is 1.52, which is greater than 1, represented insolubility.

By comparing the RED value of polymers with DI Water as solvent, both PVA and PEG polymer shows RED less than 1 having values of 0.86 and 0.63 respectively. Whereas, the RED value between CA and DI-Water is 1.065 greater than 1. This signifies that, DI-Water is a good solvent for both PVA and PEG polymer. However, CA polymer showed insolubility in DI-Water.

Through this analysis it can be concluded that, through PVA/Water/THF ternary system PVA asymmetric membrane can be developed. Whereas, CA/PEG – THF polymer solution can be casted on top of PVA support membrane for the fabrication of multi-layer composite membrane (MLCM) as THF showed insoubility towards the PVA polymer.

Chapter 4 – Materials and Experimental Methods

4.1 Materials Used

- Cellulose Acetate (CA) (Mw-50,000) from Sigma Aldrich, UK
- Tetrahydrofuran (THF) +99% Pure from Sigma Aldrich, UK
- Poly-Ethylene Glycol (PEG) (Mw-1000) from Sigma Aldrich, UK
- Poly vinyl Alcohol (PVA) (Mw-30000 – 70,000) (70 – 80 % Hydrolyzed) from Sigma Aldrich, UK
- Zeolitic Imidazolate Framework (ZIF-8) obtained from our own research group
- Deionized (DI) Water (Solvent) from Lab Care, Pakistan
- 99.9% Oxygen (O_2) gas from Linde, Pakistan
- 99.5% Nitrogen (N_2) gas from Linde, Pakistan

4.2 Synthesis of Support Membrane

PVA asymmetric membrane was used as support layer for composite membrane. These membranes were prepared using non-solvent induced phase separation (NIPS) method. PVA asymmetric membrane was optimized on the basis of two different parameters (a). Polymer Concentration (b). Coagulation residence time.

4.2.1. Optimization Study: PVA polymer concentration (PC)

The PVA solutions were prepared by dissolving PVA polymer having different concentration of 10, 12 and 14 wt. % in 10 ml de-ionized water (DI-Water) as mentioned in Table 4.1 and represented in Figure 4.1. The solutions were continuously stirred for 2 hours at constant temperature of 60 - 75 ^{o}C and then degassed for 1 hours, in-order to remove the trapped bubbles. Afterwards these solution were casted on a glass plate using automatic casting machine and then immersed in the THF coagulation bath. As thickness of membrane depends on the viscosity of solution, so variable viscosity of PVA solution were casted on a glass slab. The coagulation bath was covered with aluminum foil to prevent THF evaporation and placed in vacuum oven for 3 hours at 20 °C. Afterwards these membranes were dried for 3 – 5 hours at room temperature and then qualitatively

analyzed using different characterization techniques in-order to select the optimized concentration of PVA asymmetric membrane as support membrane for GS applications. These analytical techniques include, scanning electron microscopy (SEM), gravimetric porosity and mechanical testing (e.g. tensile testing and elongation at break percent).

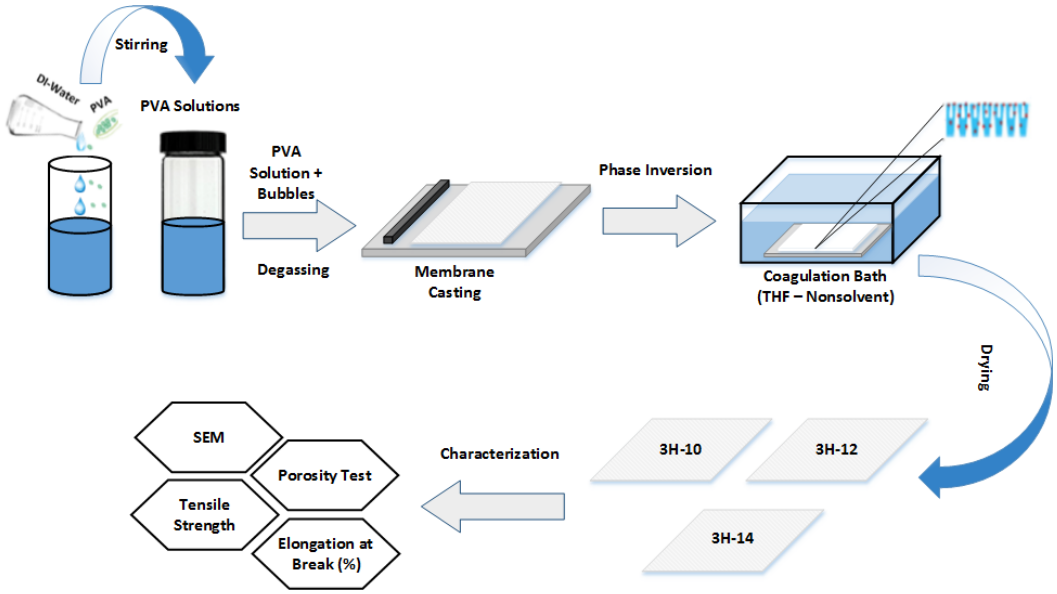

Figure 4.1. PVA Asymmetric membrane preparation at different concentration using NIPS method

4.2.2. Optimization Study: Coagulation Residence Time (CRT)

After optimization of polymer concentration of PVA asymmetric membrane, the effects of coagulation residence time was also investigated in this study. For that purpose, PVA solution having constant concentration of 12 wt. %, was prepared and casted on five (5) glass plates through automatic membrane casting machine as mentioned in Table 4.1 and represented in Figure 4.2. Which were then immersed in THF coagulation bath, covered with aluminum foil and were placed in vacuum oven at different coagulation residence from 3 to 24 hours and at a temperature of 20 °C. Afterwards asymmetric membranes were dried for 3 – 5 hours at room temperature. Then these membranes were qualitatively analyzed using different characterization techniques in-order to select the optimized coagulation residence time for the preparation of PVA asymmetric membranes. The optimized PVA asymmetric membrane was used as support layer for the preparation of composite membrane. The analytical techniques include, scanning electron microscopy

(SEM), gravimetric porosity, gas permeation test, X-Ray diffraction (XRD), Fourier transform infrared (FT-IR) spectroscopy and mechanical testing (e.g. tensile testing and elongation at break percent).

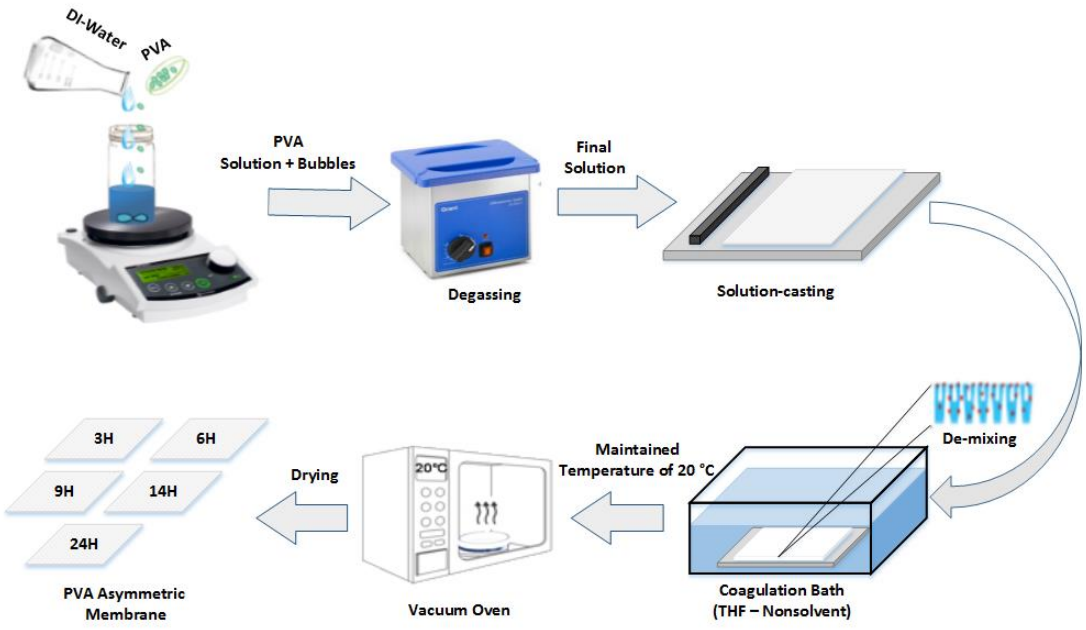

Figure 4.2. PVA Asymmetric membrane preparation at different CRT using NIPS method

Table 4.1 - PVA Asymmetric membrane composition and nomenclature table

Polymer	DI Water (ml)	Concentration (wt. %)	Coagulation Residence Time (h)	Nomenclature
PVA	10	10	3	PVA 3H-10
PVA	10	12	3	PVA 3H-12
PVA	10	14	3	PVA 3H-14
PVA	10	12	3	PVA 3H-12
PVA	10	12	6	PVA 6H-12
PVA	10	12	9	PVA 9H-12
PVA	10	12	14	PVA 14H-12
PVA	10	12	24	PVA 24H-12

4.3 Synthesis of Composite Membrane

The CA/PEG/ZIF-8 dense selective layers were synthesized using solution casting method as mentioned in Figure 4.3, by dissolving 10 (w/v) % of CA and 10 (w/w) % of PEG in 8 ml of THF and stirred for 24 hours. The solution of ZIF-8 was prepared separately by adding 5 wt. % in 2 ml of THF solvent and then stirred it for 24 hours at a continuous agitation speed of 500 RPM. Afterwards, the prepared solutions were poured in a media bottle and were mixed for 6 hours using magnetic stirrer. Then this solution was sonicated for 2 hours for complete and homogenized dispersion of ZIF-8 in polymeric solution. This solution was then degassed and again stirred for 2 hours, in-order to form a bubble free polymeric solution. The prepared solution were then poured manually on the PVA support layer at room temperature and casted a very thin layer on it. The thickness of membrane were controlled by using automatic membrane casting machine. The composite membrane was then covered with glass lid and dried for 24 hours in room temperature. After successful fabrication, the multi-layer composite membrane (MLCM) was then dried for 30 - 40 °C for 24 hours for the removal of left over solvent in polymer membrane matrix.

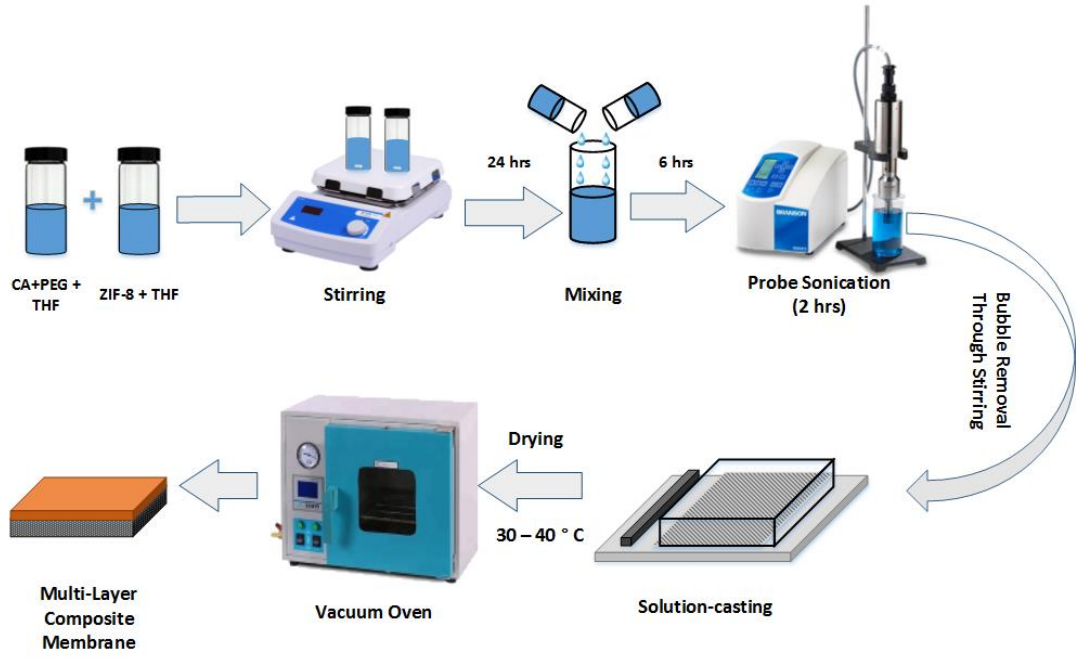

Figure 4.3. Multi-layer composite membrane (MLCM) preparation using solution casting method

4.4 Membrane Testing and Characterization

4.4.1 Cloud Point Test

The cloud point was estimated using rapid titration methodology [91]. For this characterization, different concentration between (5 – 15 wt. %) of PVA solutions were prepared by dissolving in DI-water in a sealed flask. The prepared polymeric solutions were continuously agitated at a temperature of 20 °C. Afterwards, through syringe dropwise THF (coagulant) were added in the solution and stirred for at least 1 hour. This addition of THF was continued until cloudy product was permanently formed. The final composition of each solution was recorded with its composition mass fraction and its percent, which was then represented on the phase diagram and its tabulated form.

4.4.1.1 Applications

The following are the applications of ternary phase diagram [60].

- Estimation of Mass Fraction of each components in ternary system.
- Analysis of de-mixing rate of NIPS process.
- Predicting the morphology of asymmetric membrane prepared through NIPS method.

4.4.2 Scanning Electron Microscopy (SEM)

Scanning electron microscopy (SEM) analysis were carried out to investigate the physical structure and morphology of membrane matrix at different resolution using scanning electron microscope - SEM (JSM-6490, Joel Japan). Through this analysis, in-depth information about membrane surface topography, pore size geometry, surface and cross-sectional morphology were studied. The membrane samples were prepared on copper stub, which were then sputter coating with gold [92, 93].

4.4.2.1 Components of SEM

SEM consist of following components [92, 93].

- Electron generating source
- Magnetic lenses
- Sample Stage
- Scanning system

- Electron detector
- Display (TV Scanner)
- Vacuum system
- Electronic control

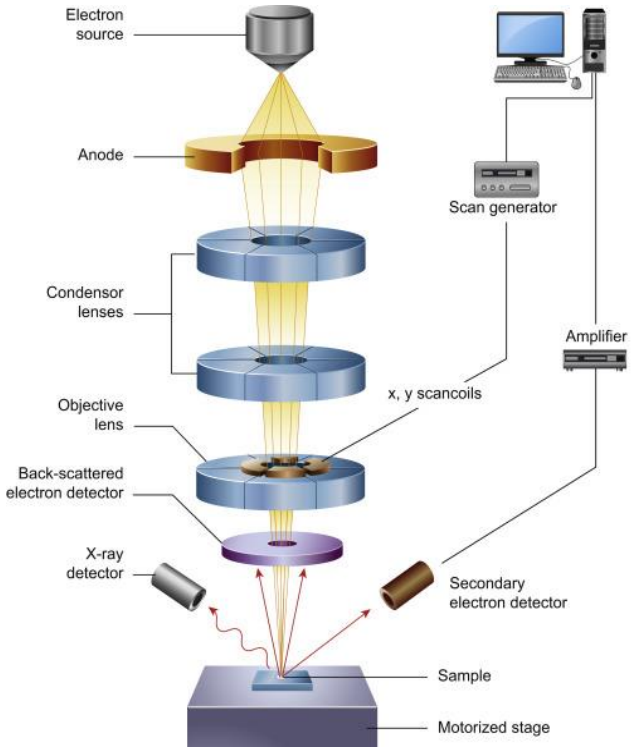

Figure 4.4. Schematic diagram of scanning electron microscopy (SEM) machine [92, 93]

4.4.2.2 SEM Working Principles

When electron beam having high energy was incidence on a membrane sample, it dissipated into various kind of signals as represented in Figure 4.4. Which focused on the surface of material. Signals generated between the interaction of membrane samples and the electron beams were collected by the electron detector. These signals were then analyzed accordingly to evaluate the morphology of membranes. The samples were analyzed in 10 KV voltage at different magnification between X500 – X20000. As samples doesn't damage in the process, SEM is considered as non-destructive analytical technique [92, 93].

4.4.3 Gravimetric Porosity Test

The interconnectivity of PVA asymmetric porous support membranes were determined by using gravimetric based porosity analysis method. Which is the fraction between the volumes of pores over total volume of porous membrane matrix. The following mentioned equation (4.1) was used to measure the porosity of membrane. In-order to evaluate standard deviation and to eliminate the errors in the estimation, three samples of each asymmetric membrane were tested. The mentioned below equation was used to estimate the gravimetric porosity of membranes [60].

$$\varepsilon = \frac{(W_w - W_d)/\rho_w}{(W_w - W_d)/\rho_w + W_d/\rho_p} \text{ X } 100 \qquad \text{Eq (4.1)}$$

In this equation, 2-propanol was taken as non-solvent displacement fluid, which have the density of ρ_w = 0.785 g/cm^3. Whereas ρ_p is the PVA polymer density having value of 1.19 g/cm^3. Initially membrane samples were dried in oven to remove unwanted moisture content and then weigh to measure the weight of fully dried samples W_d. The membrane samples were then immersed in non-solvent (2-propanol) bath for 24 hours. Through capillaries action the liquid sustained in the porous network of asymmetric membranes. Afterwards, the samples were again weigh in-order to estimate the weight of wet membrane samples (W_w) [60].

4.4.4 Fourier transform Infrared (FT-IR) Spectroscopy

Fourier transform infrared (FT-IR) spectroscopy is an analytical techniques carried out to evaluate the presence of function group in organic compounds and its modes as represented in Figure 4.5 and 4.6. Which also includes, detecting the chemical bond type in molecules, molecular structure of membrane samples. For this characterization, Perkin-Elmer spectrum 100 FT-IR spectrometer was used at a range of 4000 – 400 cm^{-1} wave number with a resolution of 4 cm^{-1} [94, 95].

4.4.4.1 Components of FT-IR Spectrometer

FT-IR spectrometer consist of the following components [94, 95].

- Infrared (IR) source
- Beam Splitter
- Fixed and movable mirrors
- Sample cell
- Detector

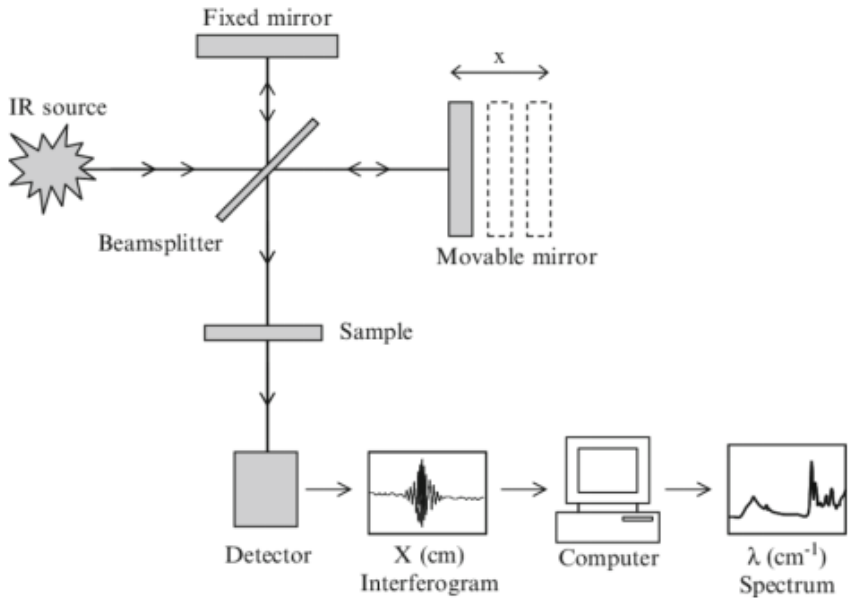

Figure 4.5. Schematic diagram of Fourier Transform Infrared (FT-IR) Spectrometer [95]

4.4.4.2 Working Principles

In FT-IR spectrometer, an IR radiation was generated through IR source as represented in Figure 4.5. Which was then absorbed by the material, this cause the molecules to raise its energy state from lower energy level towards the excited energy state. Through this mean, the molecules gained a higher vibrational states. This amount of energy that is needed to transfer the molecules to that higher state is proportional to the wavelength of the radiation absorbed. Each particular functional group present in a molecules absorbs radiation in a different specific wavelength. This formed a spectra peak called as *fingerprint* of that functional group. When all the characteristics peaks of different functional group present

in a materials are combined, it formed a spectrum of that particular molecules called as FT-IR spectrum [94, 95].

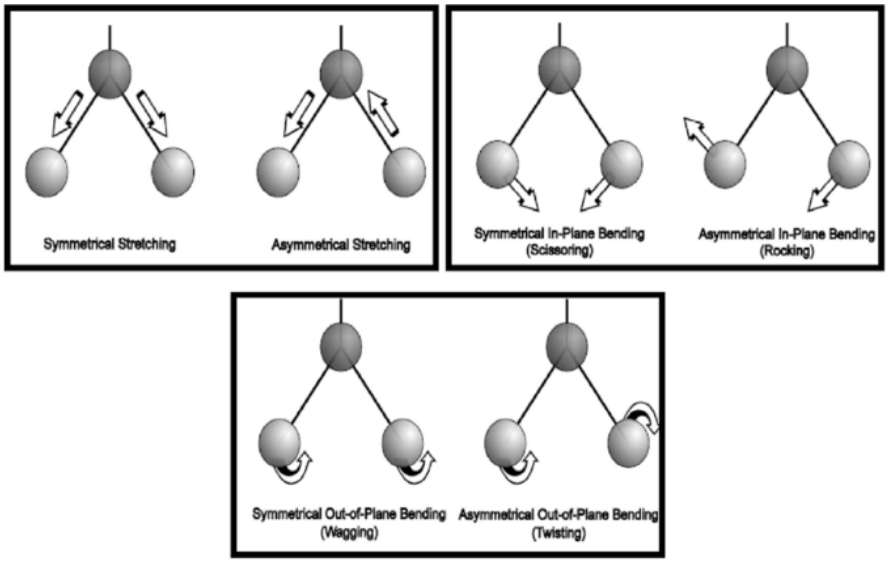

Figure 4.6. Different modes of molecular vibration in FT-IR (stretching and bending)

4.4.5 X-Ray Diffraction (XRD)

XRD characterization technique was carried out to measure the crystallinity of material (membranes). XRD provides in-depth information about the phase identity, purity, crystal structure and crystallinity of membrane [96].

4.4.5.1 Components of XRD

XRD consist of the following components [96].

- X-Ray Tube
- Sample holder
- Detector

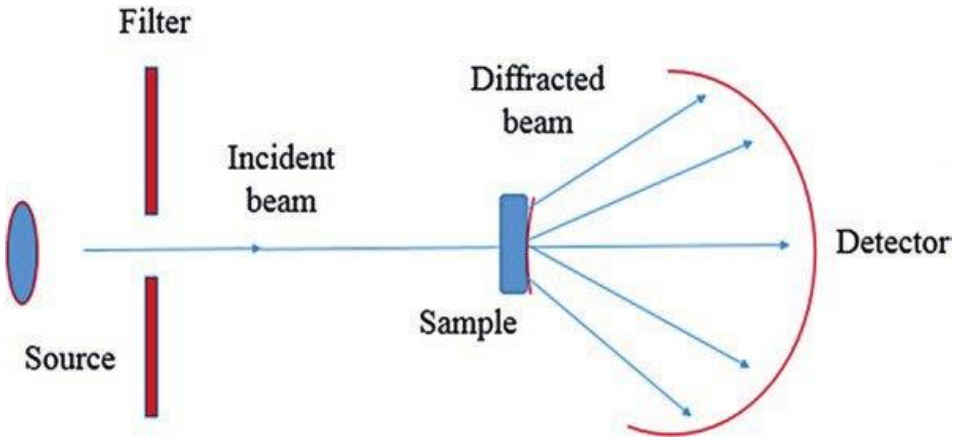

Figure 4.7. Schematic diagram of X-Ray Diffraction characterization [96]

4.4.5.2 Working Principles

XRD working principles is represented in Figure 4.7, X-Rays are produced by using X-ray tube having monochromatic nature. X-Rays are passed through collimator. These rays are then concentrated and directed towards the sample stage. A constructive interference are produced, when X-Rays interact with the test samples and some of the rays got diffracted. This applied Bragg's Law ($n\lambda = 2d \sin\theta$) conditions as depicted in Figure 4.8. Which correlates with electromagnetic radiation wavelength to the diffracted angle and the spacing between the sample lattices. By using Debye-Scherer's equation, the crystallite size of the crystals can be estimated. All crystalline material have their own unique finger print pattern for its identification [96].

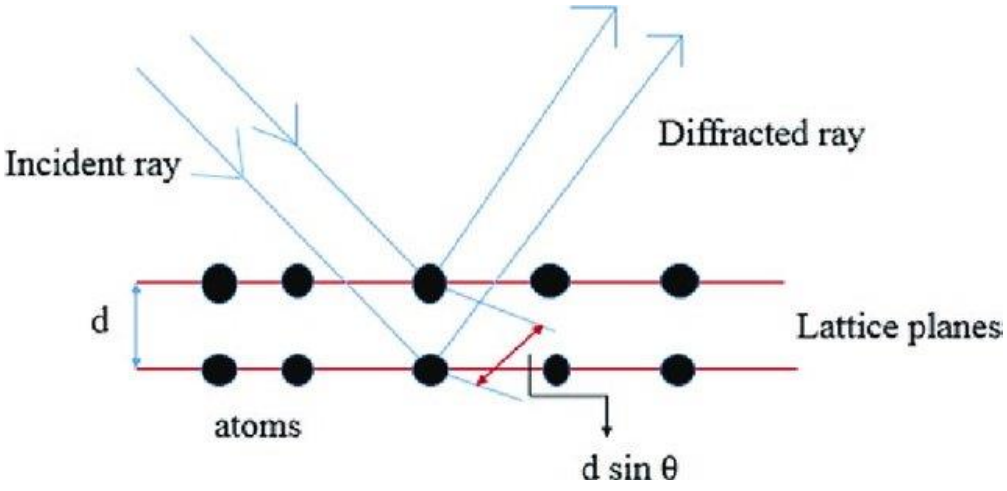

Figure 4.8. Bragg's Law X-Ray Diffraction system [96]

4.4.6 Gas Permeation Testing

Gas permeation testing analysis were carried out to investigate the perm-selective nature of the membranes. For that purpose PHILOS-Korea gas permeation testing rig was used to evaluate the gas permeation of membrane samples as depicted in Figure 4.9. Three samples of each membrane were tested in-order to calculate the standard deviation and to remove the random errors [60].

4.4.6.1 Components of Gas Permeation Testing Rig

The following are the components of gas permeation testing rigs [60].

- Membrane Cell
- Flow regulators
- Bubble flow meter
- Flow valves
- Vent tube

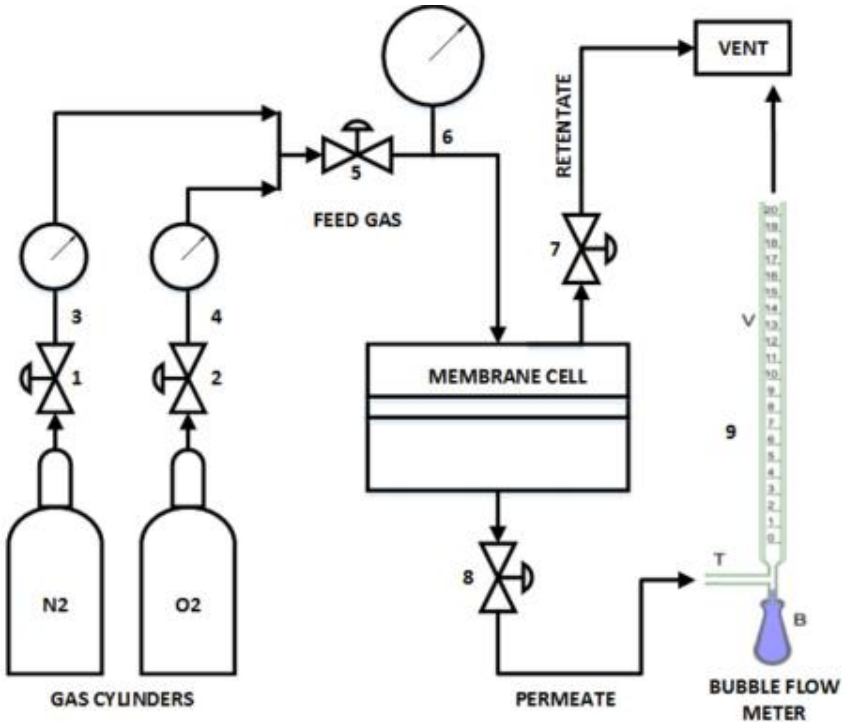

Figure 4.9. Gas permeation testing system rig [60]

4.4.6.2 Working Principle of Gas Permeation Testing Rig

The membrane samples were prepared by cutting the samples up-to 8.0 cm^2 and placed in membrane cell having two porous ceramic disk. In this study, Oxygen (O_2) and Nitrogen (N_2) gases were used as feed gas. The permeation analysis test results were recorded and calculated by using gas flow meter also called as bubble flow meter at a gauge pressure range between 2.0 to 5.0 bars at constant temperature condition of 25 °C and constant volume. In this characterization, the gas permeation works on the basis of solution-diffusion mechanism and estimated through the following mentioned equations [60].

$$P_i = \frac{Q\Delta L}{A\Delta P} \qquad \text{Eq (4.2)}$$

$$P = S \times D \qquad \text{Eq (4.3)}$$

$$\alpha_{i/j} = \frac{P(i)}{P(j)} \qquad \text{Eq (4.4)}$$

4.4.7 Mechanical Testing

Mechanical testing of a membrane samples were carried out to investigate the different mechanical characteristics, which includes tensile strength testing and elongation at break percent. In-order to estimate the standard deviation to eliminate the random errors, three samples of each membrane were used to determine the mechanical properties of membranes [60, 97].

4.4.7.1 Components of Ultimate Tensile Testing Machine (UTM)

The following are the components of the ultimate tensile testing machine (UTM) [97].

- Screw Column
- Adjustable upper crosshead
- Wedge Grips
- Adjustable Lower Crosshead
- Base and encoder assembly

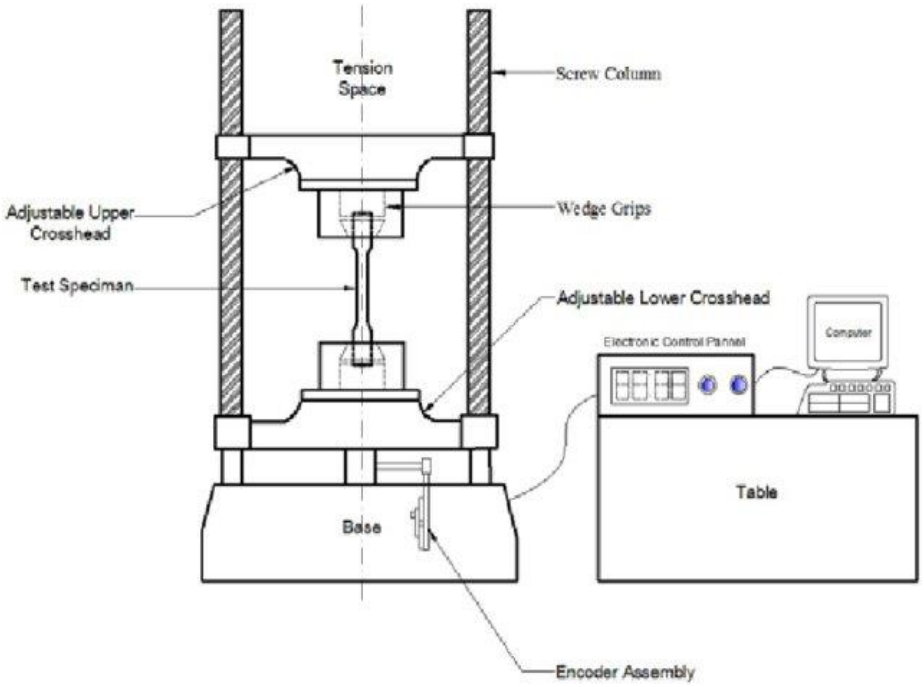

Figure 4.10. Schematic diagram of ultimate tensile testing system [97]

4.4.7.2 Working Principle of Ultimate Tensile Testing Machine (UTM)

The maximum tensile strength of a material can be estimated by the ratio of maximum stress of that material before forming a permanent deforming of the physical structure of membrane and its strain. The strength of the materials depends on the basis of their nature whether it is glassy or rubbery. For this purpose, UTM SHUMADZU AGS-X Plus Japan machine is used to determine the mechanical characteristics of the membranes as represented in Figure 4.10. The membrane samples were cut according to the ASTM standard D882-02 and mechanical testing was performed at an elongation rate of 10 mm/min [60, 97].

Chapter 5 – Results and Discussion

For this investigation different characterization techniques were used to evaluate the properties of asymmetric and composite membrane. The list of techniques are as follows:

- **Cloud Point Testing,** used to investigate the demixing rate of the ternary system of phase inversion and to predict the morphology of asymmetric membrane.
- **Scanning electron microscopy (SEM),** used to investigate the surface and cross-sectional morphology of membrane.
- **Gravimetric Porosity Testing,** used to study inter-connectivity and porosity of porous membrane.
- **Fourier Transform (FT-IR) Spectroscopy,** used to evaluate the different functional groups present in the membrane.
- **X-Ray Diffraction (XRD),** used to analyze crystalline structure of membrane.
- **Gas Permeation Testing,** used to study the perm-selective nature of different gases permeation through membrane.
- **Mechanical Testing,** used to investigate the tensile strength and elongation at break of membrane.

5.1 Cloud Point Testing Results

Table 5.1 - Phase Inversion cloud point composition data

POLYMER (PVA) (%)	CLOUD POINTS	
	SOLVENT (WATER) (%)	NON-SOLVENT (THF) (%)
2.41	57.4	40.18
3.68	58.38	37.94
4.99	59.38	35.63
5.96	59.14	34.89
7.34	58.21	34.46

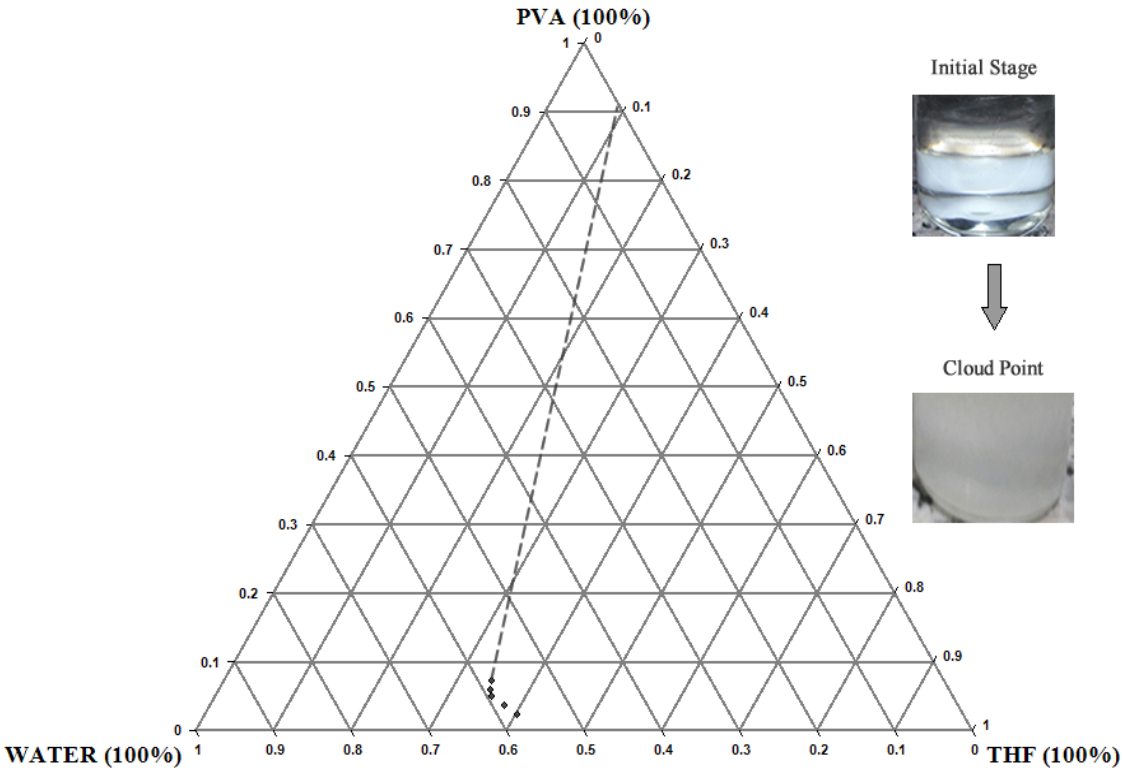

Figure 5.1. Phase inversion ternary diagram for PVA/Water/THF system at 20 ºC

The cloud point estimation of PVA/Water/THF ternary system were experimentally carried out to investigate the thermodynamic behaviour and to predict morphology of asymmetric membrane through its demixing rate. In this system coagulant drops were added in different polymer solution (PVA-Water) having concentration between 5 – 15 wt. %, which converted the clear PVA polymer solution into cloudy product as represented in Figure 5.1. The estimated cloud point's values, were plotted in the ternary phase diagram forming a curve called as binodal curve. The mass percent data of ternary phase diagram was represented in Table 5.1. The experimental binodal curve divides into two main parts. (a) The inside portion denoting the single phase region, where all the components are miscible. (b) The outside region of the curve represented the two phase consist of rich in polymer phase (solid) and lean in polymer phase (liquid).

This curve also provided the in-depth information about the coagulation power, which is the known parameter that effects the demixing rate of the phase inversion process. If there is less distance between the binodal curve and polymer solvent axis then the non-solvent as coagulant is considered as strong, this results instantaneous demixing, formation of

finger-like structure and vice versa [98, 99]. According to the Figure 5.1, as there is more distance between the binodal curve and polymer-solvent axis. Also during experimentation, it was observed that the phase inversion process took longer time to precipitate. Which concludes that, THF works as a weak coagulant for this ternary system, indicating the demixing rate of the process is slow also called as delay demixing rate. This predicted that the morphology of asymmetric membrane will have sponge-type inter-connective porous structure with top dense layer.

5.2 Scanning Electron Microscopy (SEM)

PVA asymmetric membranes and composite membrane were analyzed using SEM at a magnification range between 500X – 20,000X, to investigate its surface and cross-section matrix structure (morphology). The SEM analysis is consist of three main parts, which were divided on basis of different parameter optimization. Which includes polymer concentration, coagulation residence time and thickness of coated surface layer (dense selective layer) as mentioned below:

5.2.1 PVA Asymmetric Membrane Polymer Concentration Optimization

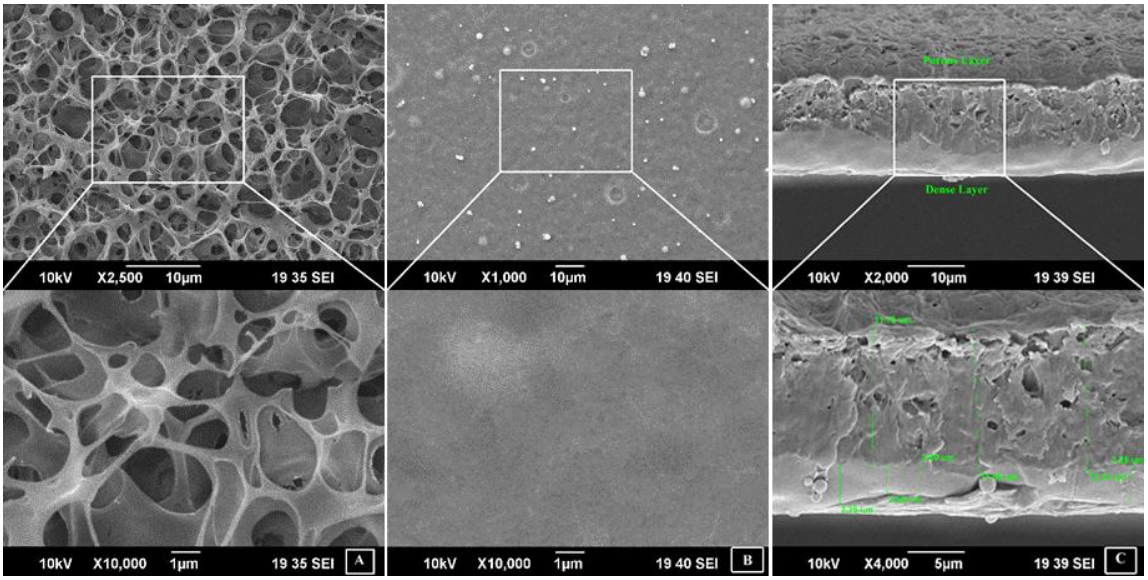

Figure 5.2. PVA 3H-10 asymmetric membrane (A) porous layer, (B) dense layer, (C) cross-section

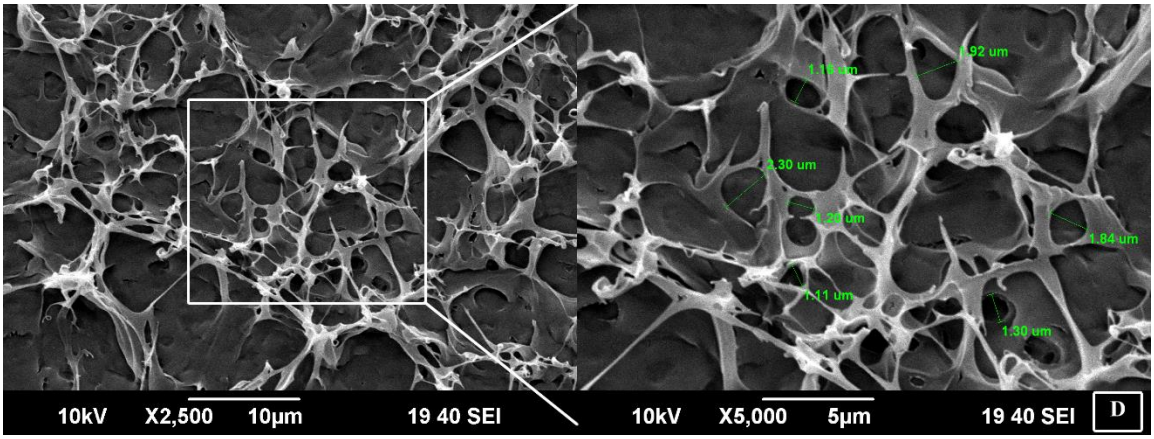

Figure 5.3. PVA 3H-10 asymmetric membrane (D) defective porous structure

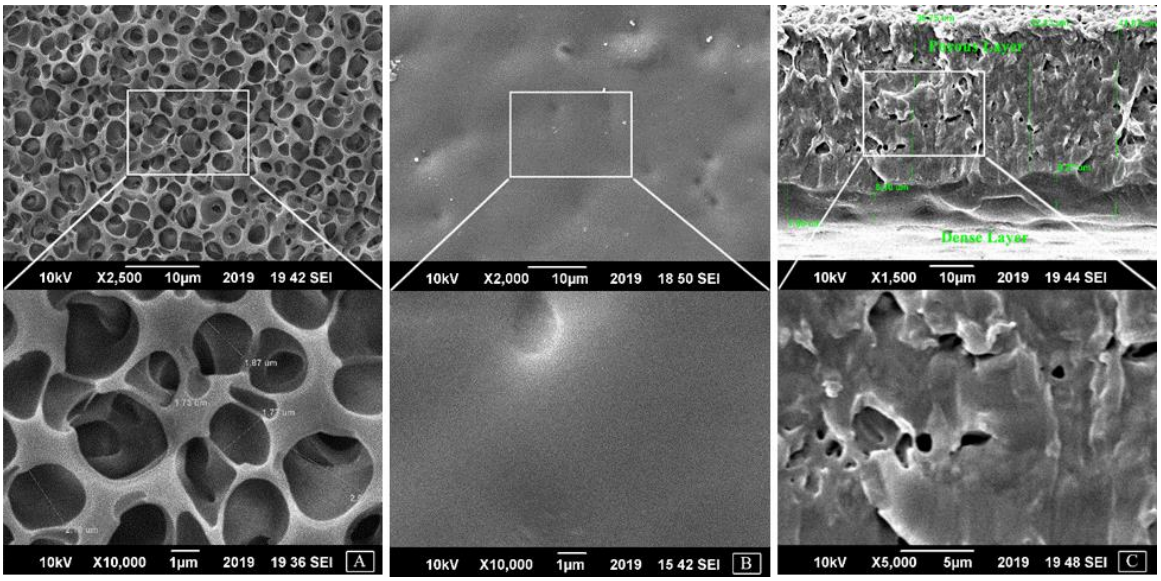

Figure 5.4. PVA 3H-12 asymmetric membrane (A) porous layer, (B) dense layer, (C) cross-section [60]

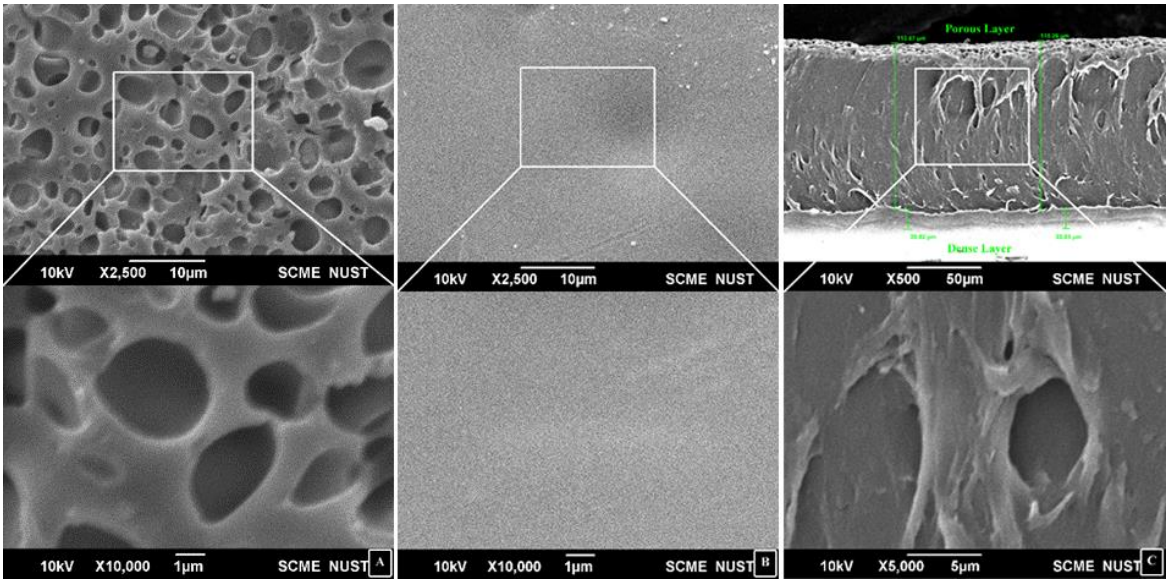

Figure 5.5. PVA 3H-14 asymmetric membrane (A) porous layer, (B) dense layer, (C) cross-section

For polymer concentration optimization, the effects of changing concentration on the morphology of membrane was investigated. Three membrane were fabricated having concentration between 10 wt. % to 14 wt. % at a constant coagulation residence time of 3 hours. The sample nomenclature are PVA 3H-10, 3H-12 and 3H-14, as mentioned in Table 4.1. Through SEM analysis, it is clearly shown from Figure 5.2 – 5.5, that PVA asymmetric membrane possessed the sponge type structure as predicted through ternary phase diagram analysis. Whereas, the information about the morphology variation occurred due to the change in polymer concentration as mentioned below:

5.2.1.1 Effect of Polymer Concentration on Membrane Thickness and Top Dense Layer

The prepared PVA membranes (PVA 3H-10, 3H-12 and 3H-14) possessed thin skin dense layer on top of sponge type porous structure. These membrane were fabricated at variable thickness of 14 – 16 µm, 40 – 42 µm and 130 – 135 µm as illustrated in cross-sectional images of Figure 5.2, 5.4 and 5.5 (C). This variation in membrane thickness were due to the change in PVA solution viscosity. As lower polymer concentration leads to lower PVA solution viscosity, which can be easily spread in a glass slab forming thinner PVA asymmetric membrane. However, by increasing polymeric concentration, PVA solution

started to show increase in viscosity. Which leads to the thicker membrane formation due to the difficulty in spreading of polymeric solution on the glass slab during membrane casting process.

From Figure 5.3, 5.4, 5.5 (B), illustrated dense skin layer of PVA asymmetric membrane. In which formation of some partial voids in the top dense layer of PVA 3H-10 were clearly visible. Which were reduced in the PVA 3H-12 and PVA 3H-14 asymmetric membrane due to the increased in polymer concentration forming uniform densified top layer. In Figure 5.3, 5.4, 5.5 (C) represents the reduction in porous structure as membrane polymer concentration increased. In PVA 3H-12 membrane, intermediate membrane matrix structure having uniform distribution of both dense and porous layer thickness was observed. Whereas, PVA 3H-14 membrane show densified structure with thicker top layer as compared to other PVA asymmetric membranes. This signifies that, by increasing polymeric concentration favours more dense and thicker skin layer of asymmetric structure [100, 101]. However, through the comparison analysis of all PVA asymmetric membrane, PVA 3H-12 asymmetric membrane shows the most optimum cross-sectional morphology for GS applications including O_2/N_2 gas separation.

5.2.1.2 Effects of Polymer Concentration on the asymmetric membrane porous morphology

Through SEM analysis of PVA asymmetric membrane porous structure from Figure 5.3 – 5.5 (A), an in-depth information about the porous morphology can be obtained. The averages pore size of PVA 3H-10, 3H-12 and 3H-14 asymmetric membrane possessed 2.486 ± 1.2 μm, 2.096 ± 0.5 μm and 1.447 ± 0.9 μm respectively, as graphically depicted in Figure 5.6. In PVA 3H-10 asymmetric membrane large and irregular connective porous structure have been observed. This membrane also contain some defective area present in the porous layer, which is illustrated in Figure 5.4 (D), representing mechanically unstable porous membrane matrix. Whereas, In PVA 3H-12 membrane these irregularity in pore sizes were reduced, having smaller pores as compared to PVA 3H-10 membrane and have the most uniform and connective porous layer. This represent a mechanically stable porous structure. However, by increasing the polymer concentration further up-to 14 wt. %, in membrane (PVA 3H-14) both voids and smaller pores appeared in the porous layer.

This concludes that, higher polymer concentration leads to the formation of denser membrane morphology [101-103]. However, there is an intermediate point of polymeric concentration (PVA 3H-12), which shows the least pore size deviation as compared to other membranes forming an uniformly distributed porous structure of asymmetric membrane. This represents that PVA 3H-12 asymmetric membrane possessed the most optimum porous structure (support layer) for GS applications.

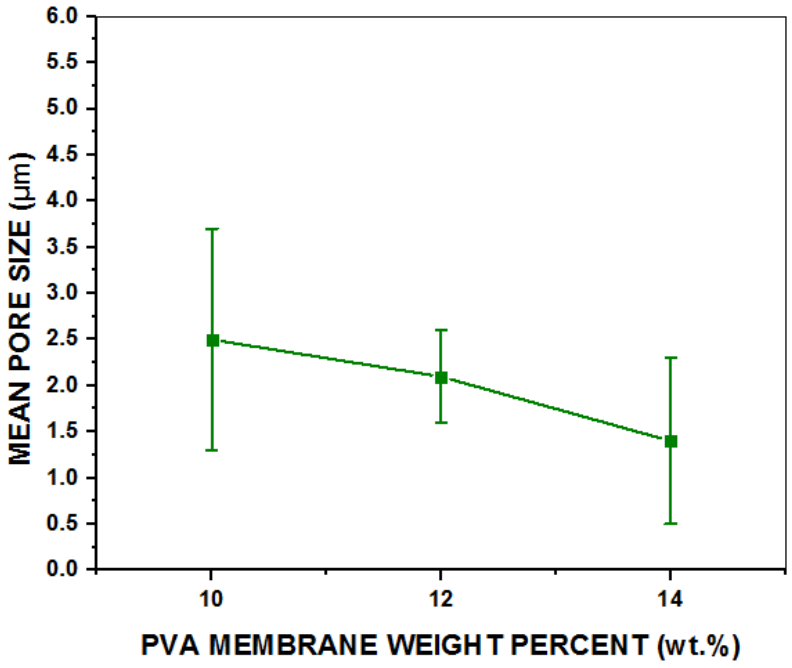

Figure 5.6. Mean pore size of PVA asymmetric membranes at different concentration

5.2.2 PVA Asymmetric Membrane Coagulation Time Optimization

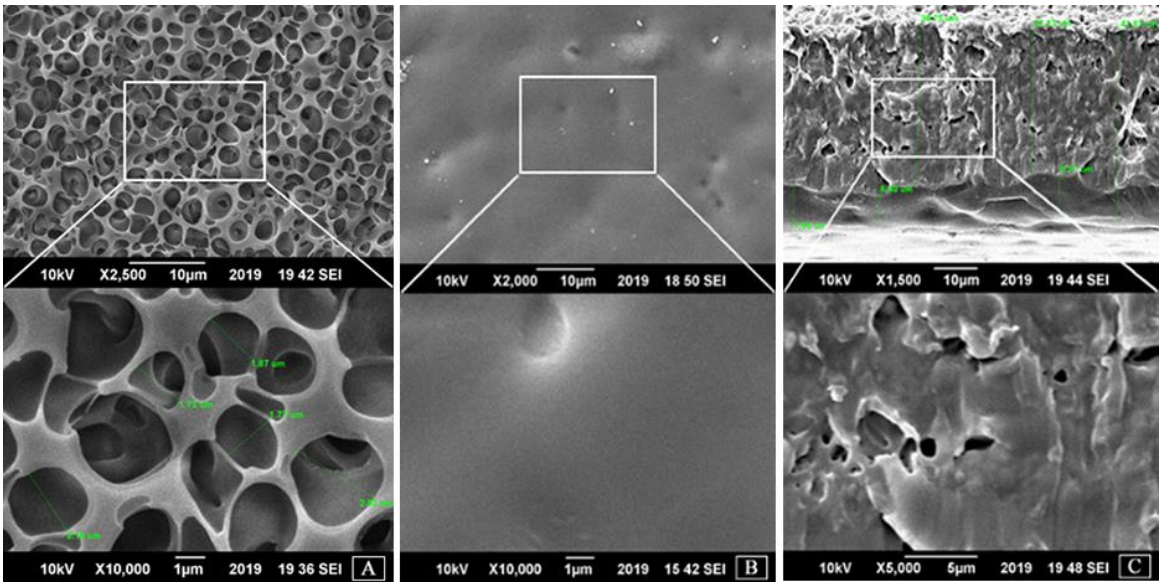

Figure 5.7. PVA 3H-12 Asymmetric membrane morphology, (A) Porous layer, (B) Dense layer, (C) Cross-section [60]

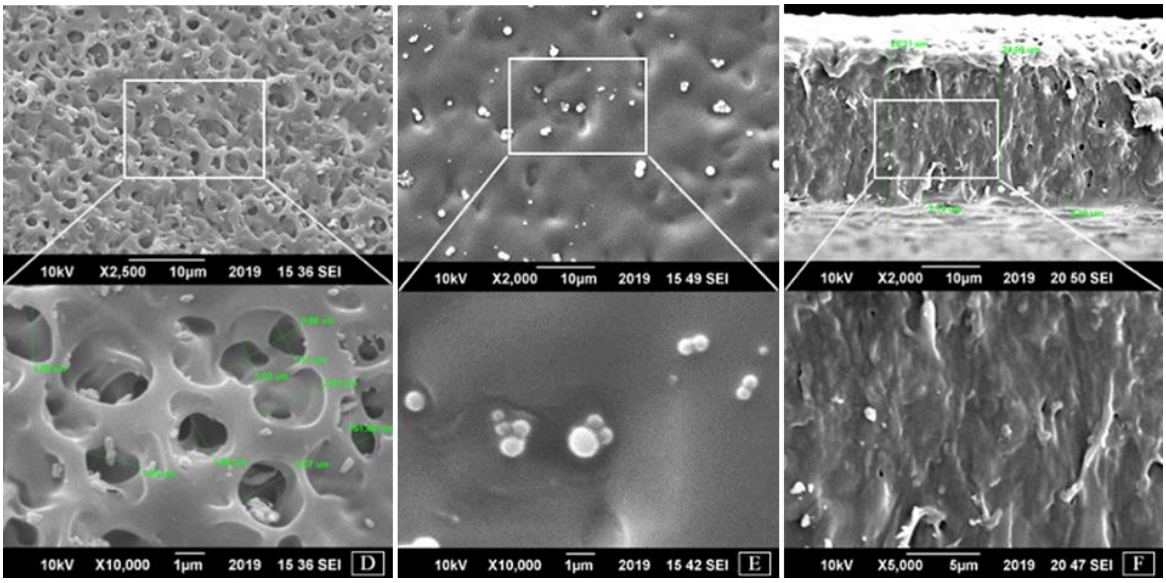

Figure 5.8. PVA 6H-12 Asymmetric membrane morphology, (D) Porous layer, (E) Dense layer, (F) Cross-section [60]

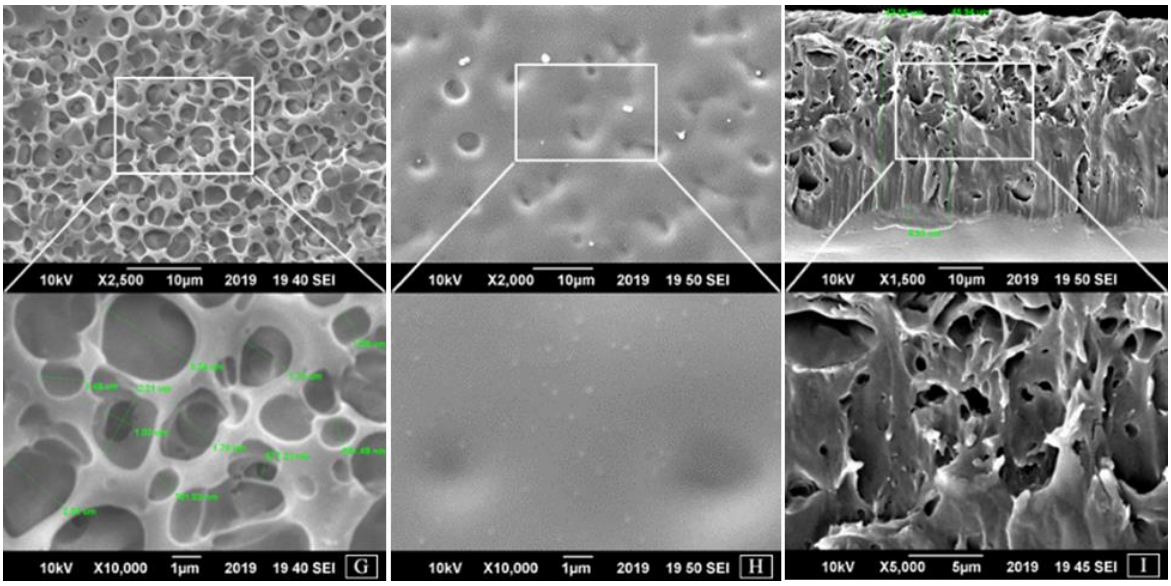

Figure 5.9. PVA 9H-12 Asymmetric membrane morphology, (G) Porous layer, (H) Dense layer, (I) Cross-section [60]

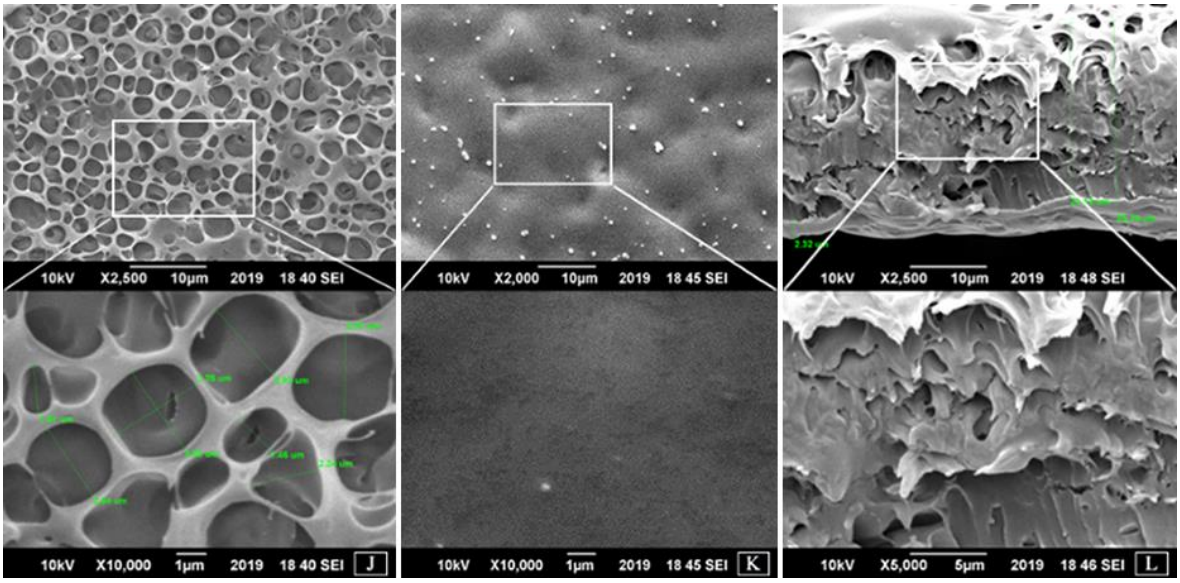

Figure 5.10. PVA 14H-12 Asymmetric membrane morphology, (J) Porous layer, (K) Dense layer, (L) Cross-section [60]

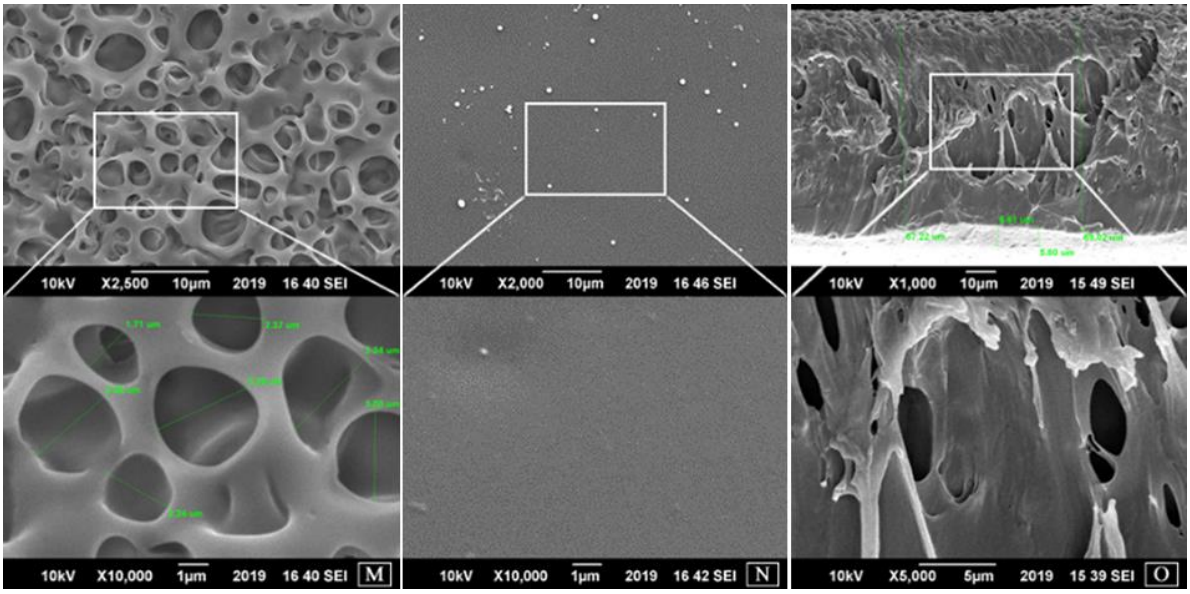

Figure 5.11. PVA 24H-12 Asymmetric membrane morphology, (M) Porous layer, (N) Dense layer, (O) Cross-section [60]

After polymer concentration optimization, the most optimum asymmetric membrane was selected (PVA 3H-12) for further optimization of its morphology in-order to utilized as porous support membrane. For that purpose, a novel parameter (coagulation residence time) was introduced to further alter the morphology of asymmetric membrane. To study the effects of this parameters, five (5) asymmetric membranes were fabricated having same polymeric concentration but at different coagulation residence time of 3 to 24 hours. The prepared membrane possessed the same sponge type morphology as predicted from cloud point testing and have top thin dense skin layer, which represent slow demixing behaviour.

Through coagulation residence time variation from 3 hours to 24 hours, membrane morphology changes were observed, which includes expansion of pore size and restructuring of porous layer of asymmetric membrane due to the change in diffusional flow time for coagulation steps in phase inversion process [60, 104-106]. The PVA 3H-12 asymmetric membrane possessed single chain porous structure, which restructured and changed to double chain porous network in PVA 24H-12 asymmetric membrane. However, the skin layer surface also got affected due to the coagulation variation, as particle formation first appeared on the surface of PVA 3H-12 asymmetric forming rough

surface of skin layer. This rough surface reduced in PVA 24H-12 skin dense layer surface, having optimum skin roughness to provide better skin fraction to the selective layer for the formation of multi-layer composite membrane (MLCM).

5.2.2.1 Effects of Coagulation residence time on membrane porous structure

SEM characterization analysis also provides the in-depth information about the pore size distribution data as graphically illustrated in Figure 5.12. These results show that, PVA 3H-12, 6H-12, 9H-12, 14H-12 and 24H-12 membranes have the mean pore sizes of 2.096, 2.224, 2.26, 2.702 and 2.736 µm accordingly. Which signifies that through increasing coagulation residence time, porous network restructuring and expansion of pore size was observed. From the time period of 3 hours to 9 hours, there is a slight effects of coagulation residence time on the mean pore size. However, from 9 hours to 14 hours, a sudden increased in mean pore size was observed in porous layer, also called as transition stage. This restructuring of membrane morphology was then completed in PVA 24H-12 asymmetric membrane, forming durable and double chain porous layer network. This phenomena of restructuring and expansion of porous network occurred due to the more time given to the diffusional flow (mass transfer) in coagulation process [60, 104-106].

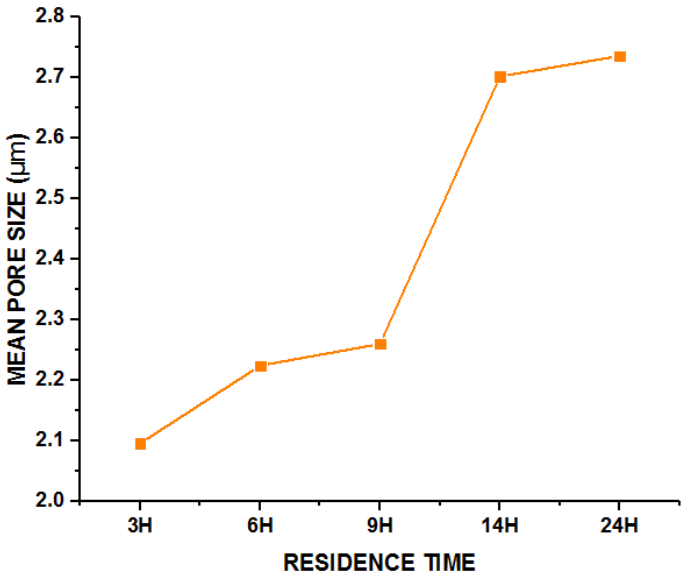

Figure 5.12. Influence of coagulation residence time on PVA asymmetric membranes pore size distribution [60]

5.2.2.2 Effects of coagulation residence time on membrane thickness ratio

The in-depth information about the effects of coagulation residence time on the membrane thickness ratio of skin layer and porous layer, was obtained through SEM characterization analysis as represented in Figure 5.13. The SEM analysis results show that, by changing coagulation residence time from 3 hours to 24 hours for fabrication of PVA asymmetric membrane, the skin layer thickness ratio percentage decreases from 17.96 $\pm$ 1.32 % to 8.35 $\pm$ 1.32 %. Whereas the porous support layer thickness ratio percentage increases from 82.04 $\pm$ 0.60 % to 91.65 $\pm$ 0.60 %.

These results signifies that, by increasing coagulation residence time, facilitated pore size expansion in porous membrane matrix was due to the more time given for the mass transfer (diffusional flow) between solvent and non-solvent in the coagulation process. Due to this pore expansion, the dense layer thickness of PVA asymmetric membrane reduces as observed from the SEM analysis of Figure 5.7 – 5.11, which is represented in tabulated data of Table 5.2 and graphically depicted in Figures 5.13 [60, 104-106].

Table 5.2 - Coagulation residence time effects on the membrane thickness ratio data obtained from SEM analysis [60]

Time	**Dense Layer**	**Porous Layer**	**Dense Layer**	**Porous Layer**
Hours	***(µm)***	***(µm)***	**(%)**	**(%)**
3	7.42 $\pm$ 0.77	33.83 $\pm$ 1.49	17.96 $\pm$ 1.32	82.04 $\pm$ 1.32
6	2.64 $\pm$ 0.03	22.48 $\pm$ 0.14	10.49 $\pm$ 0.07	89.51 $\pm$ 0.07
9	4.87 $\pm$ 0.06	42.35 $\pm$ 0.20	10.30 $\pm$ 0.08	89.70 $\pm$ 0.08
14	2.31 $\pm$ 0.17	23.29 $\pm$ 0.01	9.02 $\pm$ 0.01	90.98 $\pm$ 0.01
24	6.21 $\pm$ 0.41	68.12 $\pm$ 0.90	8.35 $\pm$ 0.60	91.65 $\pm$ 0.60

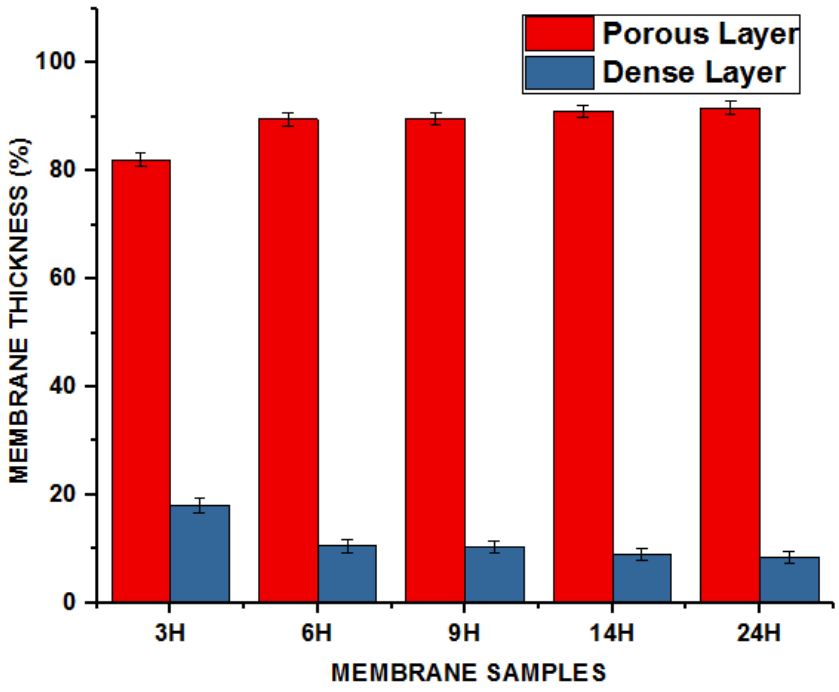

Figure 5.13. Influence of coagulation residence time on PVA Asymmetric membrane thickness ratio [60]

5.2.3 Multi-layer Composite Membrane (MLCM)

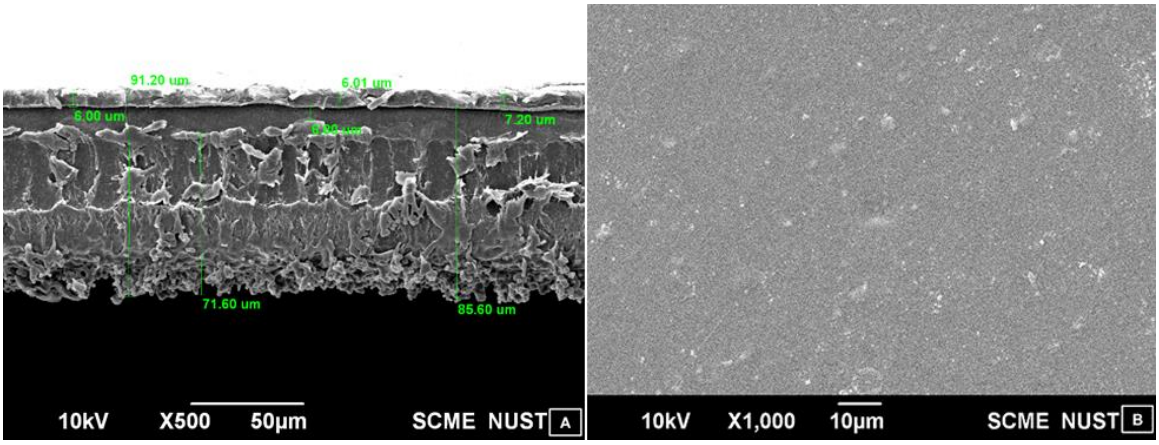

Figure 5.14 (a). Multi-Layer Composite Membrane (MLCM) (A) Cross-Section (B) Dense Layer

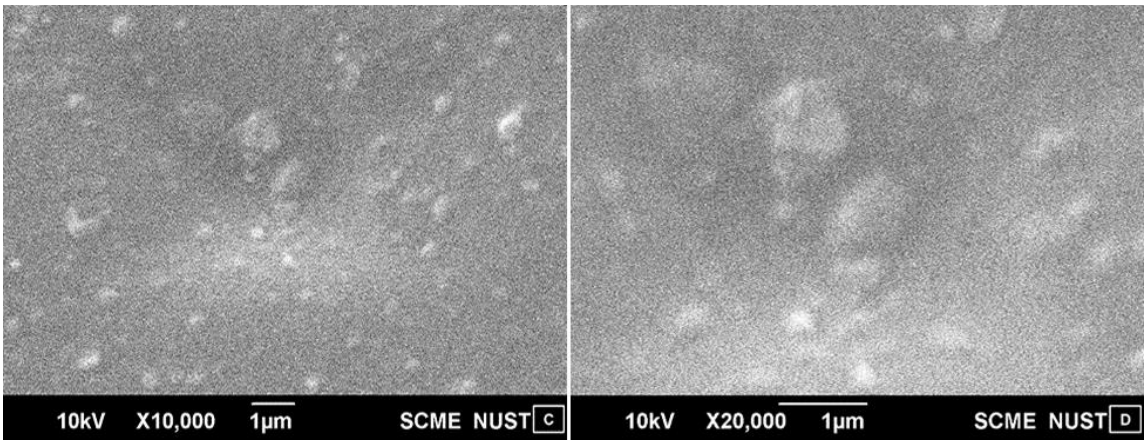

Figure 5.14 (b). Multi-Layer Composite Membrane (MLCM) (C) and (D) Dense Selective Layer

Figure 5.14 represents the multi-layer composite membrane (MLCM), composed of selective layer (CA/PEG/ZIF-8) on top of PVA asymmetric membrane (PVA 24H-12). Figure 5.14 (a) and (b), (B), (C) and (D) depicted the surface morphology of selective layer, which signifies uniformly dispersion of ZIF-8 in Cellulose acetate (CA)/ Polyethylene glycol (PEG) blend polymer.

Whereas, the cross-section image of multi-layer composite membrane is depicted in Figure 5.14 (A). Which represents the three (3) layer of multi-layer composite membrane, (a) Selective Layer composed of CA/PEG/ZIF-8 having thickness of 7.06 μm, (b) Skin layer of PVA Asymmetric membrane having thickness of 7.12 μm, (c) Porous layer of PVA Asymmetric membrane having thickness of 78.17 μm.

The particle present on the surface of PVA 24H-12 membrane, also provide skin layer friction and helps in adhesion of two layer as illustrated in Figure 5.14 (a) and (b), (B), (C) and (D). Through these SEM images it is also confirms that, selective layer is properly adhere and merged together on the surface of the PVA asymmetric membrane.

5.3 Gravimetric Porosity Testing

Gravimetric porosity analysis test were carried out on three (3) similar samples of each PVA asymmetric membrane in-order to estimate the average porosity with its mean standard deviation as illustrated in Figure 5.15 and 5.16. The gravimetric porosity test were taken in account for two optimization, as mentioned below:

(a) Effects of polymer concentration,

(b) Effects of coagulation residence time on mean porosity of PVA asymmetric membranes.

5.3.1 Polymeric Concentration Effects on membrane Gravimetric Porosity

The polymeric concentration effects were graphically represented in Figure 5.15. The results show that, the PVA 3H-10, 3H-12 and 3H-14 asymmetric membrane have inter-connected porous structure having mean porosity of 77.73 $\pm$ 15.26 %, 56.31 $\pm$ 3.6 % and 31.35 $\pm$ 11.98 %. Which signifies that, increasing polymer concentration leads to the formation of lower gravimetric porosity.

Whereas, standard deviation of each samples signifies uniform pore channel connectivity of asymmetric porous membrane. In which PVA 3H-12 asymmetric membrane has the most uniform connective channels in porous layer as compared to the other PVA asymmetric membranes. These analysis results were also supported by SEM analysis data [60, 104-106].

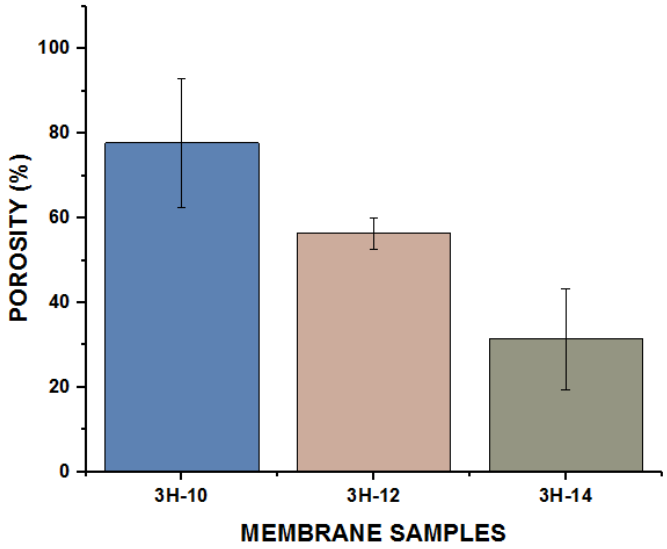

Figure 5.15. Gravimetric based mean porosity of PVA asymmetric membrane samples

5.3.2 Coagulation Residence Time Effects on membrane Gravimetric Porosity

The coagulation residence time effects on membrane gravimetric porosity were graphically represented in Figure 5.16. These results shows that PVA 3H-12, 6H-12, 9H-12, 14H-12 and 24H-12 have inter-connective mean porosity of 56.31 $\pm$ 3.60 %, 61.96 $\pm$ 6.94 %, 65.52 $\pm$ 10.47 %, 70.52 $\pm$ 14.81 % and 75.52 $\pm$ 14.24 % [60, 104-106].

Through these analysis data, it is concluded that longer coagulation residence time leads to higher gravimetric porosity of PVA asymmetric membrane. These results were also supported by SEM analysis, which signifies that by increasing coagulation residence time, more diffusional flow occurred. This increases the mean pore size and thickness of porous layer of asymmetric membrane [60, 104-106].

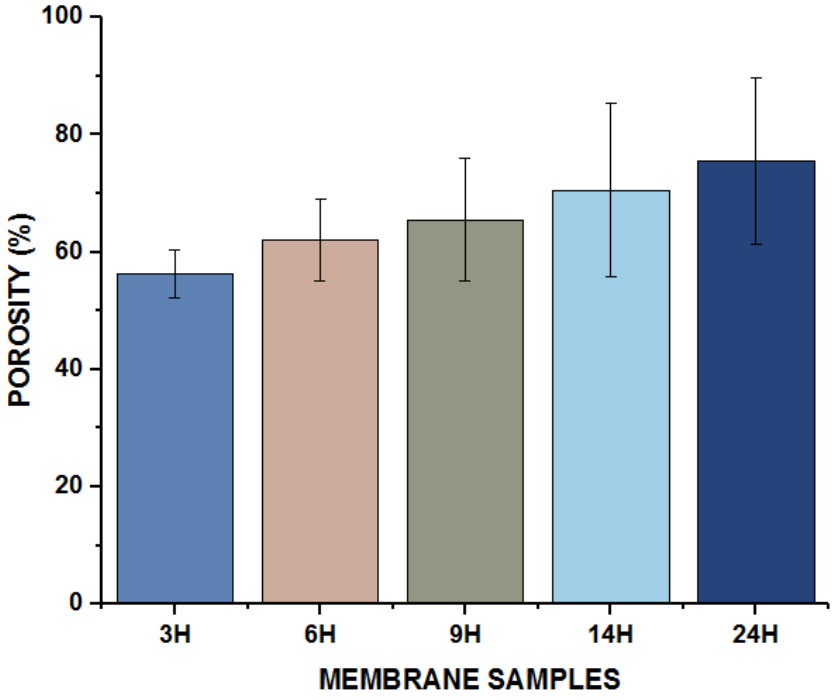

Figure 5.16. Gravimetric based mean porosity of PVA asymmetric membranes [60]

5.4 Fourier Infrared Transform (FT-IR) Spectroscopy

FT-IR spectra analysis of membrane samples were illustrated in Figure 5.17. Which confirmed the presence of different chemical bonds such as functional groups present in the material of membrane samples. The FT-IR of PVA Asymmetric membrane, CA blend (CA/PEG), Mixed matrix membrane (CA/PEG/ZIF-8) and Composite membrane (CA/PEG/ZIF-8/PVA) are discussed in this section.

In FT-IR spectra, different peaks of PVA asymmetric membrane were observed at 3417, 2943, 1731, 1428, 1375 and 1095 cm^{-1} accordingly. At peak of 3417 cm^{-1}, having bell shape like structure indicated the strong-broad Hydroxyl group (O-H) stretching of alcohol having intermolecular hydrogen bonding. Whereas at peak of 2943, 1731 and 1375 cm^{-1}, represented the stretching, blending and deformation vibration of C_{sp}^{3}-H bonding of asymmetric methyl compound accordingly. These two compounds (C_{sp}^{3}-H bond and Hydroxyl group) are the two main peaks of PVA polymer.

However at peak of 1731 and 1081 cm^{-1}, carbon double bond (C=O) and single bond (C-O) were indicated, which shows carbonyl stretching and acetyl group stretching. Through this analysis of PVA asymmetric membrane signifies that, as PVA asymmetric membrane show the similar behaviour of pure polymer, so there is no chemical interaction and effects of non-solvent (THF) on the PVA asymmetric membrane [107, 108].

CA Blend (CA/PEG) and MMMs (CA/PEG/ZIF-8) membrane exhibits, similar FT-IR peaks of 3507.02, 2956.85, 2877.25, 1740, 1442.21, 1362.54, 1238.46 and 1069.89 cm^{-1} respectively. Absorption FT-IR band at 3507.02 cm^{-1} represented intermolecular bonded of hydroxyl group (O-H) having bell shape like structure. Whereas, 2956.85 and 2877.25 cm^{-1} peaks are allocated to asymmetric and symmetric of C_{sp}^{3}-H methyl group stretching. At peak 1740 cm^{-1} exhibits strong carbon double bond (C=O) of Aldehyde group. While, 1442.21 and 1362. 54 cm^{-1} peaks represents C_{sp}^{3}-H asymmetric and symmetric bending of methyl group (deformation).

However, at 1238.46 and 1069.899 cm^{-1} shows C-O-C stretching (strong) of acetate group and primary alcohol of C-O stretching (strong) bonding accordingly [109, 110]. However, two additional absorption peak are also observed in MMMs membrane due to presence of

ZIF-8 nano-particles at 1574.2 and 421 cm^{-1} consigned to C=N and Zn-N (stretching) groups respectively [76, 111].

In Composite membrane FT-IR spectra, shows characteristics peak at 3456.68, 2924.08, 2874.91, 1740, 1574, 1425.75, 1374.24, 1247.82, 1071.07 and 421.25 cm^{-1} respectively. In which peak of 3456.68 cm^{-1} indicated the strong-broad Hydroxyl group (O-H) stretching of alcohol having intermolecular hydrogen bonding and having bell shape like structure. Whereas, 2924.08, 2874.91, 1425.75 and 1374.24 cm^{-1} peaks are consigned to $C_{sp}{}^{3}$ – H asymmetric and symmetric methyl group stretching and deformation accordingly similarly like in CA/PEG blend FT-IR spectra. In which symmetric stretching and deformation peaks shows, lower intensity as compared to asymmetric peaks. These two compounds ($C_{sp}{}^{3}$-H bond and Hydroxyl group) are the two main peaks of PVA polymer.

Whereas at peak of 1740, 1247.82, 1071.07 cm^{-1} exhibits strong carbon double bond (C=O) of Aldehyde group, stretching (strong) of acetate group and primary alcohol of C-O stretching (strong) bonding respectively. However, two additional peaks are also similarly observed at 1574 and 421 cm^{-1} allocated for C=N and Zn-N stretching bonds accordingly, which represents the characteristics peaks of ZIF-8 nano-particles [76, 107-111].

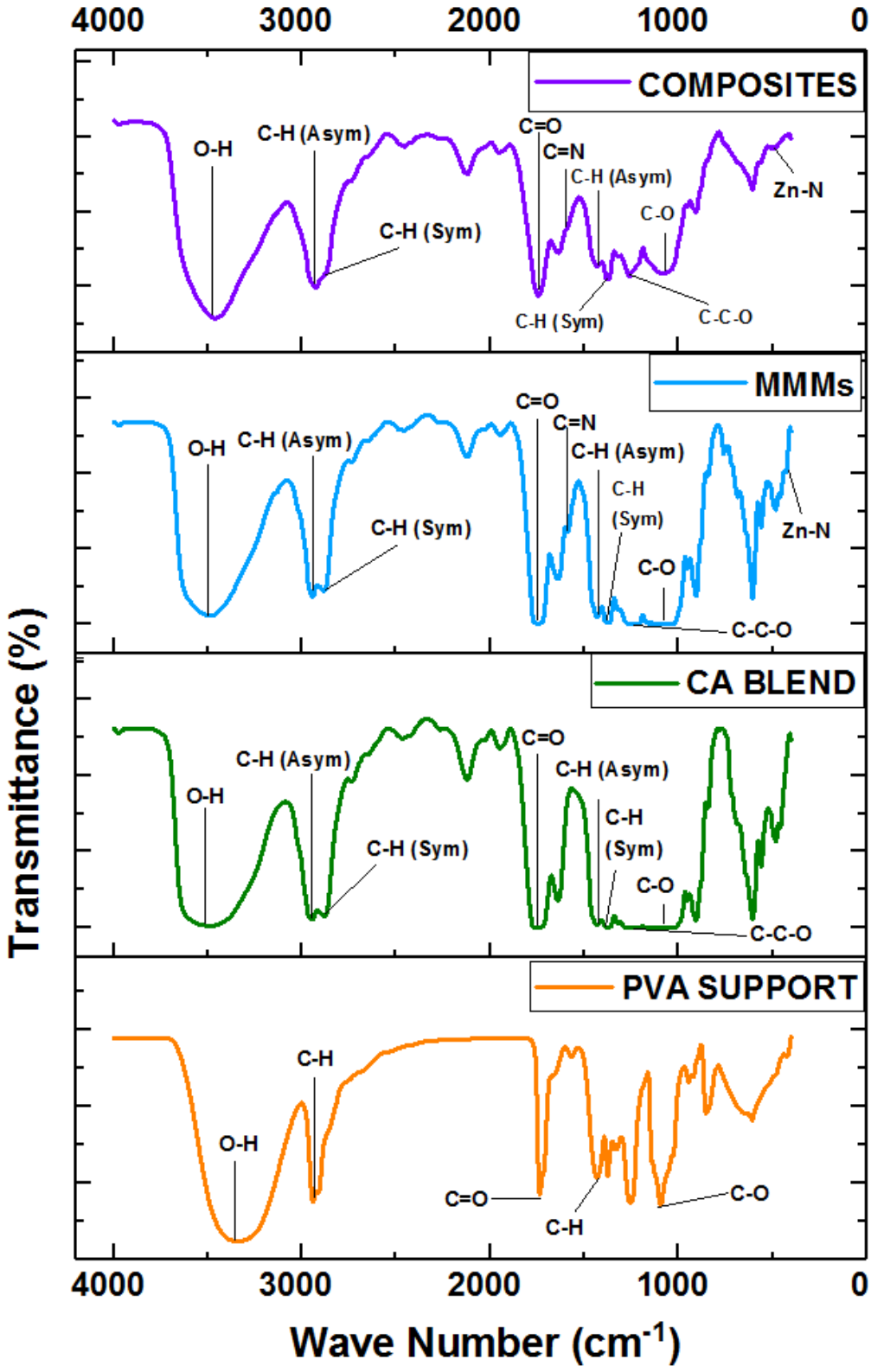

Figure 5.17. Graphically representation of Fourier Infrared Transform (FT-IR) analysis of membrane samples

5.5 X-Ray Diffraction

X-Ray Diffraction (XRD) analysis of membrane samples were illustrated in Figure 5.18, which defined the chemical structure including crystallinity and purity of different membrane samples. Which includes the sample of PVA support membrane, CA Blend (CA/PEG), ZIF-8 (nano-particle) powdered and CA/PEG/ZIF-8 based composite membrane. These XRD analysis pattern were acquired between the 2θ angle of 5° to 60° at a rate of 0.04°/s.

In XRD pattern of polymeric membrane, some parts of polymer chain are orderly arranged, which shows higher crystalline peaks. While loosely packed polymer chain represents amorphous region of polymer, which represents lower intensity in XRD spectrum.

The XRD pattern of PVA asymmetric membrane showed an prominent peak at 2θ angle of 20.04°, representing higher intensity of crystalline region. Wheras, some peaks were also observed at 2θ angle of 40° – 42° representing lower intensity of amorphous region. Which indicate the behaviour of semi-crystalline similar to pure PVA polymer [60, 112-116].

In Blend of CA/PEG XRD spectrum shows a hump-shaped like pattern between 2θ angle of 17° – 20°, as there is a absense of high intensity sharp peak, this represents the semi-crystalline behaviour of membrane [117].

The XRD spectrum of nano-particle particles ZIF-8 showed sharp and strong peaks at different 2θ angles of 7.20°, 10.28°, 12.56°, 14.58°, 16.32°, 17.92°, 22.6°, 24.36°, 25.44°, 26.48° and 29.52°, which correspond to the plane of (011), (002), (112), (022), (013), (222), (114), (223), (224), (134) and (004) accordingly. These peaks are excellent agreement with the literature [76, 118].

In Composite membrane XRD pattern, sharp peaks of nano-particles (ZIF-8) were observed at angle of 10.55°, 12.25°, 16.15° and 17.65°. Whereas the similar hump shape like pattern represent CA/PEG blend, in which at angle of 18.75° showing an peak of crystalline CA polymer [76]. At 2θ angle of 20.55° represents prominent peak of PVA polymer. Whereas, some peaks are also observed at angle of 40° – 45° representing lower

intensity of amorphous region [60]. This shift in pattern of composite signifies good interaction between polymers and ZIF-8 nano-particles.

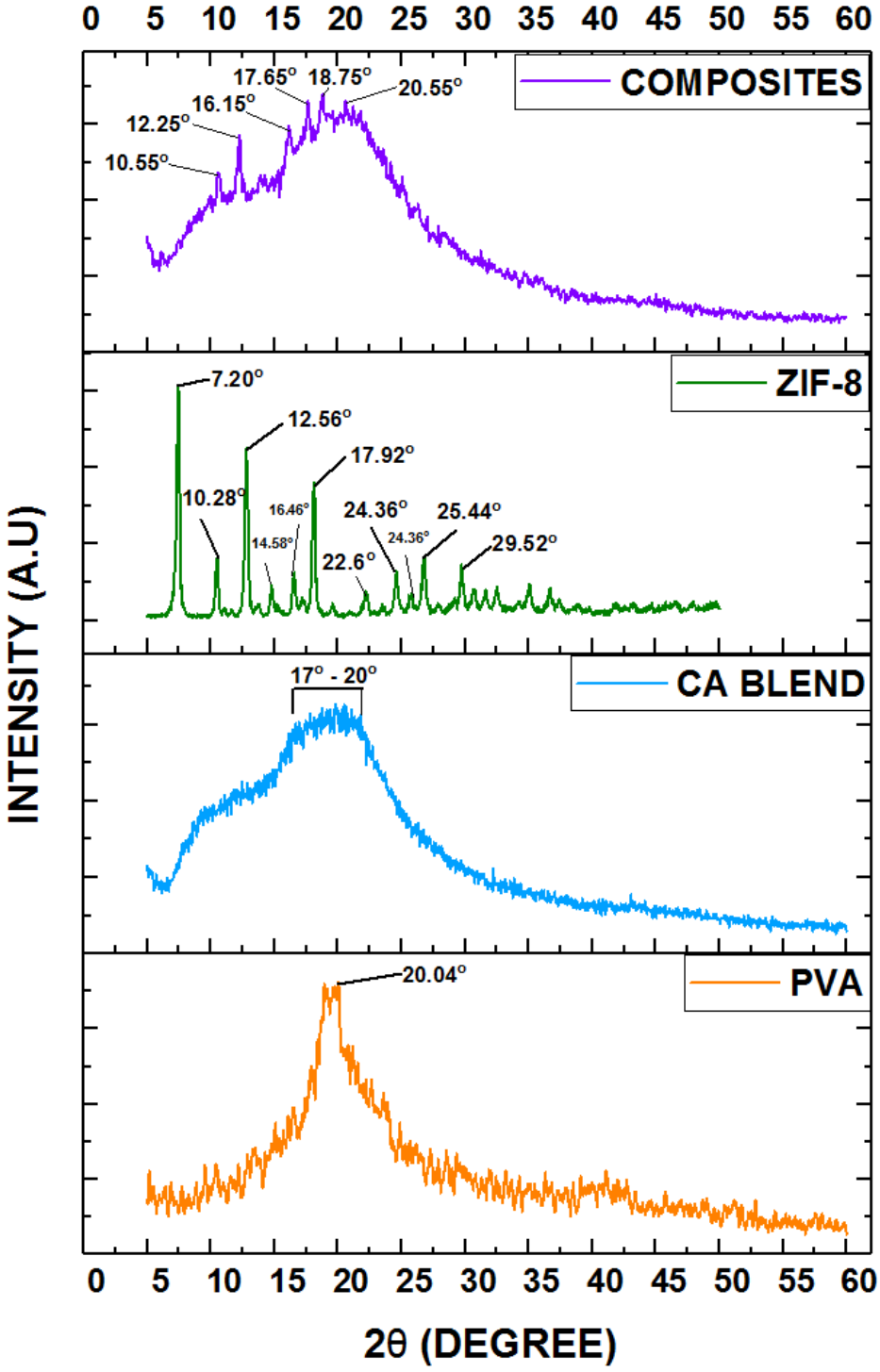

Figure 5.18. Graphically representation of X-Ray Diffraction (XRD) analysis of membrane samples

5.6 Gas Permeation Testing

The gas permeability testing were carried out in-order to investigate the gas transport behaviour of pure oxygen (O_2) gas and nitrogen (N_2) gas through PVA asymmetric membranes (support layer) and composite membrane (CA/PEG/ZIF-8/PVA). These permeation analysis were tested at a pressure range of 2 - 5 bar. The analysis results were investigated for the two main objectives:

- Effects of varying pressure
- Effects of decreasing selective layer membrane thickness and addition of plasticizer (PEG)

5.6.1 PVA Asymmetric Membrane Gas Permeation Analysis

The gas permeation testing were carried out to investigate the co-relation between the morphology of PVA asymmetric membrane and its gas transport properties. Also through this analysis, the most optimum PVA asymmetric membrane was selected for the fabrication of composite membrane for O_2/N_2 gas separation. For this investigation, three samples of each membrane were tested, to estimate the standard deviation and it also eliminate the analysis random errors. The gas permeation analysis data of PVA asymmetric membranes were represented in Table 5.3, Figure 5.19 and 5.20.

These gas permeation analysis results showed the changes were occurred in gas transport behaviour with respect to varying morphology of PVA asymmetric membrane due to change in coagulation residence time. The oxygen (O_2) gas has slightly higher permeation rate than Nitrogen (N_2) gas, as O_2 gas shows higher diffusion rate as compared to N_2 gas in the dense skin layer of PVA asymmetric membrane. The kinetic diameter (K.D) of O_2 gas is 3.46 °A, which is smaller than N_2 gas having K.D of 3.64 °A. Due to this difference of K.D between two gases, smaller molecule (O_2) gas passes with less restriction through the polymeric chain. Whereas, larger gas molecules (N_2) passes slowly within chains of polymer material due to more resistance. As increase in gas molecule size leads to decreased in diffusion co-efficient. Which satisfied the co-relation between the gas molecular size and diffusion coefficient [60, 119, 120].

From analysis data it has also been observed that, change in membrane thickness ratio also affects the gas permeation rate. As PVA 3H-12 asymmetric membrane having membrane thickness ratio between skin layer and porous layer of 17.96 $\pm$ 1.32 % and 82.04 $\pm$ 1.32 % accordingly, shows lower gas permeation rate as compared to PVA 24H-12 asymmetric membrane having skin layer and porous layer thickness ratio of 8.35 $\pm$ 0.60 and 91.56 $\pm$ 0.60 respectively. Through these gas permeation analysis results, it is concluded that longer coagulation residence time favours higher gas permeation rates due to decrement in thickness of skin layer and higher gravimetric porosity of PVA asymmetric membrane. However, the O_2/N_2 selectivity (α) of all PVA asymmetric membranes are in the range of (1 – 1.5). These single gas permeation analysis confirms the occurrence of solution diffusion mechanism through the dense skin layer of PVA asymmetric membrane [60, 121-123].

Table 5.3 – PVA Asymmetric membranes gas permeation analysis for O_2/N_2 separation[60]

Membrane Nomenclature	Gas Pressure	Gas Permeance (GPU)		Gas Selectivity $\alpha_{(O2/N2)}$
		$P_{(O2)}$	$P_{(N2)}$	
	(bars)	(GPU)	(GPU)	
PVA 3H-12	2	4.53 $\pm$ 0.10	3.1 $\pm$ 0.12	1.46 $\pm$ 0.033
	3	6.56 $\pm$ 0.16	6.18 $\pm$ 0.14	1.06 $\pm$ 0.002
	4	10.69 $\pm$ 0.23	8.55 $\pm$ 0.19	1.25 $\pm$ 0.0002
	5	16.04 $\pm$ 0.19	14.69 $\pm$ 0.16	1.09 $\pm$ 0.0023
PVA 6H-12	2	8.99 $\pm$ 0.34	6.8 $\pm$ 0.03	1.32 $\pm$ 0.05
	3	14.03 $\pm$ 0.17	11.88 $\pm$ 0.05	1.18 $\pm$ 0.01
	4	19.79 $\pm$ 0.39	17.19 $\pm$ 0.12	1.15 $\pm$ 0.01
	5	27.04 $\pm$ 0.09	20.93 $\pm$ 0.4	1.29 $\pm$ 0.03

PVA 9H-12	2	8.83 ± 0.04	6.93 ± 0.03	1.27 ± 0.01
	3	14.36 ± 0.12	12.34 ± 0.1	1.16 ± 0.01
	4	21.16 ± 0.27	18.64 ± 0.18	1.14 ± 0.01
	5	31.16 ± 0.84	24.34 ± 0.3	1.28 ± 0.03
PVA 14H-12	2	8.93 ± 0.45	6.96 ± 0.35	1.28 ± 0.01
	3	14.63 ± 0.27	12.29 ± 0.43	1.19 ± 0.03
	4	21.75 ± 0.4	18.21 ± 0.35	1.19 ± 0.03
	5	33.15 ± 0.19	26.86 ± 0.62	1.23± 0.06
PVA 24H-12	2	9.13 ± 0.67	6.63 ± 0.3	1.38 ± 0.16
	3	17.57 ± 1.13	12.93 ± 0.53	1.36 ± 0.04
	4	22.34 ± 1.9	18.41 ± 0.43	1.21 ± 0.1
	5	33.72 ± 2.1	27.62 ± 0.67	1.22 ± 0.06

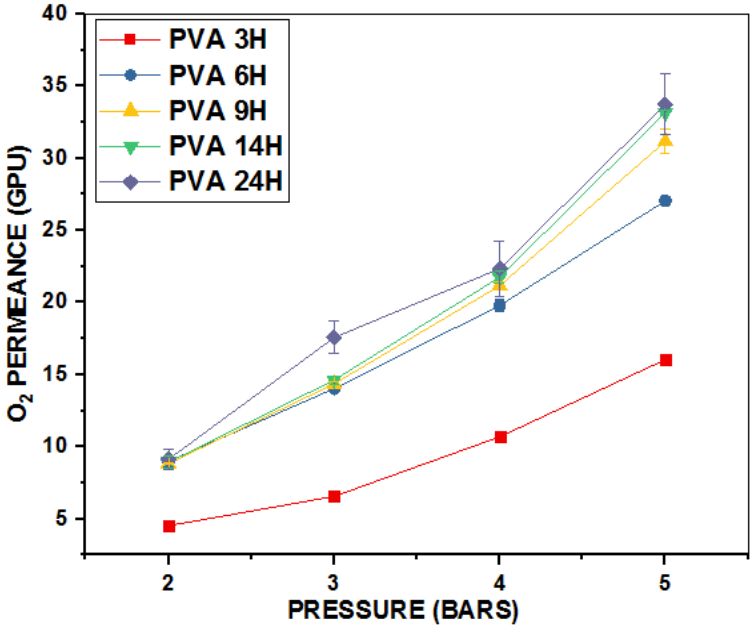

Figure 5.19. PVA Asymmetric membrane Oxygen (O_2) gas permeation analysis results [60]

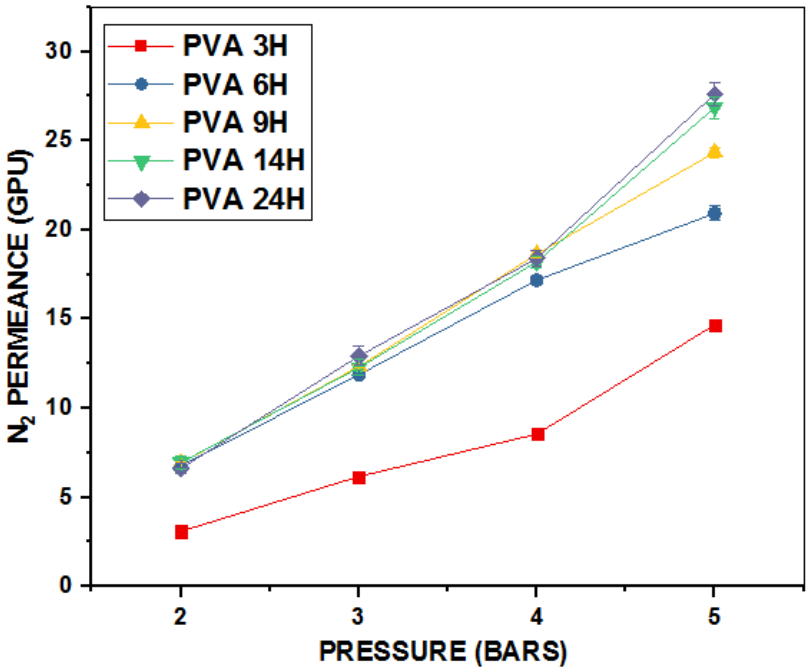

Figure 5.20. PVA Asymmetric membrane Nitrogen (N_2) gas permeation analysis results [60]

5.6.2 Multi-Layer Composite Membrane (MLCM) Gas Permeation Analysis

As among all PVA asymmetric membrane, PVA 24H-12 membrane shows the most optimum and highest gas permeation rate. Due to this reason, it was selected as support layer for the fabrication of composite membrane for O_2/N_2 separation. This support membrane showed O_2 and N_2 gas permeance up-to 33.72 $\pm$ 2.1 (GPU) and 27.62 $\pm$ 0.67 (GPU) respectively. Whereas, the O_2/N_2 selectivity were in the range of 1 – 1.5 [60].

In-order to enhance its gas selectivity, a highly selective dense layer is coated on the top surface of PVA 24H-12 asymmetric membrane, which formed a multi-layer composite membrane (MLCM). The coated dense is composed of CA/PEG/ZIF-8. This composite membrane was then tested through gas permeation unit, in-order to analyze single gas permeation performance with respect to varying pressure. In this membrane, ZIF-8 nano-particle possessed the property of gas molecules sieving due to its similarity with zeolites [25]. These nano-sieves have pore aperture of 3.40 °A, which is nearly similar to the K.D of O_2 gas having size of 3.46 °A. However, N_2 gas have K.D greater than the size of ZIF-8 pore aperture [124]. Which is the reason ZIF-8 nano-sieves are one of the most suitable candidate for incorporation in CA/PEG blend membrane for O_2/N_2 separation.

From Table 5.4 and Figure 5.21 – 5.22, single gas permeation data shows decrement in O_2 and N_2 gas permeance with increased in pressure difference. However, the O_2/N_2 gas selectivity increased. This phenomena occurred due to the polymer chain compression, which effects the free volume presents within the polymer chains of membrane [125]. At this points the transport behaviour depends on ZIF-8 particles. Which acts as an excellent nano-sieves that passes O_2 gas due to its nearly similar K.D and its higher condensability, while K.D of N_2 gas molecules is greater than pore aperture size of nano-sieve, it retains. For these reason the composite membrane showed, the maximum O_2/N_2 selectivity of 8.78 $\pm$ 0.011 at higher pressure of 5 bar. This also showed that the non-selective voids is not present in the membrane selective layer and there is good interaction between ZIF-8 and CA/PEG based selective layer of composite membrane [76].

Table 5.4 – Multi-layer composite membranes gas permeation analysis for O_2/N_2 separation

Gas Pressure	**Gas Permeance (GPU)**		**Gas Selectivity $\alpha_{(O2/N2)}$**
	$P_{(O2)}$	**$P_{(N2)}$**	
(bar)	**(GPU)**	**(GPU)**	
2.0	0.7545 $\pm$ 0.024	0.3419 $\pm$ 0.019	2.2065 $\pm$ 0.053
2.5	0.6832 $\pm$ 0.030	0.2432 $\pm$ 0.016	2.8092 $\pm$ 0.45
3.0	0.6208 $\pm$ 0.017	0.1691 $\pm$ 0.012	3.6713 $\pm$ 0.30
3.5	0.5804 $\pm$ 0.0075	0.0969 $\pm$ 0.040	5.9896 $\pm$ 0.52
4.0	0.5593 $\pm$ 0.0030	0.0790 $\pm$ 0.0002	7.0764 $\pm$ 0.20
4.5	0.5126 $\pm$ 0.0062	0.0610 $\pm$ 0.030	8.4032 $\pm$ 0.013
5.0	0.4808 $\pm$ 0.0054	0.0547 $\pm$ 0.010	8.7897 $\pm$ 0.011

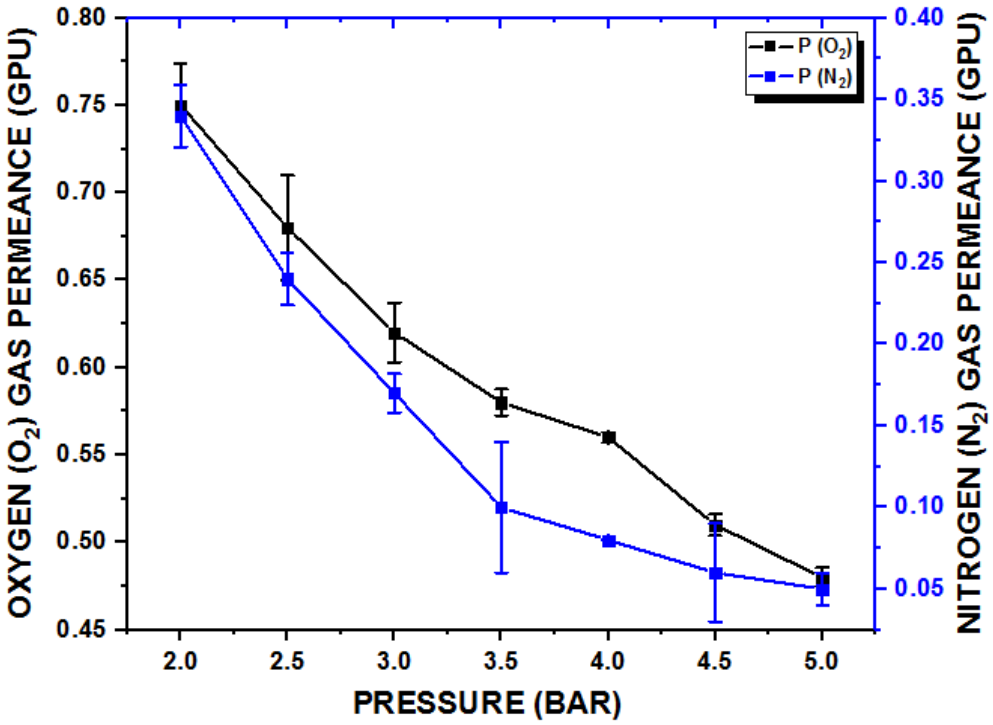

Figure 5.21. Multi-layer composite membrane gas permeation analysis results

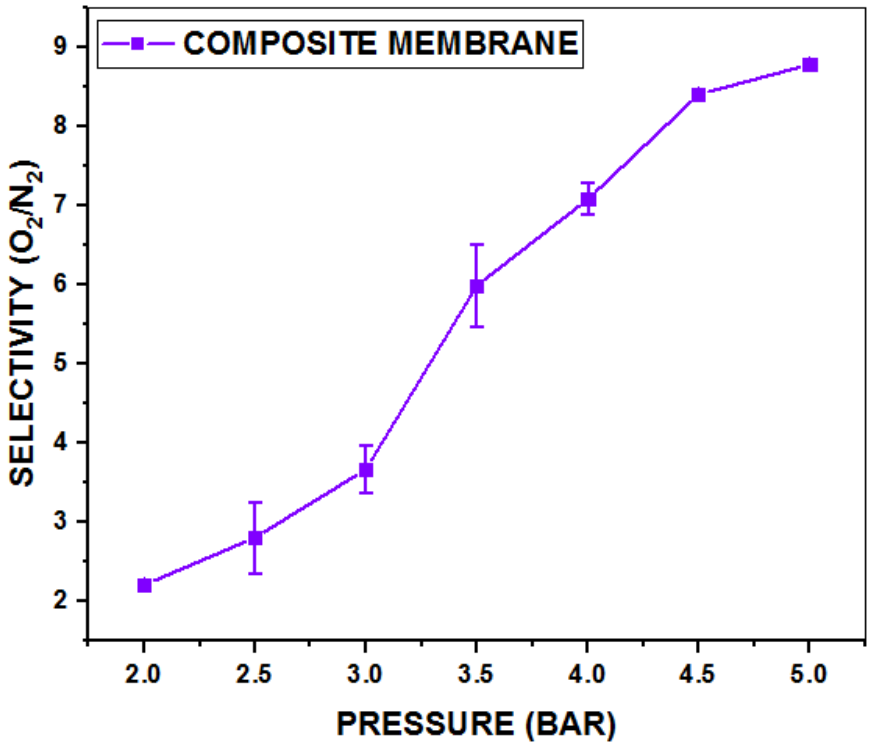

Figure 5.22. Multi-layer composite membrane O_2/N_2 selectivity results

5.6.3 Effects of Plasticizer (PEG) and selective layer thickness on gas permeance

In this section, gas permeance results of multi-layer composite membrane (MLCM) are compared with previous work of CA/ZIF-8 based mixed matrix membrane (MMMs) as represented in Table 5.5 – 5.6 and Figure 5.23 – 5.24. Which showed significantly improvement in gas permeance as compared to MMMs due to (a) lowered thickness of selective layer and (b) PEG addition.

In composite membrane, the thickness of selective layer is reduced from 25 µm to 7.06 µm. In MLCM, the highest permeance of O_2 gas was achieved up-to 0.6832 GPU at 2.5 bar, whereas MMMs show maximum O_2 gas permeance of 0.2024 GPU at 2.5 bar. Similarly N_2 gas permeance was also increased in MLCM from 0.0588 to 0.2432 GPU at 2.5 bar. These results signifies that MLCM showed higher gas permeance up-to three times than MMMs.

This improvement of gas permeance depends on two main factors, (i) Thickness variation of selective layer: As seen from Figure 5.23 and 5.24, the permeance of both gases has significantly improved, when dense layer thickness is reduced from 25 µm to 7.06 µm. This improvement in the gas permeance was also confirmed and supported by many researchers including Firpo et al. [126], Alsari et al. [127] and Nikpour N. et al. [81]. In which they showed that the permeability of gas significantly increases as thickness is reduced.

Another factor is (ii) Plasticizer (PEG) addition, which is used to enhance the polymer chain flexibility of selective layer. Which also lowers the resistance present between the polymer chains, caused increases in gas permeance rate of O_2 and N_2 through membrane. This phenomena was also supported by J. Li et al. [89] in their research work, they also explained that by PEG addition up-to 10 wt. % in CA membrane, increases gas permeation rate of O_2 and N_2, whereas O_2/N_2 selectivity reduced by one factor. This increase in diffusion rate occurred due to enhancement of polymeric chain flexibility.

However, as seen from Table 5.5 and Figure 2.5, the O_2/N_2 gas selectivity decreased from 9.58 to 7.07 in MLCM at 4 bar. This signifies that, even with the addition of PEG and variation of thickness does not greatly affected like gas permeance. Which was also supported by Pakizeh et al. [128] and J. Li et al. [89]. Another aspect to this effects are

also that, due to presence of ZIF-8 nano-particle the selectivity doesn't drastically reduced, as at higher pressure polymer chains were compressed and the gas transport behaviour becomes depended to the sieving properties of ZIF-8 nano-particles [76].

Table 5.5 – MMMs and MLCM O_2 and N_2 gas permeance comparison analysis data

Gas Pressure	MMMs Gas Permeance (GPU)		MLCM Gas Permeance (GPU)	
	$P_{(O2)}$	$P_{(N2)}$	$P_{(O2)}$	$P_{(N2)}$
(bars)	(GPU)	(GPU)	(GPU)	(GPU)
2.5	0.2024 ± 0.0204	0.0588 ± 0.0152	0.6832 ± 0.030	0.2432 ± 0.016
3.0	0.174 ± 0.014	0.0456 ± 0.01	0.6208 ± 0.017	0.1691 ± 0.012
3.5	0.1536 ± 0.0064	0.022 ± 0.032	0.5804 ± 0.0075	0.0969 ± 0.040
4.0	0.1344 ± 0.0048	0.014 ± 0.0004	0.5593 ± 0.0030	0.0790 ± 0.0002

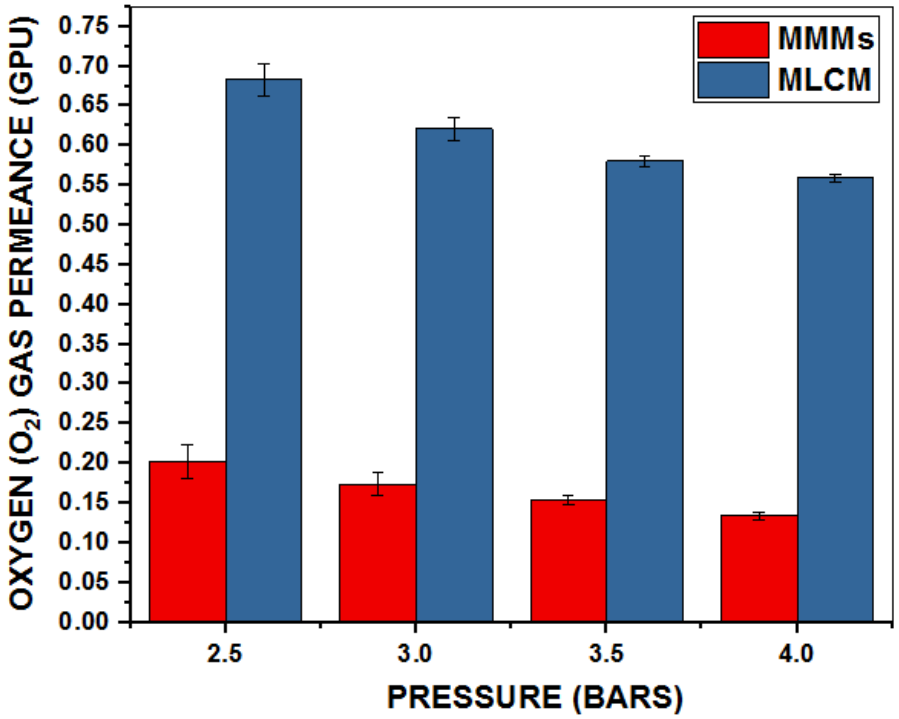

Figure 5.23. MMMs and MLCM Oxygen (O_2) gas permeance comparison

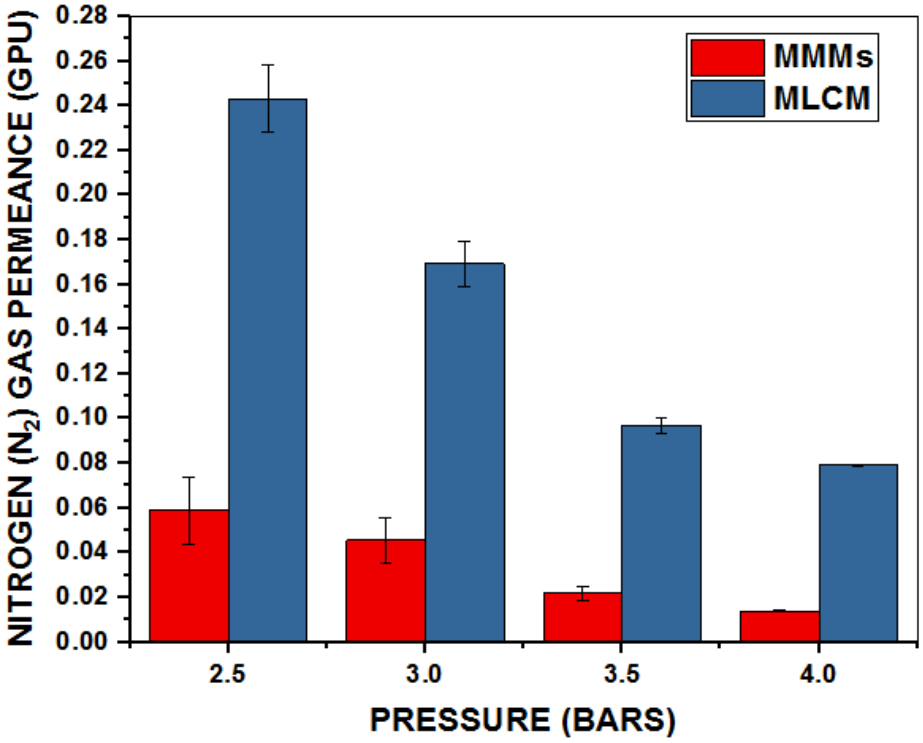

Figure 5.24. MMMs and MLCM Nitrogen (N_2) gas permeance comparison

Table 5.6 – MMMs and MLCM O_2/N_2 selectivity comparison data for O_2/N_2 separation

Gas Pressure	Gas Selectivity (O_2/N_2)	
(bar)	MMMs	MLCM
2.5	3.44 ± 0.49	2.80 ± 0.45
3.0	3.81 ± 0.49	3.67 ± 0.30
3.5	6.98 ± 0.71	5.98 ± 0.52
4.0	9.58 ± 0.18	7.07 ± 0.20

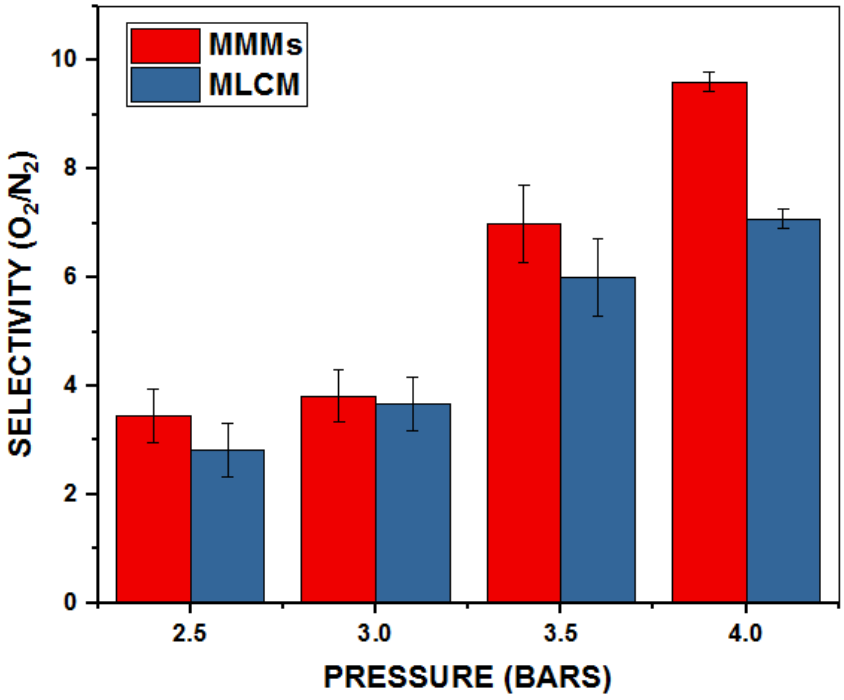

Figure 5.25. MMMs and MLCM O_2/N_2 gas selectivity comparison

5.7 Mechanical Testing

The mechanical testing of all fabricated membrane samples were carried out at an elongation rate (ER) of 10 mm/min. Through this characterization tensile strength (TS) and elongation at break percent (EAB) % of different membrane samples were analyzed as illustrated in Figure 5.26, 5.27, and 5.28. This analysis is divided into three main section as mentioned below:

5.7.1 Effects of Polymer concentration on PVA asymmetric membranes

The mechanical properties were performed to investigate the tensile strength and (EAB) % of PVA asymmetric membranes having different polymer concentration from 10 – 14 wt. % as depicted in Figure 5.25. The recorded tensile strength of PVA 3H-10, PVA 3H-12 and PVA 3H-14 asymmetric membrane were 14.5 $\pm$ 1.2 MPa, 19.4 $\pm$ 2.88 MPa [60] and 26.6 $\pm$ 1.2 MPa respectively. The analysis results showed an increasing trend of tensile strength with respect to increasing polymeric concentration from 10 wt. % to 14 wt. % [100].

However (EAB) % of PVA 3H-10 to PVA 3H-12 asymmetric membrane initially increased from 158.4 $\pm$ 30.2 % to 247 $\pm$ 48.77 % [60]. After increasing the polymer concentration from 12 wt. % to 14 wt. %, the (EAB) % decreased from 247 $\pm$ 48.77 % to 121.5 $\pm$ 38.2 %. This trend of (EAB) % signifies that, when polymer concentration increased from 10 wt. % to 12 wt. %, the membrane matrix showed enhancement in mechanical properties due to formation of smaller pores.

However, after increasing polymer concentration from 12 wt. % to 14 wt. %, the PVA membrane rigidified [100]. Due to this reason PVA 3H-14 asymmetric membrane shows increased in tensile strength with reduced (EAB) % as compared to lower polymeric (PVA) concentration based asymmetric membrane [100, 129-131]. Through this analysis, it is concluded that, at 12 wt. % PVA asymmetric membrane have the most optimum mechanical properties showing higher durability for GS applications.

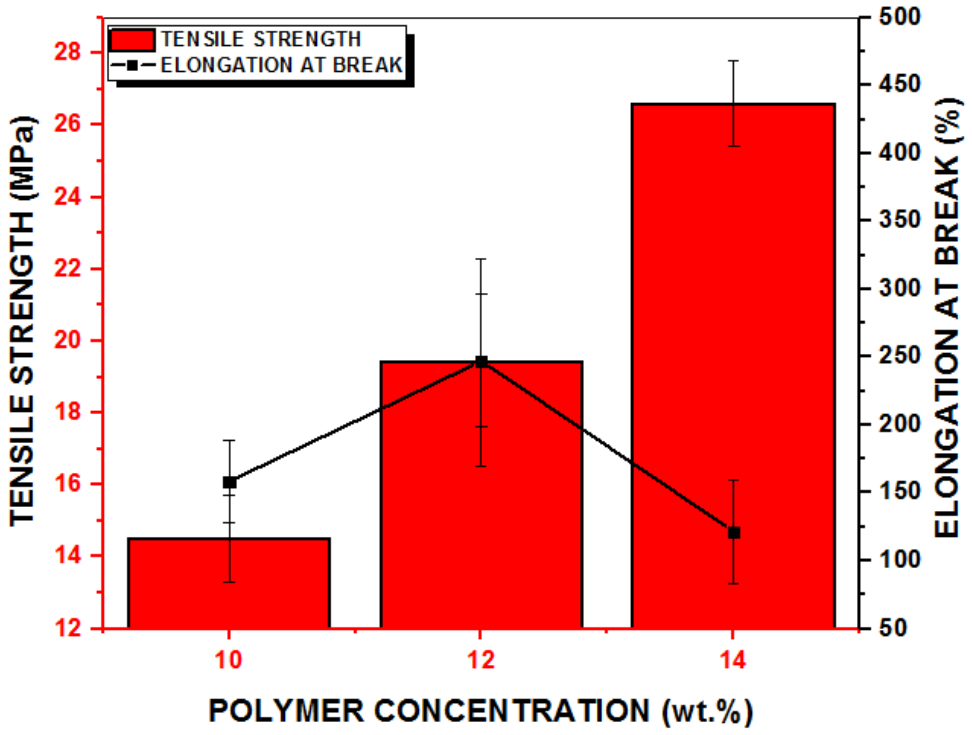

Figure 5.26. Effect of Polymer Concentration on mechanical properties of PVA asymmetric membranes

5.7.2 Effects of coagulation residence time on PVA asymmetric membranes

The effects on mechanical properties of PVA asymmetric membrane samples fabricated at different coagulation residence time between 3 hours to 24 hours were analyzed, which were illustrated in Figure 5.26. The analysis results showed that, PVA 3H-12, PVA 6H-12, PVA 9H-12, PVA 14H-12 and PVA 24H-12 asymmetric membrane have tensile strength of 19.44 $\pm$ 2.88, 15.51 $\pm$ 1.11, 12.61 $\pm$ 1.26, 18.08 $\pm$ 2.76 and 19.19 $\pm$ 1.41 MPa accordingly. Whereas (EAB) %, are 247.89 $\pm$ 48.77 %, 205.81 + 20.99 %, 129.25 + 13.55 %, 152.34 + 87.83 % and 141.60 + 80.61 % respectively [60]. These results showed that PVA 3H-12 possessed the highest mechanical strength and ductility as compared to other membrane. Whereas these mechanical properties were decreased in PVA 6H-12 membrane. Which were further reduced in PVA 9H-12 membrane. This decrement of mechanical properties represents changes occurred in polymer matrix due to the variation of coagulation residence time. This is due to the formation of weaker inter-connective porous structure and thinner dense layer [60].

However, after 9 hours the membrane started to developed proper inter-connective stronger porous network as mechanical properties was enhanced in PVA 14H-12 asymmetric membrane. This durability was further enhanced in PVA 24H-12 asymmetric membrane due to the formation of double chain porous network. The PVA 24H-12 membrane showed, the similar mechanical strength of PVA 3H-12 membrane in-spite more porous structure and thinner skin layer. This concludes that, PVA 24H-12 asymmetric membrane possessed the most optimum mechanical properties in-order to utilized it as support layer for the fabrication of multi-layer composite membrane [60].

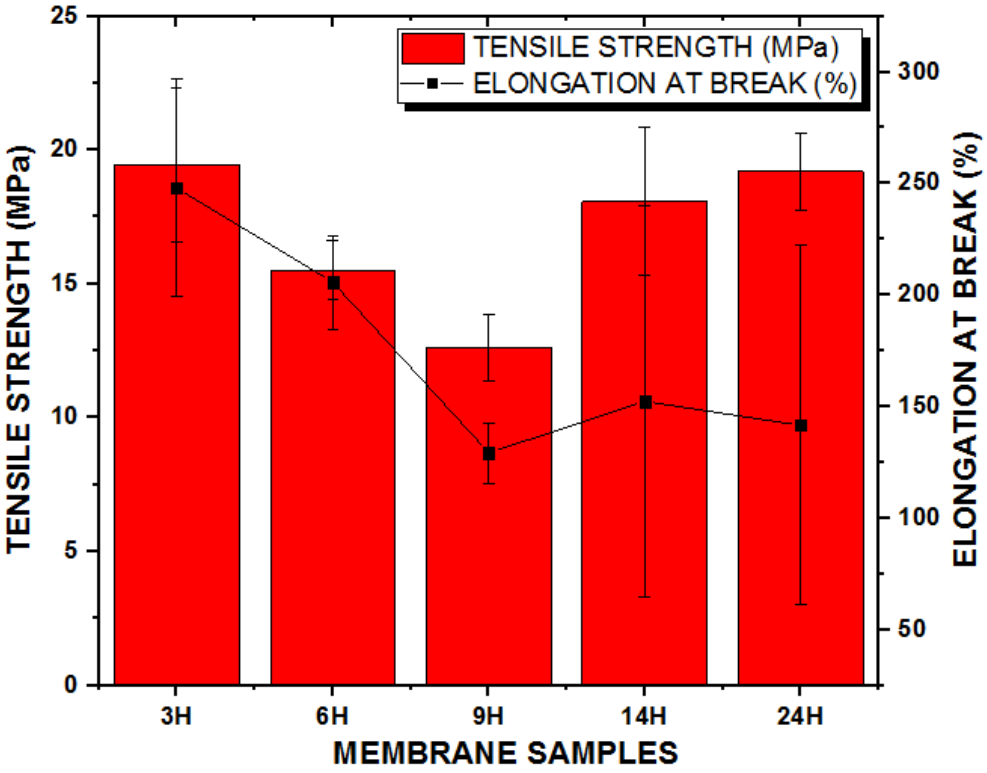

Figure 5.27. Effect of coagulation residence time on mechanical properties of PVA asymmetric membranes

5.7.3 Composite membrane mechanical properties

Figure 5.28, represented the graphical data of tensile strength comparison between different membrane samples. The results showed that, PVA support (P.S) membrane (PVA 24H-12) has the tensile strength of 19.19 $\pm$ 1.41 MPa. The single layer dense selective membrane composed of CA/PEG blend, incorporated with ZIF-8 nano-particles has a tolerable stress of 26.69 $\pm$ 0.43 MPa. Whereas, multi-layer composite membrane

(MLCM) results showed the highest tensile strength of 30.50 ± 1.5 MPa. Which signifies that, when both membranes are combined together a significant increase of tensile strength was observed in-spite of lower thickness of selective layer. This increased occurred in MLCM, was due to the support layer of PVA asymmetric membrane. This concludes that, the composite membrane having dense selective layer thickness of 7.06 µm can tolerate higher stress as compared to single layer mixed matrix membrane (MMMs).

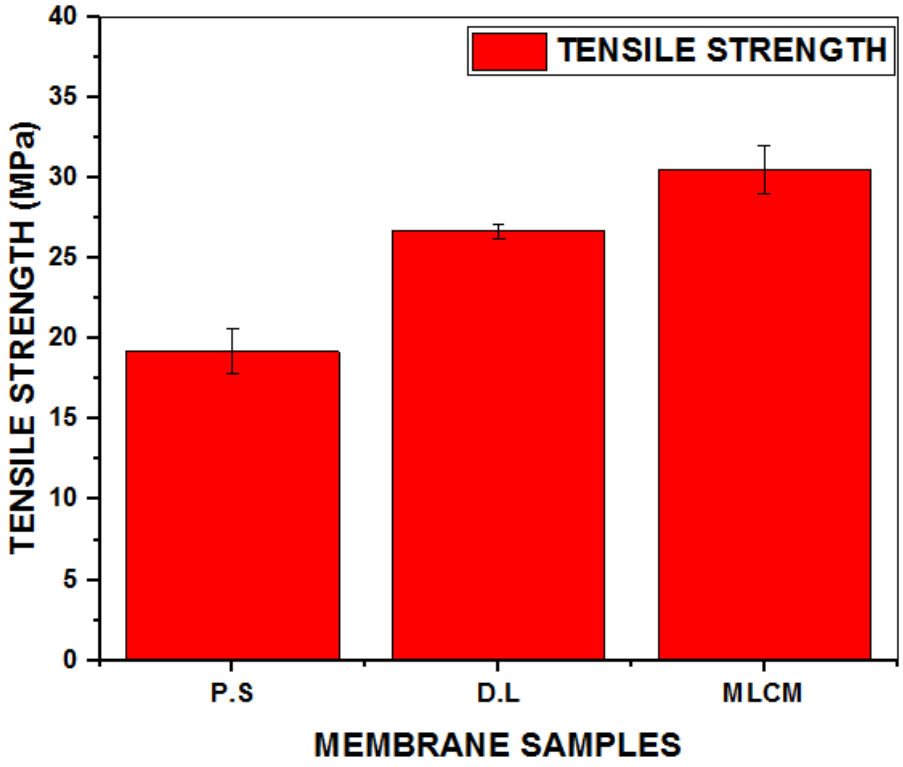

Figure 5.28. Comparison of tensile strength between different membranes

*P.S = PVA asymmetric support membrane

*D.L = Dense Layer composed of CA/PEG/ZIF-8

*MLCM = Multi-layer composite membrane (CA/PEG/ZIF-8/PVA)

Conclusion

In this research work, multi-layer composite membrane was fabricated for O_2/N_2 separation. For this purpose, a MMMs based selective layer composed of CA/PEG blend, incorporated with ZIF-8 as filler was coated on support membrane. In which PVA asymmetric membrane was used as support layer, fabricated through PVA/Water/THF ternary system by using NIPS method. The compatibility between different layers of composite membrane was ensured through theoretical solubility model. The support layer possessed the same sponge type inter-connective porous structure with top dense layer as predicted through experimental phase diagram. The PVA asymmetric membrane morphology and physical properties were improved through optimizing two different parameters of NIPS process. Which include (i) polymer concentration and (ii) coagulation residence time. It was reported that, by increasing polymer concentration from 10 wt. % to 14 wt. % leads to more densified PVA asymmetric membrane. However, 12 wt. % PVA asymmetric (3H-12) membrane showed the most optimum durable structure. Then coagulation residence time was changed from 3 hours to 24 hours, which leads to more porous membrane morphology and thinner dense layer. At 24 hours, the membrane possessed the most optimum structure having double chain porous network with thinnest top dense layer of 8.35 %. This optimized support membrane (PVA 24H-12) asymmetric membrane have the enhanced physical durability of 19.19 MPa, similar to PVA 3H-12 membrane in spite of its higher porosity and thinner dense layer. It was also reported that, the gas permeation was directly linked to gravimetric porosity and reduction of dense layer (skin layer) thickness of PVA asymmetric membrane. The highest O_2 gas permeance of 33.72 GPU with selectivity of 1 – 1.5 was achieved by PVA 24H-12 support membrane at pressure of 5 bar.

Then improvement in gas separation performance and mechanical properties was observed by coating a thin layer of CA/PEG/ZIF-8 on support membrane. The coating layer thickness was reduced from 25 µm to 7.06 µm. The addition of plasticizer (PEG) up-to 10 wt. % and reduction of selective layer thickness to 7.06 µm, resulted in improvement of gas permeance up-to 0.75 (GPU) at pressure of 2 bar. We report that the

increment in the gas permeance was directly linked to the reduction in the thickness of selective layer and addition of PEG content. However, the selectivity of the membrane was not that much affected. The highest O_2/N_2 selectivity of 8.78 was achieved by composite membrane at maximum pressure of 5 bar. The resulting membranes were also characterized by SEM, FT-IR, XRD and UTM. Which showed excellent compatibility and adhesion between the layers of composite membrane. The mechanical test showed that, the use of composite membrane instead of single flat sheet membrane also showed improvement in tensile strength, which can tolerate higher stress of 30.5 MPa as compared to single layer membrane.

Future Recommendations

The following are the recommendation for future research works.

- Further reduction of selective layer thickness up-to nano-meters should be consider to increase the O_2 gas permeation rate.
- There lies a need to incorporate different MOFs (e.g. MOF-5 and MIL-101-Cr) in the polymer matrix to fabricate high performance composite membrane.

References

[1]. Chong, K., et al., *Recent progress of oxygen/nitrogen separation using membrane technology.* J. Eng. Sci. Technol, 2016. **11**(7): p. 1016-1030.

[2]. Stafford, T.M., *Indoor air quality and academic performance.* Journal of Environmental Economics and Management, 2015. **70**: p. 34-50.

[3]. Naito, N., et al., *Artificial lungs for lung failure: JACC Technology Corner.* Journal of the American College of Cardiology, 2018. **72**(14): p. 1640-1652.

[4]. Rosso, D., L.E. Larson, and M.K. Stenstrom, *Aeration of large-scale municipal wastewater treatment plants: state of the art.* Water Science and Technology, 2008. **57**(7): p. 973-978.

[5]. Norkool, D.M. and J.N. Kirkpatrick, *Treatment of acute carbon monoxide poisoning with hyperbaric oxygen: a review of 115 cases.* Annals of emergency medicine, 1985. **14**(12): p. 1168-1171.

[6]. Jin, Y.-H., et al., *A rapid advice guideline for the diagnosis and treatment of 2019 novel coronavirus (2019-nCoV) infected pneumonia (standard version).* Military Medical Research, 2020. **7**(1): p. 4.

[7]. Mohandas, B., A. Jagadeesh, and S. Vikram, *Impact of monitoring cerebral oxygen saturation on the outcome of patients undergoing open heart surgery.* Annals of cardiac anaesthesia, 2013. **16**(2): p. 102.

[8]. Federspiel, W.J. and K.A. Henchir, *Lung, artificial: basic principles and current applications.* Encyclopedia of biomaterials and biomedical engineering, 2004. **9**: p. 910.

[9]. Baker, R.W., *Membrane technology.* Kirk-Othmer Encyclopedia of Chemical Technology, 2000.

[10]. Bernardo, P., E. Drioli, and G. Golemme, *Membrane gas separation: a review/state of the art.* Industrial & engineering chemistry research, 2009. **48**(10): p. 4638-4663.

[11]. Abetz, V., et al., *Developments in membrane research: from material via process design to industrial application.* Advanced Engineering Materials, 2006. **8**(5): p. 328-358.

[12]. Shen, Y., et al., *MoS2 nanosheets functionalized composite mixed matrix membrane for enhanced CO2 capture via surface drop-coating method.* ACS applied materials & interfaces, 2016. **8**(35): p. 23371-23378.

[13]. Wang, M., et al., *Post-combustion CO2 capture with chemical absorption: a state-of-the-art review*. Chemical engineering research and design, 2011. **89**(9): p. 1609-1624.

[14]. Brimblecombe, P., *Air composition and chemistry*. 1996: Cambridge University Press.

[15]. Ismail, A.F., K.C. Khulbe, and T. Matsuura, *Gas separation membranes.* Switzerland: Springer, 2015.

[16]. Breck, D.W., *Zeolite molecular sieves: structure, chemistry and use*. 1984: Krieger.

[17]. Matteucci, S., et al., *Transport of gases and vapors in glassy and rubbery polymers.* Materials science of membranes for gas and vapor separation, 2006. **1**: p. 1-2.

[18]. Pinnau, I. and B.D. Freeman, *for Membrane Separations*, in *Encyclopedia of Separation Science*. 2000, Academic Press. p. 1755-1764.

[19]. Dai, Z., L. Ansaloni, and L. Deng, *Recent advances in multi-layer composite polymeric membranes for CO2 separation: A review.* Green Energy & Environment, 2016. **1**(2): p. 102-128.

[20]. Mulder, M., *Basic principles of membrane technology*. 2012: Springer Science & Business Media.

[21]. Browall, W.R., *Method for sealing breaches in multi-layer ultrathin membrane composites*. 1976, Google Patents.

[22]. Henis, J.M. and M.K. Tripodi, *Multicomponent membranes for gas separations*. 1980, Google Patents.

[23]. Khalilpour, R., et al., *Membrane-based carbon capture from flue gas: a review.* Journal of Cleaner Production, 2015. **103**: p. 286-300.

[24]. Koros, W., et al., *Polymeric membrane materials for solution-diffusion based permeation separations.* Progress in Polymer Science, 1988. **13**(4): p. 339-401.

[25]. Ordonez, M.J.C., et al., *Molecular sieving realized with ZIF-8/Matrimid® mixed-matrix membranes.* Journal of Membrane Science, 2010. **361**(1-2): p. 28-37.

[26]. Hussain, A., et al., *Carbon capture from natural gas using multi-walled CNTs based mixed matrix membranes.* Environmental technology, 2019. **40**(7): p. 843-854.

[27]. Moghadam, F., et al., *The effect of TiO2 nanoparticles on gas transport properties of Matrimid5218-based mixed matrix membranes.* Separation and Purification Technology, 2011. **77**(1): p. 128-136.

[28]. Nagar, H., et al., *Air separation by facilitated transport of oxygen through a Pebax membrane incorporated with a cobalt complex.* RSC Advances, 2015. **5**(93): p. 76190-76201.

[29]. Deng, L., T.-J. Kim, and M.-B. Hägg, *Facilitated transport of CO2 in novel PVAm/PVA blend membrane.* Journal of Membrane Science, 2009. **340**(1-2): p. 154-163.

[30]. Deng, L., et al. *PVA/PVAm blend FSC membrane for natural gas sweetening*. in *Proceedings of the 1st Annual Gas Processing Symposium*. 2009. Elsevier.

[31]. Menning, M. and M.A. Aegerter, *Sol-Gel Technologies for Glass Producers and Users*. 2004: Kluwer Academic Publishers.

[32]. Castro, R.P., R.W. Baker, and J.G. Wijmans, *Multilayer interfacial composite membrane*. 1991, Google Patents.

[33]. Larson, R.G. and T.J. Rehg, *Spin coating*, in *Liquid Film Coating*. 1997, Springer. p. 709-734.

[34]. Buschow, K.J., et al., *Encyclopedia of materials.* Science and technology, 2001. **1**: p. 11.

[35]. Martin, P.M., *Handbook of deposition technologies for films and coatings: science, applications and technology*. 2009: William Andrew.

[36]. Asatekin, A. and K.K. Gleason, *Polymeric nanopore membranes for hydrophobicity-based separations by conformal initiated chemical vapor deposition.* Nano letters, 2011. **11**(2): p. 677-686.

[37]. Yang, R. and K.K. Gleason, *Ultrathin antifouling coatings with stable surface zwitterionic functionality by initiated chemical vapor deposition (iCVD).* Langmuir, 2012. **28**(33): p. 12266-12274.

[38]. Wang, Q., et al., *PVDF membranes with simultaneously enhanced permeability and selectivity by breaking the tradeoff effect via atomic layer deposition of TiO2.* Journal of membrane science, 2013. **442**: p. 57-64.

[39]. Cai, Y., et al., *Gas transport property of polyallylamine–poly (vinyl alcohol)/polysulfone composite membranes.* Journal of Membrane Science, 2008. **310**(1-2): p. 184-196.

[40]. Kuang, P.-Y., et al., *Double-shelled CdS-and CdSe-cosensitized ZnO porous nanotube arrays for superior photoelectrocatalytic applications.* ACS applied materials & interfaces, 2015. **7**(30): p. 16387-16394.

[41]. Zhao, Y. and W.W. Ho, *CO2-selective membranes containing sterically hindered amines for CO2/H2 separation.* Industrial & Engineering Chemistry Research, 2013. **52**(26): p. 8774-8782.

[42]. Zou, J. and W.W. Ho, *CO2-selective polymeric membranes containing amines in crosslinked poly (vinyl alcohol).* Journal of Membrane Science, 2006. **286**(1-2): p. 310-321.

[43]. Jansen, J.C., *Glassy Polymer*, in *Encyclopedia of Membranes*, E. Drioli and L. Giorno, Editors. 2015, Springer Berlin Heidelberg: Berlin, Heidelberg. p. 1-1.

[44]. Budd, P.M. and N.B. McKeown, *Highly permeable polymers for gas separation membranes.* Polymer Chemistry, 2010. **1**(1): p. 63-68.

[45]. McKeown, N.B., et al., *Polymers of intrinsic microporosity (PIMs): bridging the void between microporous and polymeric materials.* Chemistry–A European Journal, 2005. **11**(9): p. 2610-2620.

[46]. Haraya, K. and S.-T. Hwang, *Permeation of oxygen, argon and nitrogen through polymer membranes.* Journal of membrane science, 1992. **71**(1-2): p. 13-27.

[47]. Borandeh, S., A. Abdolmaleki, and M. Sadeghi, *Poly (vinyl alcohol)/methoxy poly (ethylene glycol) methacrylate-TiO 2 nanocomposite as a novel polymeric membrane for enhanced gas separation.* Journal of the Iranian Chemical Society, 2019. **16**(3): p. 523-533.

[48]. Baker, R.W., *Membrane Technology*, in *Kirk-Othmer Encyclopedia of Chemical Technology*.

[49]. Reid, B.D., et al., *Gas permeability properties of polysulfone membranes containing the mesoporous molecular sieve MCM-41*. Chemistry of materials, 2001. **13**(7): p. 2366-2373.

[50]. Espeso, J., et al., *Effect of substituents on the permeation properties of polyamide membranes.* Journal of Membrane Science, 2006. **280**(1-2): p. 659-665.

[51]. Merkel, T., et al., *Gas sorption, diffusion, and permeation in poly (dimethylsiloxane).* Journal of Polymer Science Part B: Polymer Physics, 2000. **38**(3): p. 415-434.

[52]. Srinivasan, R., S. Auvil, and P. Burban, *Elucidating the mechanism (s) of gas transport in poly [1-(trimethylsilyl)-1-propyne](PTMSP) membranes.* Journal of Membrane Science, 1994. **86**(1-2): p. 67-86.

[53]. Bos, A., et al., *Suppression of gas separation membrane plasticization by homogeneous polymer blending.* AIChE journal, 2001. **47**(5): p. 1088-1093.

[54]. Aryanti1a, P., et al., *Performance and characterization of PEG400 modified PVC ultrafiltration membrane.* 2015.

[55]. Rezakazemi, M., M. Sadrzadeh, and T. Matsuura, *Thermally stable polymers for advanced high-performance gas separation membranes.* Progress in Energy and Combustion Science, 2018. **66**: p. 1-41.

[56]. Li, X.-G., et al., *Morphology and gas permselectivity of blend membranes of polyvinylpyridine with ethylcellulose.* Polymer, 2001. **42**(16): p. 6859-6869.

[57]. Komatsuka, T., A. Kusakabe, and K. Nagai, *Characterization and gas transport properties of poly (lactic acid) blend membranes.* Desalination, 2008. **234**(1-3): p. 212-220.

[58]. Ghalei, B. and M.A. Semsarzadeh. *A novel nano structured blend membrane for gas separation*. in *Macromolecular Symposia*. 2007. Wiley Online Library.

[59]. George, S.C., K. Ninan, and S. Thomas, *Permeation of nitrogen and oxygen gases through styrene–butadiene rubber, natural rubber and styrene–butadiene rubber/natural rubber blend membranes.* European polymer journal, 2001. **37**(1): p. 183-191.

[60]. Karim, S.S., et al., *Effects of Coagulation Residence Time on the Morphology and Properties of Poly (vinyl) Alcohol (PVA) Asymmetric Membrane via NIPS Method for O 2/N 2 Separation.* Journal of Polymers and the Environment, 2020: p. 1-13.

[61]. Mohamed, F., et al. *Effect of coagulant bath on the gas permeation properties of cellulose acetate asymmetric membrane*. in *IOP Conference Series: Earth and Environmental Science*. 2016.

[62]. Kawakami, H., M. Mikawa, and S. Nagaoka, *Gas permeability and selectivity through asymmetric polyimide membranes.* Journal of applied polymer science, 1996. **62**(7): p. 965-971.

[63]. Pesek, S. and W. Koros, *Aqueous quenched asymmetric polysulfone hollow fibers prepared by dry/wet phase separation.* Journal of Membrane Science, 1994. **88**(1): p. 1-19.

[64]. Mohamed, F., et al., *Gas permeation performance of poly (lactic acid) asymmetric membrane for O 2/N 2 separation*, in *ICGSCE 2014*. 2015, Springer. p. 149-156.

[65]. Robeson, L., et al., *An empirical correlation of gas permeability and permselectivity in polymers and its theoretical basis.* Journal of Membrane Science, 2009. **341**(1-2): p. 178-185.

[66]. Aroon, M., et al., *Performance studies of mixed matrix membranes for gas separation: a review.* Separation and purification Technology, 2010. **75**(3): p. 229-242.

[67]. Xu, Z.-l., L.-y. Yu, and L.-f. Han, *Polymer-nanoinorganic particles composite membranes: a brief overview.* Frontiers of Chemical Engineering in China, 2009. **3**(3): p. 318-329.

[68]. Moore, T.T. and W.J. Koros, *Gas sorption in polymers, molecular sieves, and mixed matrix membranes.* Journal of applied polymer science, 2007. **104**(6): p. 4053-4059.

[69]. Chung, T.-S., et al., *Mixed matrix membranes (MMMs) comprising organic polymers with dispersed inorganic fillers for gas separation.* Progress in polymer science, 2007. **32**(4): p. 483-507.

[70]. Mahajan, R., et al., *Challenges in forming successful mixed matrix membranes with rigid polymeric materials.* Journal of Applied Polymer Science, 2002. **86**(4): p. 881-890.

[71]. Patel, R., et al., *Use of block copolymer as compatibilizer in polyimide/zeolite composite membranes.* Polymers for Advanced Technologies, 2011. **22**(5): p. 768-772.

[72]. Yong, H.H., et al., *Zeolite-filled polyimide membrane containing 2, 4, 6-triaminopyrimidine.* Journal of Membrane Science, 2001. **188**(2): p. 151-163.

[73]. Vu, D.Q., W.J. Koros, and S.J. Miller, *Mixed matrix membranes using carbon molecular sieves: I. Preparation and experimental results.* Journal of membrane science, 2003. **211**(2): p. 311-334.

[74]. Chen, J.-T., et al., *Zeolite-filled porous mixed matrix membranes for air separation.* Industrial & Engineering Chemistry Research, 2014. **53**(7): p. 2781-2789.

[75]. Goh, P., et al., *Effect of dispersed multi-walled carbon nanotubes on mixed matrix membrane for O2/N2 separation.* Separation Science and Technology, 2011. **46**(8): p. 1250-1261.

[76]. Azam, S.U., et al., *Enhancement in the selectivity of O 2/N 2 via ZIF-8/CA mixed-matrix membranes and the development of a thermodynamic model to predict the permeability of gases.* Environmental Science and Pollution Research, 2020: p. 1-17.

[77]. Jeazet, H.B.T., C. Staudt, and C. Janiak, *A method for increasing permeability in O 2/N 2 separation with mixed-matrix membranes made of water-stable MIL-101 and polysulfone.* Chemical Communications, 2012. **48**(15): p. 2140-2142.

[78]. Perez, E.V., et al., *Mixed-matrix membranes containing MOF-5 for gas separations.* Journal of Membrane Science, 2009. **328**(1-2): p. 165-173.

[79]. Ismail, A., W. Rahman, and F. Aziz. *Development of Polysulfone (PSF)-Carbon Molecular Sieve (CMS) Mixed Matrix Membrane (MMM) For O 2/N 2 Gas Separation*. in *AIP Conference Proceedings*. 2009. American Institute of Physics.

[80]. Liang, C.Z., T.-S. Chung, and J.-Y. Lai, *A review of polymeric composite membranes for gas separation and energy production.* Progress in Polymer Science, 2019. **97**: p. 101141.

[81]. Nikpour, N. and B. Khoshnevisan, *Enhanced selectivity of O2/N2 gases in co-casted mixed matrix membranes filled with BaFe12O19 nanoparticles.* Separation and Purification Technology, 2020: p. 116815.

[82]. Chong, K.C., et al., *Preparation and characterization of polysulfone membrane coated with poly (ether block amide) for oxygen enrichment process.* Malaysian Journal of Fundamental and Applied Sciences, 2019. **15**(1): p. 50-53.

[83]. Maleh, M.S. and A. Raisi, *Comparison of porous and nonporous filler effect on performance of poly (ether-block-amide) mixed matrix membranes for gas separation applications.* Chemical Engineering Research and Design, 2019. **147**: p. 545-560.

[84]. Moradi, M.R., et al., *PDMS coating of used TFC-RO membranes for O2/N2 and CO2/N2 gas separation applications.* Polymer Testing, 2017. **63**: p. 101-109.

[85]. Habibiannejad, S., A. Aroujalian, and A. Raisi, *Pebax-1657 mixed matrix membrane containing surface modified multi-walled carbon nanotubes for gas separation.* RSC advances, 2016. **6**(83): p. 79563-79577.

[86]. Son, W.-I., J.-M. Hong, and B.-S. Kim, *Polypyrrole composite membrane with high permeability prepared by interfacial polymerization.* Korean Journal of Chemical Engineering, 2005. **22**(2): p. 285-290.

[87]. Han, J., et al., *Highly Selective Oxygen/Nitrogen Separation Membrane Engineered Using a Porphyrin-Based Oxygen Carrier.* Membranes, 2019. **9**(9): p. 115.

[88]. Robeson, L.M., *The upper bound revisited.* Journal of membrane science, 2008. **320**(1-2): p. 390-400.

[89]. Li, J., et al., *Preparation of polyethyleneglycol (PEG) and cellulose acetate (CA) blend membranes and their gas permeabilities.* Journal of applied polymer science, 1995. **58**(9): p. 1455-1463.

[90]. Hansen, C.M., *Hansen Solubility Parameters: A User's Handbook, Second Edition*. 2007: Taylor & Francis.

[91]. Wijmans, J., et al., *Phase separation phenomena in solutions of polysulfone in mixtures of a solvent and a nonsolvent: relationship with membrane formation.* Polymer, 1985. **26**(10): p. 1539-1545.

[92]. Goldstein, J.I., et al., *Scanning electron microscopy and X-ray microanalysis*. 2017: Springer.

[93]. Zhang, Y., et al., *Recent advances in gold nanostructures based biosensing and bioimaging.* Coordination Chemistry Reviews, 2018. **370**: p. 1-21.

[94]. Berthomieu, C. and R. Hienerwadel, *Fourier transform infrared (FTIR) spectroscopy.* Photosynthesis research, 2009. **101**(2-3): p. 157-170.

[95]. Ojeda, J.J. and M. Dittrich, *Fourier transform infrared spectroscopy for molecular analysis of microbial cells*, in *Microbial Systems Biology*. 2012, Springer. p. 187-211.

[96]. Hitkari, G., S. Singh, and G. Pandey, *Nanoparticles: An Emerging Weapon for Mitigation/Removal of Various Environmental Pollutants for Environmental Safety*, in *Emerging and Eco-Friendly Approaches for Waste Management*. 2019, Springer. p. 359-395.

[97]. Chellamuthu, S., S. Muthu, and M.N. Ali, *Experimental Study on Tensile Behavior of Multi Wall Carbon Nanotube Reinforced Epoxy Composites.* Journal of Applied Sciences Research, 2012. **8**: p. 3253-5259.

[98]. Ebrahimpour, M., et al., *Phase separation analysis in the ternary system of poly (butylene succinate)/1, 1, 2, 2,-tetrachloethane/non-solvent in relation to membrane formation.* Int. Bus. Manag, 2016. **10**: p. 5876-5884.

[99]. Peydayesh, M., et al., *Fabrication optimization of polyethersulfone (PES)/polyvinylpyrrolidone (PVP) nanofiltration membranes using Box–Behnken response surface method.* RSC advances, 2017. **7**(40): p. 24995-25008.

[100]. Ismail, N., et al., *Effect of polymer concentration on the morphology and mechanical properties of asymmetric polysulfone (PSf) membrane.* Journal of Applied Membrane Science & Technology, 2017. **21**(1).

[101]. Mustaffar, M., A. Ismail, and R. Illias. *Study on the effect of polymer concentration on hollow fiber ultrafiltration membrane performance and morphology*. in *Reg. Conf. Eng. Educ. RCEE 2005*. 2004.

[102]. Julian, H. and I. Wenten, *Polysulfone membranes for CO2/CH4 separation: State of the art.* J. Eng, 2012. **2**(3): p. 484-495.

[103]. Ismail, A.F. and L.P. Yean, *Review on the development of defect-free and ultrathin-skinned asymmetric membranes for gas separation through manipulation of phase inversion and rheological factors.* Journal of applied polymer science, 2003. **88**(2): p. 442-451.

[104]. Strathmann, H., et al., *The formation mechanism of asymmetric membranes.* Desalination, 1975. **16**(2): p. 179-203.

[105]. Smolders, C., et al., *Microstructures in phase-inversion membranes. Part 1. Formation of macrovoids.* Journal of Membrane Science, 1992. **73**(2-3): p. 259-275.

[106]. Boom, R., et al., *Microstructures in phase inversion membranes. Part 2. The role of a polymeric additive.* Journal of membrane science, 1992. **73**(2-3): p. 277-292.

[107]. Abdel-Hady, E.E., et al., *Physical and electrochemical properties of PVA/TiO2 nanocomposite membrane.* Advances in Polymer Technology, 2018. **37**(8): p. 3842-3853.

[108]. Tahalyani, J., K.K. Rahangdale, and K. Balasubramanian, *The dielectric properties and charge transport mechanism of π-conjugated segments decorated with intrinsic conducting polymer.* RSC advances, 2016. **6**(74): p. 69733-69742.

[109]. Mark, J.E., *Polymer data handbook.* 2009: Oxford university press.

[110]. Mansur, H.S., R.L. Oréfice, and A.A. Mansur, *Characterization of poly (vinyl alcohol)/poly (ethylene glycol) hydrogels and PVA-derived hybrids by small-angle X-ray scattering and FTIR spectroscopy.* Polymer, 2004. **45**(21): p. 7193-7202.

[111]. Hu, Y., et al., *In situ high pressure study of ZIF-8 by FTIR spectroscopy.* Chemical communications, 2011. **47**(47): p. 12694-12696.

[112]. Hemalatha, K., et al., *Synthesis, characterization and optical properties of hybrid PVA–ZnO nanocomposite: a composition dependent study.* Materials Research Bulletin, 2014. **51**: p. 438-446.

[113]. Mansour, A., S. Mansour, and M. Abdo, *Improvement structural and optical properties of ZnO/PVA nanocomposites.* IOSR Journal of Applied Physics, 2015. **7**(2): p. 60-69.

[114]. Abdullah, O.G., S.B. Aziz, and M.A. Rasheed, *Structural and optical characterization of PVA: KMnO4 based solid polymer electrolyte.* Results in physics, 2016. **6**: p. 1103-1108.

[115]. Hema, M., et al., *FTIR, XRD and ac impedance spectroscopic study on PVA based polymer electrolyte doped with NH4X (X= Cl, Br, I).* Journal of Non-Crystalline Solids, 2009. **355**(2): p. 84-90.

[116]. Nasar, G., M.S. Khan, and U. Khalil, *Structural study of PVA composites with inorganic salts by X-ray diffraction.* J. Pak. Mater. Soc, 2009. **3**: p. 67-70.

[117]. Mubashir, M., et al., *Efficient CO2/N2 and CO2/CH4 separation using NH2-MIL-53 (Al)/cellulose acetate (CA) mixed matrix membranes.* Separation and Purification Technology, 2018. **199**: p. 140-151.

[118]. Zhou, K., et al., *Characterization and properties of Zn/Co zeolitic imidazolate frameworks vs. ZIF-8 and ZIF-67.* Journal of Materials Chemistry A, 2017. **5**(3): p. 952-957.

[119]. Ziegel, K., *Gas transport in segmented block copolymers.* Journal of Macromolecular Science, Part B: Physics, 1971. **5**(1): p. 11-21.

[120]. Eusébio, T.M., et al. *Polyurethane urea membranes for membrane blood oxygenators: synthesis and gas permeation properties*. in *2019 IEEE 6th Portuguese Meeting on Bioengineering (ENBENG)*. 2019. IEEE.

[121]. Rozuki, N., M. Tajuddin, and N. Yusof, *Effect of different solvent on asymmetric polysulfone (Psf) membranes for CO2/CH4 separation.* Env Ecosys Sci, 2018. **2**(2): p. 1114.

[122]. Baker, R.W., *Membrane technology and applications*. 2012: John Wiley & Sons.

[123]. Raza, A., S. Farrukh, and A. Hussain, *Synthesis, characterization and NH 3/N 2 gas permeation study of nanocomposite membranes.* Journal of Polymers and the Environment, 2017. **25**(1): p. 46-55.

[124]. Ghosal, K. and B.D. Freeman, *Gas separation using polymer membranes: an overview*. Polymers for advanced technologies, 1994. **5**(11): p. 673-697.

[125]. Isfahani, A.P., et al., *Plasticization resistant crosslinked polyurethane gas separation membranes.* Journal of Materials Chemistry A, 2016. **4**(44): p. 17431-17439.

[126]. Firpo, G., et al., *Permeability thickness dependence of polydimethylsiloxane (PDMS) membranes.* Journal of Membrane Science, 2015. **481**: p. 1-8.

[127]. Alsari, A., B. Kruczek, and T. Matsuura, *Effect of pressure and membrane thickness on the permeability of gases in dense polyphenylene oxide (PPO) membranes: thermodynamic interpretation.* Separation Science and Technology, 2007. **42**(10): p. 2143-2155.

[128]. Pakizeh, M., et al., *Modification of PSf membrane nanostructure using different fabrication parameters and investigation of the CO2 separation properties of PDMS-coated PSf composite membranes.* Brazilian Journal of Chemical Engineering, 2013. **30**(2): p. 345-354.

[129]. Yunos, M.Z., et al. *Effects of water as non-solvent additive on performance of polysulfone ultrafiltration membrane*. in *Advanced Materials Research*. 2012. Trans Tech Publ.

[130]. Amirabedi, P., R. Yegani, and M.K. Razavi Aghje, *Experimental design applied to fabrication of PSf membranes via NIPS method Part1: Influential parameters on membrane porosity and mechanical strength.* Journal of Textiles and Polymers, 2013. **1**(1): p. 24-30.

[131]. Jung, J.T., et al., *Understanding the non-solvent induced phase separation (NIPS) effect during the fabrication of microporous PVDF membranes via thermally induced phase separation (TIPS).* Journal of Membrane Science, 2016. **514**: p. 250-263.